

République Algérienne Démocratique et Populaire
Ministère de l'Enseignement Supérieur et de la Recherche Scientifique
Université d'Echahid Cheikh Larbi Tebessi



Faculté des Sciences Exactes et des Sciences de la Nature et de la Vie

Département : Science de la terre et l'univers

PRESENTÉE EN VUE DE L'OBTENTION DU DIPLOME DE DOCTORAT

TROISIÈME CYCLE (LMD)

Option: Géologie de l'ingénieur

Thème:

**Shallow landslides of the Souk Ahras region: influence
of soil geotechnical properties and rainfall.**

Présenté par: **BENABID Ibtissam**

Devant le jury:

Président : BOUBAYA .Djamel	Professeur	Université de Tebessa
Encadreur : FEHDI.Chemeseddine	Professeur	Université de Tebessa
Co-encadreur: BOUMEZBEUR Abderrahmane	Professeur	Université d'Oum El Bouaghi
Examineur : HADJI Rihab	Professeur	Université de Sétif 1
Examineur : GHRIEB.Lassaad.	Professeur	Université de Guelma
Examineur :BAALI.Fethi	Professeur	Université de Tebessa

Date de soutenance:



ACKNOWLEDGEMENT

First of all, I would like to thank god Almighty for guiding me through all these years of scientific research and giving me the will, patience and courage to finish this humble work.

Following people contributed to this work in various ways. My infinite thanks to;

I would like to express my deep gratitude to my supervisor ***Professor Fehdi Chemseddine***, who has done me the honor of accompanying this work throughout its implementation, would like to accept my sincere thanks.

I express my heartfelt gratitude to the co-supervisor ***Professor Boumezbeur Abderrahmane*** from Laarbi Ben Mehidi University (Oum El Bouaghi) for the trust he has placed in me by co-supervising my PhD thesis, for his commitment, availability and advice.

I would like to thank ***Prof. Boubaya Djemal***, Professor at the University of Tebessa, who did me the honour of presiding over my jury.

My sincere thanks to ***Prof. Hadji Rihab***, Professor at the University of Setif 1 ***Prof. Ghrieb Lassad*** Professor at the University of Guelma, and ***Pr. Baali Fethi*** Professor at the University of Tebessa who did me the honor of agreeing to review this work.

My thanks also go to all my teachers in the Department of Earth Sciences and the Universe of the University of Tebessa, who shared their scientific

experiences with me and for the valuable lessons and advice they gave me during my study trip.

I do not forget to thank *Hassane Hamaidia*, responsible for the geology laboratory of the University of Laarbi Tebessi (Tebessa), who made it easier for me to carry out my tests in the laboratories.

In particular, I would like to thank *Prof. Kamil Kayabili*, Professor at Ankara University (Turkish), for his availability, advice, encouragement and documentation.

I also thank all the staff of the Directorate of Water Resources – Souk-Ahras for their warm welcome and for facilitating my work in every possible way.

Many thanks also to the staff of the central library and our faculty library.

I will not be able to end these thanks without including my family, my parents, my brothers and sisters, and so many others without whose support I would not have been able to complete this degree.

I would like to thank everyone who, with their help and encouragement, made this work possible.

Dedication

I have the honor to dedicate this humble work to *my parents*. I can never thank them enough, may God bless them.

To my dear brothers;

To my dear sisters and their children;

To all my friends and colleagues;

To everyone who helped me to complete this work.

Ibtissam ✍

Abstract

In the Souk Ahras area of northeastern Algeria, shallow landslides typically happen after heavy rain. To investigate these landslides and the circumstances surrounding their occurrence, three sectors—Zaarouria, Hammam Tassa, and Mechroha—were selected. They have been seen to predominantly impact the transportation system, major supply locations, and agricultural land. The purpose of this research is to determine how soil characteristics, geology, and geomorphology relate to precipitation. A number of field excursions to the research locations were planned, and while there, landslide masses were characterized, mapped, and some field measurements, such as sampling and determining the natural moisture content, were made. We measure the density, Atterberg limits, reinforcement size distribution, effective cohesion, and internal friction in the lab. The hydraulic function and the soil water characteristic curve (SWCC) of unsaturated soil were then calculated. GeoStudio 2020 software was used to do the stability calculation, which is a coupled study where Seep/W mimics infiltration and Slope/W the safety factor. According to the findings, the studied sector contains clay sands with gravel (SC), well-graded sands with silt and gravel (SW-SM), and silt sands (SM), with hydraulic conductivity ranging from $4.5 \cdot 10^{-6}$ to $4 \cdot 10^{-5}$ and 10^{-3} m/s. The safety factor ranges from 0.8 to 1.16 and back to 0.8. In conclusion, our research supports field findings that a number of shallow landslides occurred in March 2019 when rainfall totaled 110 mm. Additionally, the safety factor progressively declines in the two other less permeable soils, Zaarouria and Hammam Tassa, whereas the high permeability soils in Mechrouha exhibit a bigger reduction at the 100 mm rainfall level.

Keywords: Unsaturated Soil, Shallow Landslide, Rainfall, Seep/w-Slope/w, Souk Ahras.

Résumé

Les glissements de terrain peu profonds dans la région de Souk Ahras, dans le nord-est de l'Algérie, se produisent généralement après des précipitations prolongées. Trois sites, Zaarouria, Hammam Tassa et Mechroha ont été choisis pour étudier ces glissements de terrain et les conditions de leur occurrence. On a observé qu'elles affectent principalement les terres agricoles, les principales zones d'approvisionnement et le réseau routier. Le but de ce travail est de découvrir la relation entre les précipitations, les propriétés du sol, la géologie et la géomorphologie. Plusieurs visites sur le terrain dans les zones d'étude ont été organisées, au cours desquelles les masses de glissements de terrain ont été décrites et cartographiées et certaines mesures sur le terrain ont été effectuées, telles que la teneur en humidité naturelle et l'échantillonnage. En laboratoire, nous déterminons la distribution de la taille des armatures, les limites d'Atterberg, la densité ainsi que la cohésion effective et le frottement interne. Nous avons ensuite déterminé les propriétés non saturées du sol, comme la courbe des caractéristiques de l'eau du sol (SWCC) et la fonction hydraulique. Le calcul de stabilité a été effectué à l'aide du logiciel GeoStudio 2020, une analyse couplée où Seep/W simule l'infiltration et Slope/W le facteur de sécurité. Les résultats indiquent que l'étude sectorielle comprend les sables limoneux (SM), les sables bien nivelés avec du limon et du gravier (SW-SM) et les sables argileux avec du gravier (SC), tandis que la conductivité hydraulique varie de $4.5 \cdot 10^{-6}$, $4 \cdot 10^{-5}$ and 10^{-3} m/s.. Le facteur de sécurité varie entre 0.8, 1.16 et 0.8. En résumé, notre étude confirme les observations sur le terrain, car il y a eu de nombreux glissements de terrain peu profonds en mars 2019 lorsque les précipitations ont atteint 110 mm. En outre, les sols à haute perméabilité à Mechrouha présentent une diminution plus importante du facteur de sécurité lorsqu'ils atteignent le niveau de pluie de 100 mm, tandis qu'ils diminuent progressivement dans les deux autres sols moins perméables à Zaarouria et Hammam Tassa.

Mots-clés : Sol non saturé, Glissement de terrain superficiel, Précipitations, Seep/w-Slope/w, Souk Ahras.

ملخص

عادة ما تحدث الانهيارات الأرضية الضحلة في منطقة سوق أهراس في شمال شرق الجزائر بعد هطول الأمطار لفترات طويلة. اختيرت ثلاثة مواقع هي الزعرورية وحمام تاسا ومشروحة لدراسة هذه الانهيارات الأرضية وظروف حدوثها. لوحظ أنها تؤثر بشكل أساسي على الأراضي الزراعية ومناطق الإمداد الرئيسية وشبكة الطرق. الهدف من هذا العمل هو معرفة العلاقة بين هطول الأمطار وخصائص التربة والجيولوجيا والجيومورفولوجيا. تم تنظيم العديد من الرحلات الميدانية إلى مناطق الدراسة، حيث تم وصف كتل الانهيارات الأرضية ورسم خرائط لها وتم إجراء بعض القياسات الميدانية مثل محتوى الرطوبة الطبيعية وأخذ العينات. في المختبر، نحدد توزيع حجم التعزيز، وحدود Atterberg، والكثافة بالإضافة إلى التماسك الفعال والاحتكاك الداخلي. ثم حددنا وظائف خاصية التربة غير المشبعة مثل منحني ماء التربة (SWCC) والوظيفة الهيدروليكية. تم إجراء حساب الثبات باستخدام برنامج GeoStudio 2020، وهو تحليل مقترن حيث يحاكي Seep/W التسلسل و Slope/W عامل الأمان. تشير النتائج إلى أن دراسة القطاع تشمل: رمال الطمي (SM)، والرمال المصنفة جيداً مع الطمي والحصى (SW-SM) والرمال الطينية مع الحصى (SC)، بينما تتراوح الموصلية الهيدروليكية من $4.5 \cdot 10^{-6}$ و $4 \cdot 10^{-5}$ و 10^{-3} م/ث. يتراوح عامل الأمان بين 0.8 و 1.16 و 0.8. باختصار، تؤكد دراستنا الملاحظات الميدانية حيث كان هناك العديد من الانهيارات الأرضية الضحلة في مارس 2019 عندما وصل هطول الأمطار إلى 110 ملم. بالإضافة إلى ذلك، تظهر التربة ذات النفاذية العالية في المشروحة انخفاضاً أكبر في عامل الأمان عند الوصول إلى مستوى هطول الأمطار 100 ملم، بينما تتخفف تدريجياً في الترتيبين الأخيرين الأقل نفاذية في الزعرورية وحمام تاسا.

الكلمات المفتاحية: التربة غير المشبعة، الانهيار الأرضي الضحل، هطول الأمطار، المنحدر/ث - التسرب/ث، سوق أهراس

TABLE OF CONTENTS

General Introduction	1
CHAPTER I: Overview on Shallow Landslide and Slope Instability Model	
1. Introduction.....	5
2. Landslides classification	5
3- Shallow landslides and slope stability mechanisms.....	6
4- Debris flow and shallow landslides	7
5- Data needed for landslide modeling.....	7
6- Hazard evaluation and assessment.....	9
6.1 Spatial prediction	10
6.2 Temporal prediction.....	10
7 Slope stability models	11
8 Development of shallow landslides	12
8.1- Failure criterion, effective tension and interstitial water pressures	12
8.2- Apparent cohesion in unsaturated soils	13
9. Infinite slope model for stability analysis	15
10. Slope stability models for shallow landslides	17
11. Rainfall triggered shallow landslides (Iverson’s model).....	19
12. Hydrological processes	19
13. Slope stability analysis software	21
14. Conclusion.....	22
CHAPTER II: Presentation of The Souk Ahras Region	
1. Introduction:.....	24
2. The study area:	24
3. Socioeconomic context	25
4. Plant cover	26
5. The seismic context.....	27
6. Geological setting	28
6.1. The internal domain:.....	29
6.2. The Flysch domain :	29
6.3. The external domain:	30
7. The structural setting of Souk Ahras region.....	30

8. Litho-stratigraphy According to this litho-stratigraphic assemblage covering the study area:	31
8.1. Allochthonous units	31
8.2- Atlas para autochthonous and autochthonous units	32
8.2.1. The Paleozoic:	32
8.2.2- The Mesozoic:	32
8.2.3- The Cenozoic.....	33
8.2.4- Quaternary.....	34
9. Tectonic setting	38
10. Conclusion.....	39
CHAPTER III: Climatology	
1. Introduction.....	40
2. The climatic evolution of northern Algeria.....	40
3. Climatological characteristics of the study area	41
4. Analysis of climatic factors.....	42
4.1- Rainfall:	42
4.1.1. Seasonal variations in precipitation:	43
4.2- Temperature	44
4.2.1. Seasonal variations in temperature.....	45
4.3- Temperature-Precipitation Relationship (Umbro-Thermal Diagram)	46
5. Determination of climatic indices	47
5.1- Emberger climagram	47
5.2- Soil moisture.....	49
5.3- Water balance.....	51
5.4- Evapotranspiration.....	51
5.4.1. Actual evapotranspiration ETR.....	52
5.4.2. Potential evapotranspiration ETP.....	52
5.5- Runoff.....	53
5.6- Water infiltration calculation	54
6. Comments on the water balance	55
7. Conclusion	57
CHAPTER IV: Historical Development of Unsaturated Soil Mechanic	
1. Introduction.....	58
2. Historic of soil mechanics.....	58
3. The effective stress.....	59
4. Development of unsaturated soil mechanics.....	60

4.1. Definition:.....	60
4.2- Matric suction:.....	61
4.3- Solute (or osmotic) suction:.....	61
5. What Is an Unsaturated Soil?.....	63
6. Typical profiles of unsaturated soils	64
7. Unsaturated soil properties determination	65
8. Soil physical properties.....	67
8.1- Grain-size distribution curve	67
8.2- Atterberg Limits.....	70
8.3- The shrinkage limit.....	71
9. Unsaturated soil phase properties	71
9.1- The contractile skin	72
9.2- Solid phase.....	72
9.3- Water phase.....	73
9.4- Air Phase.....	75
9.5- Interaction of Air and Water	76
9.6- Surface tension	76
10. Volume-mass relations	78
10.1- Volume Relationship.....	78
11. Water content relationships	80
11.1- Volume-Mass Relations	81
12. Basic Volume-Mass Relationship.....	83
13. Shear strength of unsaturated soils.....	83
14. Effective stress equations	86
14.1- Stress State Variables for Unsaturated Soils.....	87
14.2- Stress state variables	87
15. Equations for Mohr circle.....	87
15.1- Construction of Mohr circles for unsaturated soils	91
16. Hydraulic properties	93
17. Flow of water in unsaturated soils.....	93
18. Factors affecting unsaturated hydraulic conductivity	94
19. Conclusion.....	95
CHAPTER V: Inventory of Shallow Landslides and Soil Characterization of The area Study.....	

1. Introduction.....	96
2. Methodology.....	96
3. Landslide inventory	98
4. Landslide material characterization	99
5. Laboratory and field tests.....	100
5.1- Atterberg Limits.....	101
5.2- Grain size distribution	101
5.3- Soil water characteristic curve.....	101
6. Landslide analysis	102
CHAPTER VI: Numerical Simulation, Results and Discussion.....	
1. Introduction.....	106
2. Interpretation of map's inventory	106
2.1- Land use and cover	107
2.2- Slope inclination map	108
2.3- Slope aspect ratio map.....	109
2.4- Elevation map	110
3. Laboratory and field data analysis	111
4. Rainfall and landslide	113
5. Numerical analyses	115
6. Conclusion	119
GENERAL CONCLUSION AND RECOMMENDATIONS.....	121
Reference	124
Annexes.....	135

LIST OF FIGURES

Figure (I)	Rainfall-induced slope instability mechanism (Rahardjo et al., 2019).	2
Figure (I.1)	Infinite slope model for unsaturated soil in a slope(Shaojie Zhang et al 2016).	15
Figure (I.2)	Vector components of gravity and position of groundwater table.	16
Figure (I.3)	Bingham model on infinite slope (from Iverson et al. 1997).	17
Figure (I.4)	Takahashi model on an infinite slope (from Iverson et al. 1997).	18
Figure (II.1)	Geographical location of the study area.	25
Figure (II.2)	The main railway line and road map of the study area	26
Figure (II.3)	NDVI map of study area.	27
Figure (II.4)	Seismicity in northern Algeria from the CRAAG database.	28
Figure (II.5)	The major structural domains and tectonic map of northern Algeria (Abdelkarim Yelles, et al. 2022).	29
Figure (II.6)	Geological map of the study area.	35
Figure (II.7)	Compilation of geological maps (1/50.000).	36
Figure (II.8)	Geological section in the study area (Hadji et al. 2012).	37
Figure (II.9)	Fault map of the study area.	38
Figure (III.1)	Mean annual and winter climate changes, precipitation projected for the Mediterranean basin between 2040 and 2070 compared to 1960-1990 by nine general circulation models.(García-Ruiz et al., 2011)	42
Figure (III.2)	Map showing the average annual rainfall in Eastern Algeria .	43
Figure (III.3)	Variation in average monthly rainfall in the study region.	44
Figure (III.4)	Variation of seasonal rainfall in the study area.	45
Figure (III.5)	Variation in average annual precipitation (2000-2019).	45
Figure III.6	Variation of monthly average temperatures (2000-2019).	46
Figure (III.7)	Variation in seasonal mean temperatures (2000-2019).	47
Figure (III.8)	Variation in average annual temperature (2000-2019).	47
Figure (III.9)	Rainfall-thermal diagram of the study area.	48
Figure (III.10)	Representation of the climate of the study area on the Emberger climagram	49

Figure (III.11)	Representation of the study area on the Martone Aridity Index abacus (1923). (HR).	50
Figure (III.12)	Variation of monthly average soil moisture (mm) (2000-2019).	51
Figure (III.13)	Variation in monthly average relative soil moisture (%) (2000-2019).	52
Figure (III.14)	Variation of monthly average runoff (mm) (2000-2019).	55
Figure (III.15)	Variation in monthly average relative runoff (%) (2000-2019).	55
Figure (III.16)	Graphic representation of Thorn Thwaite's water balance sheet (Souk Ahras 2000-2019)	57
Figure III.17	Graphic representation of the hydrological balance (Souk Ahras 2000-2019).	58
Figure IV.1	Capillary model of unsaturated soil.	63
Figure IV.2	Subdivision of the unsaturated soil zone (vadose zone) at local and regional level.	65
Figure IV.3	Schematic representation of the typical tropical residual soil profile (Little, 1969).	66
Figure IV.4	Methods for determining unsaturated soil property functions (Fredlund et al 2013).	68
Figure IV.5	Grain size distribution curve data with unimodal fit for clay mud, best fit of grain size distribution data for clay mud (from M.D.Fredlund et al., 2000).	69
Figure IV.6	Gap bottom fit using the unimodal and bimodal grain size distribution equation (M.D. Fredlund et al., 2000).	70
Figure IV.7	Determination of percentage passage for selected particle sizes, (Fredlund et al., 2000).	71
Figure IV.8	Typical desorption SWCC with clear desaturation zones.	72
Figure IV.9	Relationship of Atterberg limits to shrinkage curve for initially highly plastic clay (data points generated).	73
Figure IV.10	Phase diagram for unsaturated soil, it simplifies four phases.	74
Figure IV.11	Element of unsaturated soil with continuous air phase (modified from Fredlund and Rahardjo).	74
Figure IV.12	Density of pure water for different applied pressures and temperatures (from Dorsey, 1940).	77
Figure IV.13	Surface tension phenomenon at air-water interface.	79

Figure IV.14	Relationship between volume and mass of unsaturated soil.	80
Figure IV.15	Relationship between volume-mass properties of unsaturated soil.	84
Figure IV.16	Relationship between volume and mass of unsaturated soil.	85
Figure IV.17	Effective stress parameter v versus degree of saturation (from Zerhouni 1991).	88
Figure IV.18	Stress state variables for unsaturated soil.	89
Figure IV.19	Net normal and shear stresses on inclined plane at point in soil mass below horizontal ground surface.	91
Figure IV.20	Using the Extended Mohr Diagram to represent stress states in unsaturated soils .	92
Figure IV.21	Construction of Mohr circle using net normal stresses	94
Figure IV.22	Illustration demonstration non-uniform wetness and thus, variation in unsaturated hydraulic conductivity k , volumetric water content θ and matric potential ψ_m (after Hillel 1971).	96
Figure (V.1)	Generalized flowchart adopted in the current study	98
Figure (V.2)	Deformation and infiltration phenomena in a near-surface deposit of unsaturated expansive soil.	105
Figure (V.3)	Forces on an element of infinite slope.	106
Figure (VI.1)	The landslide inventory map.	107
Figure (VI.2)	Land use / cover map	108
Figure (VI.3)	Slope inclination map	110
Figure (VI.4)	Slope aspect ratio map	111
Figure (VI.5)	Elevation map	112
Figure (VI.6)	Grain size distribution curves of representative samples from the three studied areas.	114
Figure (VI.7)	Rainfall intensity and cumulative rainfall from GEE for 2019.	115
Figure (VI.8)	The SWCC for soils from the three sectors studies	118
Figure (VI.9)	Soil conductivity and matric suction	118

Figure (VI.10)	The results of safety factor (FOS)	118
Figure (VI.11)	Numerical slope model in coupled of seep/w –slop/w of the Geoslope Software (2020).	119

LIST OF PHOTO

Photo (V.1)	Shallow landslide in the study area (Hammam Tassa and Zaarouria).	100
Photo (V.2)	Photos of shallow landslides from the three studied areas.	101

LIST OF TABLE

Table I.1	Landslides classification of Varnes	06
Table III.1	Monthly averages of precipitation in the study area, (period: 2000-2019).	44
Table III.2	Monthly average temperatures of Souk Ahras (period 2000-2019).	46
Table III.3	Martonne classification of climate type, according to the values of "I"	50
Table III.4	Monthly averages of soil moisture in the study area, (period: 2000-2019).	51
Table III.5	Monthly averages of Runoff in the study area, (period: 2000-2019).	54
Table III.6	Showing the water balance of Souk Ahras region.	56
Table IV.1	The search for a description of effective stress in an unsaturated soil.	64
Table IV.2	Specific Gravity of Several Mineral..	75
Table IV.4	Composition of Dry Air	76
Table IV.5	Shear strength equations for unsaturated soils.	77
Table IV.6	Equivalent X for shear strength equations listed in Table 5	87
Table IV.1	Summary of the laboratory test results	88
Table IV.3	Shows more accurate water densities over a temperature range.	113
Table VI.2	Table showing the rainfall data from GEE for 2019.	115

General

Introduction

GENERAL INTRODUCTION

Introduction

Landslides are among the main geo-hazards phenomena that constitute a serious threat to man and its environment. They are the most effective cause of the earth's surface landscape shaping (Eckle 1958). A landslide is defined as "the movement of a mass of rock, debris, or earth down a slope" (Cruden, 1991). They occur in mountains and hilly areas in many regions of the world and are an important means of mass wasting and material removal from the highlands to the valleys (Lu and Godt 2013).

Landslides can move slowly (millimeters per year) or fast and catastrophically, as is the case with shallow landslides. The term shallow landslide is used to describe movements that displace material over a discrete area of sliding near the land surface. Shallow landslides are particularly important with regard to natural hazards, as they often result in fast-flowing debris flows (Iverson et al., 1997). Shallow landslides can be triggered by a variety of factors, either natural or caused by human activity. Among the natural factors, precipitation and the resulting water infiltration is certainly one of the most common causes of the occurrence of landslides. Landslides caused by precipitation occur mainly in tropical and subtropical regions and are the result of a change in groundwater conditions, especially in the unsaturated zone.

Landslides in Algeria, similar to many countries of the world, have caused significant damage and casualties, especially in recent years. Landslides are a ubiquitous natural phenomenon in northeastern Algeria especially on the steep slopes of the Tellian Atlas mountain ranges (hadji.R).

In Souk Ahras region, as in the rest of the Tellian Atlas, shallow landslides affect almost virtually all natural slopes and particularly areas with little or no vegetation cover. Several road cuts are effected by landslides every rainy year and affects agroforestry production in general (Jones et al., 2008). The latter will reappear, despite stabilization works, when the climatic conditions that first triggered them return (Mehdadi, F,).

Landslide activity, in the Souk Ahras region, has been extensively studied either individually for a specific project (PhD, Magester, Masters etc.) or for general purposes (LTPE) to assess slope stability. Many studies have confirmed the occurrence of landslides, which usually occur after every heavy rain.

GENERAL INTRODUCTION

In regions like Souk Ahras, many researchers have been advanced to explain the cause of this type failure. Some recent studies state that this approach implies that landslides occur due to excessive pore water pressure, independent of rain infiltration (Reid et al., 1997) or groundwater exfiltration due to rain (Montgomery et al., 1997). On the other hand, several studies (Morgenstern and de Matos, 1975; Lu and Likos, 2004; Rahardjo et al., 2007 and Godt et al., 2009) show failures occur as a consequence of suction changes due to infiltration/exfiltration saturation pressure and Ng and Shi (1998) and Rahardjo et al. (2007) proved this numerically.

Because of this approach, many slopes, particularly in the drier/more unsaturated regions of the world, experience negative pore water pressures relative to atmospheric pressure (i.e. suction). The suction (or negative pore water pressure) contributes to increasing the shear strength of the soil and keeping the slope stable. As rain seeps in, the suction effect is reduced, leading to a reduction in strength that can trigger failure (Toll et al., 2011). The slope's safety factor (F.S.) decreases as soil suction (and hence shear strength) decreases. Fig. 1 shows a schematic representation of this process for soil slope that is initially dry where the groundwater table is at a considerable depth. When the water starts to seep into the soil the pore water pressure increases inducing a reduction in the shear strength which leads to slope failure.

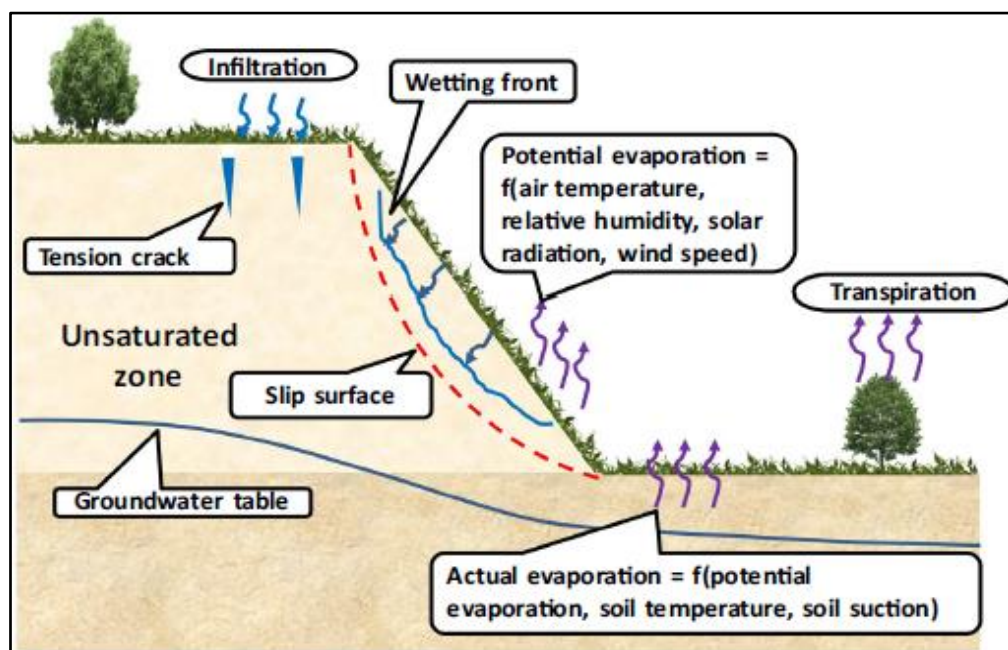


Figure .1: Rainfall-induced slope instability mechanism (Rahardjo et al., 2019).

GENERAL INTRODUCTION

For this work, only rain-triggered landslides were studied, excluding all other minor initiating factors such as earthquakes, rapid snowmelt, erosion ...etc. It is important to distinguish between saturated and unsaturated soils as they behave differently in terms of shear strength. In saturated soils, according to the laws of active stress during infiltration, the shear strength decreases with increasing pore pressure. In unsaturated soils, the additional strength given by the matric suction effect must be taken into account instead (Fredlund & Rahardjo, 1993).

The objective this thesis is to examine these shallow landslides. We adopted a model that accounts for the change in stability state of unsaturated soils on slopes due to sudden changes in their water content. We applied a coupled stability analysis model to an established geological model established using inventory maps and factor maps such as slope maps, elevation maps, geological maps, etc., which made the work easier and more accurate. The stability analysis is carried out using Seep/w-Slop/w software and considered different precipitation scenarios. The analysis results are then compared to the established landslide susceptibility maps.

The objective of the thesis is achieved following the steps bellow:

Chapter I: Describes the background to the classification of landslides and the initiating factors of landslides. It also describes the data needed for landslide modeling and the different approaches to assessing landslide risk. Contains general knowledge about the trigger mechanisms of shallow landslides and a summary of the most important existing slope stability models.

Chapter II: Describes the study area in its general context. It seemed useful to provide an overview of the geology of the region, attempting to identify the key lithological and tectonic features related to the geological history of the region, as well as the seismic context of the region, cover plant and socio-economic context.

Chapters III: The third chapter was dedicated to the climatology of the region. The homogenization of the climate data has enabled the spatialization of the interannual precipitation and temperature averages (2000-2019). We also determined the climate index to create a water balance. This knowledge is fundamental to a rational approach to hazard and landslide risk assessment.

Chapter IV: Brief history of soil mechanics and general knowledge of modern soil mechanics and various mechanisms of unsaturated soils.

GENERAL INTRODUCTION

Chapter V: Describes the methodology of the area study and its application in the different steps: inventory map, field test, laboratory tests and numerical simulation.

Chapter VI: In the last chapter we presented the results of the field and laboratory work and how they can be applied to the seep/w-slope/ coupling. By compiling these results, the data will be used to address the issue of assessing and mapping the hazard, hazard and landslide risk in the study area.

The thesis ends with a conclusion where the essential of the results are presented and where recommendations for further work are suggested.

CHAPTER I: Overview
on Shallow Landslide
and Slope Instability
Model

1. Introduction

Landslides are natural hazards where masses of rock/earth slide down a slope due to gravity. It is a natural phenomenon caused by a number of geological, atmospheric and anthropogenic factors. Both natural conditions and human activities play critical roles in preparing and initiating landslides. Every year, landslide phenomena occur in many places in and around the city of Souk Ahras, especially in hilly areas and open land, posing challenges to researchers, engineers and planners. Landslides, which damage the country's wealth and human resources, are one of the main obstacles to development in the areas affected by these phenomena. They are among the external geodynamic phenomena that contribute to the formation of landslides, but received serious attention only in the late 20th century. An International Decade (1990–2000) for the Reduction of Natural Disasters was launched by UNESCO to map landslides worldwide (International Geotechnical Societies 1993).

2. Landslides classification

The most widely used classification of slope motion was proposed by Varnes in 1978 in Table (01). This classification is primarily based on the type of movement, but also takes into account the type of material. Five basic types of movement are considered: falls, tumbles, slides (rotation and translation), lateral spread, and flow. A sixth type, complex motion, is defined as a combination of two or more basic motion types. The material in question is divided into two classes: rocks and earths. The latter are divided into two further classes: predominantly fine soils and predominantly coarse soils (Varnes, 1978). Varnes (1978) proposes a classification based on movement type and material type.

Table I.1: Landslides classification of Varnes

<i>Type of Movement</i>			<i>Type of Material</i>		
			Bedrock	Engineering Soils	
				Predominantly Coarse	Predominantly Fine
Falls			Rock Fall	Debris Fall	Earth Fall
Topples			Rock Topple	Debris Topple	Earth Topple
Slides	Rotational	Few Units	Rock Slump	Debris Slump	Earth Slump
	Translational		Rock Block Slide	Debris Block Slide	Earth Block Slide
			Many Units	Rock Slide	Debris Slide
Lateral Spreads			Rock Spread	Debris Spread	Earth Spread
Flows			Rock Flow (Deep Creep)	Debris Flow (Soil Creep)	Earth Flow
Complex – Combination of Two or More Principal Types of Movement					

Examination of the terrain during the compilation of the landslide inventory led us to conclude that most of the landslides in the Souk Ahras area are shallow in nature.

3- Shallow landslides and slope stability mechanisms

Landslide processes are the downward movement of soil or rock under the influence of gravity (USGS, 2004). Shallow landslides (SLs) are a subset of these processes, usually involving soil masses less than 2 m thick (Phillips et al., 2021), which generally occur at or near discontinuities in the soil profile or near of discontinuities along the fracture surface occur in the contact between soil profile and bedrock. This definition includes mass movements along natural and man-made embankments or stockpiles, as well as deep creep movements in rock faces. SLs are of interest for several areas of study related to soil science (Tofani et al., 2017). Landslide classification is quite difficult as the phenomena are not perfectly repeatable, making it impossible to develop a taxonomic classification. (Leonis, 2008)

In general, slope stability is defined as the state of equilibrium of the soil mass that can resist the downward movement of gravity and is maintained despite changes in hydrological and mechanical conditions (e.g. increased soil weight due to storm water infiltration). Loss of stability describes the situation where the state of equilibrium has failed and favors shallow landslides. Furthermore, the definition of slope stability acquires different meanings

depending on the study area and the main goals of the users (McColl, 2015). In general, it takes into account:

- i) The predisposition (preparatory) factors that setup the conditions for the slope to become instable;
- ii) The triggering factors (e.g. precipitation) which are the primary cause that break the state of equilibrium in favor of instability;
- iii) The sudden changes in soil properties (Dias et al., 2017)

Landslides are therefore usually characterized by different morphologies, types of movement, triggering factors and genetically different material. For this reason, landslides are classified according to various distinguishing features, such as the type of movement or the type of material involved.

4- Debris flow and shallow landslides

One of the main goals of this thesis is to study the initiation of shallow landslides by heavy rainfall. As mentioned above, a shallow landslide can be described as a slope movement of limited extent that develops mainly in the upper part of the ground down to a depth of a few meters. Debris flows are among the most dangerous landslides that can be described as shallow landslides. The dangerousness of these phenomena is possibly related to the high speed they can reach while running and even the almost complete lack of warning signals. In addition, debris flows of different origins can combine in gorges and greatly increase their destructive power. Debris flows, usually associated with heavy rain, are triggered suddenly and can reach runoff speeds of up to 20 m/s (Hungr et al., 2001). Due to these high speeds, they have a large kinetic energy and are therefore dangerous for buildings and infrastructure.

5- Data needed for landslide modeling

Many types of data are required for landslide modeling and risk assessment. Some methods rely on the study of past landslide events to derive an association between the events and the factors driving landslide formation and development. This relationship, which can be reduced to a deterministic or statistical equation, can be used to predict the future distribution of landslides based on current conditions and the behavior of the driving factors. Therefore, for models that use past events to calibrate a threshold or to derive an equation, it is very important to have a comprehensive and up-to-date knowledge of historical landslides that

have occurred in the studied area. This record of landslides, if it includes the date and time of occurrence, can even be very useful to validate the results of physically based models.

For methods based on the physical simulation of landslides, the most important data are the topographic and physical properties of the terrain. These models, also called physically based models, use topographical and geotechnical properties to simulate water intrusion into the soil and calculate slope stability from a geometrically simplified representation of the slope. Obviously, in distributed models, all input data must be distributed. For each cell or pixel where slope stability is calculated, the value of each input data set is required (cell-by-cell calculation).

- **Topographic data**

Gravity is the main reason that makes a slope unstable and greatly affects the final slope stability calculation. The most important topographic data are therefore the angle of inclination. In order to obtain a distributed map of the angle of inclination, a digital elevation model (DEM) must be derived. These tools are based on different algorithms, but all calculate the rate of maximum change in z-score from each cell to its neighbors. The maximum change in elevation over distance between each cell and its neighbors identifies the steepest descent. Other minor DEM-derived topographical features that may play a role in slope stability are slope orientation, length, and curvature.

- **Geological and geotechnical data**

Naturally, the parameters of the physical behavior of a soil play a central role in physically based slope stability modelling. In particular, geotechnical data such as cohesion, internal friction angle and soil weight significantly influence the stability balance between shear strength and destabilizing forces. It is very important to have a robust set of geotechnical data to describe the spatial variations in soil properties as well as possible. In fact, these fluctuations are quite abrupt and difficult to capture in detail. It is quite common in distributed models to extend the value of a given soil property to an entire area expected to have similar properties (Iverson, 2000; Wu & Sidle, 1995; Baum et al., 2005; Salciarini et al., 2006). ; Crosta & Frattini, 2003). For example, if a detailed geological map is available, it is possible to assign an average value of a particular soil property to each cell in the same geological or lithologic formation.

- **Rainfall data**

A slope can become unstable when the water table rises due to intruding rain as pore water pressure increases and shear strength decreases. The total amount and intensity of precipitation is therefore very important as it is the main trigger for shallow landslides. All other data such as slope and cohesion help define the spatial distribution of shallow landslides as they can determine how easily a slope can become unstable, which is very useful for assessing shallow landslide susceptibility. Instead, precipitation data is the basic input parameter that allows the system to overcome the threshold and trigger a new slope movement. When calculating slope stability for a large area or basin, an accurate distributed representation of precipitation intensity is very important. A storm is often characterized by high spatial and temporal variability, making it quite difficult to obtain a high-quality representation of the precipitation event. One of the more competent tools for obtaining a distributed precipitation map is data collected from satellites and radar. With the help of this tool it is possible to significantly improve a simulation and explain the usual non-uniform distribution of landslides (Crosta & Frattini, 2003).

6- Hazard evaluation and assessment

The landslide hazard for a given area is defined as the probability of a destructive event of a given intensity occurring over a defined period of time (Varnes, 1984). It is very important for risk assessment to distinguish between predisposing factors, the characteristics of a slope that make it vulnerable to instability and the factors that can lead to release. The group of predisposing factors includes all geological, structural, geomorphological and hydrological features such as soil conditions, slope inclination, soil depth and any faults that may be present. This set of features represents the quasi-static variables of slope stability equilibrium (Wu & Sidle, 1995) as they do not show significant changes over time.

The predisposing factors have a major impact on the spatial distribution of landslides and on risk assessment. Initiating factors, on the other hand, are those that alter the natural balance and dynamically change over time, resulting in the initiation of a landslide. Rain events, earthquakes, and volcanic eruptions can be included in the category of these dynamic variables. The dynamic variables are of great importance for the temporal prediction of landslides. Analysis of the predisposing factors is therefore useful to spatially predict hazards and slip susceptibility, while the precipitating factors are also useful to predict them over time.

6.1- Spatial prediction

Spatial hazard prediction is the estimation of the relative stability of a particular slope compared to another. It represents the spatial probability of a landslide occurrence in different zones of a given area or basin. Two main approaches to spatial prediction of landslide hazards can be distinguished:

- ✓ A qualitative approach that provides a descriptive and qualitative assessment of the hazard.
- ✓ A quantitative approach that provides a numerical estimate (in terms of probability of occurrence or safety factor) of the spatial hazard.

The first group includes methods based on an empirical assessment of instability susceptibility based on geomorphological knowledge, as described by Kienholz (1978), Brundsen et al. described. described. (1975) or Humbert (1977). Other quantitative approaches to hazard assessment are to assign a weight to each factor responsible for slope instability and rank them to obtain an index of landslide susceptibility. This ranking of factors can be subjective when the weights are set a priori (Gee, 1992; Anbalagan & Singh, 1996; Pareschi et al., 2002) or objective when it is possible to quantify the relative importance of each factor (Brabb, 1984). ; Lee et al., 2002). Other proposed methods for assessing landslide vulnerability are based on bivariate or multivariate statistical analysis (Yin & Yan, 1988; Bonham-Carter et al., 1989; Baeza & Corominas, 2001) and on stochastic hydrological simulations (Hammond et al., 1992). . . or on neural network analysis (Lee et al., 2003, 2004; Ermini et al., 2005) to determine the failure probability of a slope.

The quantitative approach is used by physically based models. These models can provide a probabilistic result (probability of failure) or a deterministic result (safety factor) and use physical laws to describe the formation and propagation of landslides (Crosta & Frattini, 2003; Dhakal & Sidle, 2004; Dietrich et al., 1995 ; Wu & Sidle, 1995; Iverson, 2000). The main advantage of using physically based models is that they can account for the dynamic variables of the system and control long-term and short-term behavior. However, in order to achieve these results, a detailed characterization of the soil is required as input data. However, this is not always possible, especially when data is sparse or not representative of the entire area.

6.2- Temporal prediction

The temporal forecast should give the probability of landslide occurrence as an absolute hazard value (H), which could be expressed as:

$$H(N) = 1 - (1 - P)^N$$

Where: P is the probability that an event will occur over a period of N years.

Typical approaches to predicting the risk of landslides over time are (Canuti & Casagli, 1996):

- ✓ Analysis of time series associated with landslide impacts to obtain return periods directly.
- ✓ Analysis of time series related to the causes of landslides. With this approach, the return periods are calculated using the time series of natural hazards such as rain and earthquakes, which are identified as initiating factors.
- ✓ Use of in situ or remote monitoring systems.

The first approach is useful for studying single recurring phenomena or localized areas where landslide occurrence is fairly uniform and homogeneous.

Unfortunately, this approach has to be applied to a fairly long and statistically significant time series of landslides. For this reason it is not useful for large areas where it is quite difficult to obtain a homogeneous and densely populated landslide database.

For large areas, it is better to use the time series of causes of landslides. In this case, it is necessary to collect and analyze historical data on the initiating factors such as precipitation, earthquakes, erosion and human activities. The most important factor, especially in shallow landslides, is precipitation, while earthquakes only need to be considered in seismic areas. Erosion can be important on river banks and escarpments. Instead, anthropogenic activity is not related to hazard prediction but to prevention and needs to be considered in urban planning and risk assessment (Leoni, 2008).

7. Slope stability models

In recent years, many physically based models for spatially distributed assessment of shallow landslide hazard have been proposed in the literature (Montgomery & Dietrich, 1994; Hsu, 1994; Wu & Sidle, 1995; Borga et al., 1998; Burton & Bathurst, 1998; Cho & Lee, 2001; Baum et al., 2002; Casadei et al., 2003; Crosta & Frattini, 2003; Montrasio & Valentino, 2003; Frattini et al., 2004; Tsai et al., 2007; Simoni et al., 2008). These models are usually based on the coupling of a hydrological model and a slope stability model such as the Infinite-Slope model.

The applicability of these models depends on many factors such as the knowledge of the study area, the availability of soil properties data and topography. As far as slope stability is

concerned, during the rainfall event, the hydrological part of the model calculates the groundwater pressure distribution. These pressures are then used in the slope stability model to obtain a probability of failure (Simoni et al., 2008; Schmidt et al., 2008) or a factor of safety (Iverson, 2000; Crosta & Frattini, 2003).

8. Development of shallow landslides

A soil mass can become unstable and eventually flow in two ways: by Coulomb failure within the soil or bedrock along a steep slope, or by liquefaction of the soil mass due to high interstitial water pressure (Iverson et al., 1997). These behaviors may occur independently, but in many cases they appear to act simultaneously and synergistically. Physically-based models, created as a coupling of a hydrological model and a slope stability model, can account for these two conditions and derive how a variation in the water pressure distribution can affect the transition between Coulomb failure and liquefaction.

Understanding where and when a shoal occurs In order for a landslide to be triggered, not only is sufficient knowledge of the area in terms of morphology and soil composition required, but also knowledge of the physical and mechanical processes that can lead to slope instabilities. All proposed models are based on physical laws and some rational approximations to develop a theoretical model intended to represent the geomechanical changes in slope during infiltration.

8.1- Failure criterion, effective tension and interstitial water pressures

In order to provide a framework for evaluating shallow landslide initiation, it is necessary to introduce some principles of soil mechanics and grain flow mechanics.

$$\tau = \sigma' \tan \phi + c' \dots\dots\dots 01$$

where τ is the shear stress acting on the surface, σ' is the effective normal stress (by convention, normal stress is positive in compression), ϕ is the internal angle of friction of the material, and c' is the effective cohesion.

The angle of internal friction is comes the internal friction between soil clasts and their interlocking. The product $\sigma' \tan \phi$ represents the frictional component of soil strength. Rather, cohesion is the component of soil shear strength that is independent of interparticle friction. It depends mainly on electrostatic forces and on interclast cementation due to secondary mineralization (Mitchell & Soga, 2005). Even cohesion from secondary causes such as vegetation roots can add some strength to the soil. The contribution of cohesion to overall strength can be small, but becomes important when it exceeds friction strength at shallow depths on steep slopes where random loading is relatively small (Iverson et al., 1997).

The effective stress, σ' Equation 01, is the difference between total normal stress σ (Terzaghi, 1936) and the effects of pore water pressure (u_w), which is:

$$\sigma' = \sigma - u_w \dots \dots \dots 02$$

The state of stress, in a plane containing the principal stresses (σ_1) and (σ_3), can be determined on a diagram constructed using shear stress versus normal stress; this plot is known Mohr circle for stress. A stress state represented any point on the intrinsic curve or the tangent to the Mohr circles is called the ultimate stress state. In this state of stress, failure occurs.

Pore pressures can vary with depth, so it is fundamental to model the spatial distribution of pore pressure $p(x, y, z)$ where x, y, z are spatial coordinates. Groundwater flow is driven by the height distribution $h(x, y, z)$ which is defined as a measure of water pressure per unit weight above a given depth, usually measured in meters of water surface height. The pore pressure distribution depends on the pressure head with this simple equation:

$$p = \gamma_w(h + z) \dots \dots \dots 03$$

Where γ_w is the unit weight of the water and z is a vertically downward space coordinate. The origin of z is fixed here and in the next sections at a point on the ground surface. The Darcian-specific discharge q , which controls groundwater flow, is represented by the following equation:

$$q^{\rightarrow} = K \nabla h \dots \dots \dots 04$$

Where: K is the tensor of the hydraulic conductivity of the soil and ∇h is the gradient of the pressure head.

Equations 01 to 04 show that the knowledge of the pore pressure distribution is absolutely fundamental for evaluating the slope stability.

8.2- Apparent cohesion in unsaturated soils

There are many forces in soil that are not included in the effective stress equation 3 and 1 that can have measurable effects on strength. One of them is the van der Waals forces; attractive or repulsive physico-chemical forces between molecules, which can play an important role, especially in fine-grained soils (Bolt, 1956). Another important force, especially in unsaturated soils, is capillary forces (Bishop, 1959; Mitchell & Soga, 2005). This force is associated with a partially macroscopic increase in shear and tensile strength and must therefore be taken into account when describing the stress state in unsaturated soils. This force is negative by convention and is called matric suction ($u_a - u_w$).

There are different approaches to describe the stress state in unsaturated soils (Lu et al., 2006)

The modified effective stress approach proposed by Bishop (1959) with a modified form of the classic effective stress equation:

$$\sigma' = \sigma - u_a + X(u_a - u_w) \dots \dots \dots 05$$

Where: u_a is the air pore pressure and X is a parameter that varies between zero and 1 depending on the degree of saturation of the pore water. The difference between u_a and u_w represents the matric suction. The classic Mohr-Coulomb criterion for unsaturated soils can then be written as:

$$\tau_f = c' + [(\sigma - u_a) + X(u_a - u_w)] \tan \phi' \dots \dots \dots 06$$

Where: c' is the effective cohesion (the intersection of the expanded Mohr-Coulomb fracture envelope where the net normal stress and matric suction are zero) and ϕ' is the effective angle of internal friction.

The independent stress state variable approach proposed by Fredlund & Rahardjo (1993), where net normal stress and die suction are treated independently within the shear strength equation:

$$\tau_f = c' + (u_a - u_w) \tan \phi' + (u_a - u_w) \tan \phi^b \dots \dots \dots 07$$

Where: the first two terms represent the classical Mohr-Coulomb criterion and the last term uses an additional angle of friction ϕ^b to account for the contribution of die suction to shear strength. The effective cohesion indicates an increase in strength with increasing matric suction. This increase can be defined using the ϕ^b angle as follows:

$$c = c' + (u_a + u_w) \tan \phi^b \dots \dots \dots 08$$

Where: c is the intersection of the overall cohesion measured as the intersection of the extended Mohr-Coulomb fracture envelope with the shear stress axis at a given matric suction.

Many other authors have proposed a different approach in the form of modified stress variables, such as Alonso et al. (1990) who includes the volume expansion by matric suction in the critical state of soil mechanics, or Gallipoli et al. (2003) who introduces a dependency between a stress variable and the degree of saturation and matric suction.

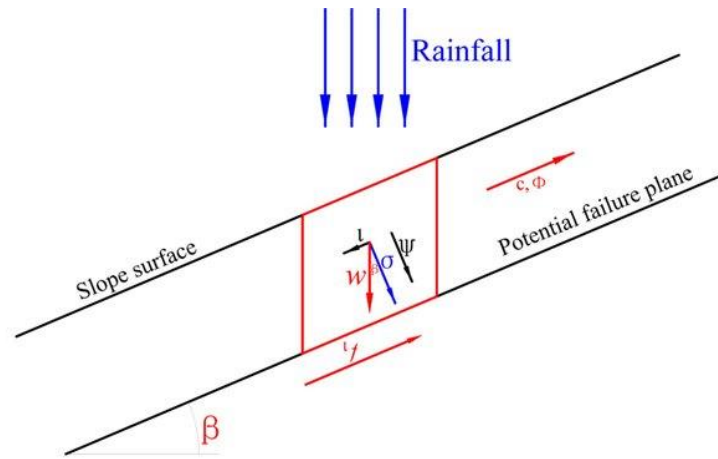


Figure I.1: Infinite slope model for unsaturated soil in a slope(Shaojie Zhang et al 2016).

Equations 05 to 08 show that when computing the stability for unsaturated soils, the increase in strength and cohesion due to matric suction must always be taken into account. Using the simple form of the shear failure equation which is valid only for saturated conditions would result in an underestimated value of the safety factor.

9. Infinite slope model for stability analysis

Many slope stability models have been proposed for different types of simulations and for different types of landslides (Bishop, 1955; Spencer, 1967; Janbu, 1973; Morgenstern & Price, 1965). All these models require a large amount of data in order to be applied successfully. However, if some simplifications are made, it is possible to get a model that is easier to use and requires less input data.

For shallow landslides we can observe that they are usually characterized by an elongated shape and that the influence of the toe and head sections is usually negligible, so they can be represented as a single layer with the sliding surface roughly parallel to the ground surface.

When the landslide is of shallow depth compared to its length and width, as is often the case with shallow landslides, the landslide geometry can be assumed to be simplified, characterized by a flat sliding surface on an infinitely extended flat slope both laterally and distally. This approach is known as the infinite slope (Skempton & DeLory, 1957). It is assumed that the failure is the result of translational slip, that the failure plane and the water table are parallel to the surface of the earth, and that the failure occurs along a single layer of infinite length. The forces acting at a point along the potential failure plane are shown in Figure (02).

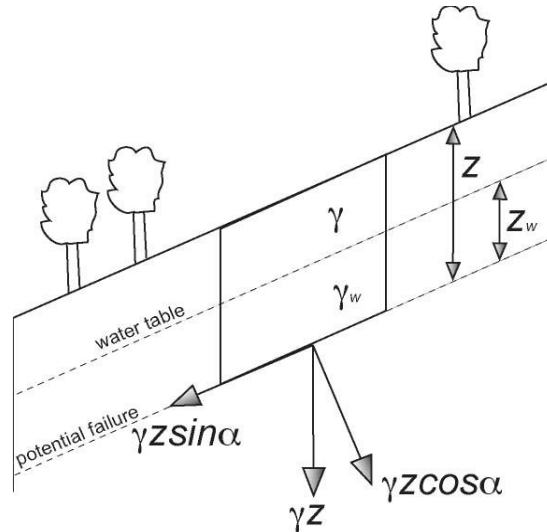


Figure II.2: Vector components of gravity and position of groundwater table.

γ : is the unit weight of soil, γ_w is the unit weight of water, z is the thickness of the slope material above the slip plane, z_w is the water table depth, and α is the angle of repose.

The resistivity of earth materials is the shear strength s described by the Terzaghis equation:

$$s = (\sigma - u_w) \tan \phi + c \dots\dots\dots 09$$

The slope normal component of gravity resisting downward motion is the normal stress σ , which can be written as:

$$\sigma = \gamma z \cos \alpha \cos \alpha \dots\dots\dots 10$$

Where γ the unit weight of the soil is, z is the thickness of the slope material above the slip plane, and α is the slope angle.

The pore fluid pressure, which reduces the resisting forces and shear strength of the material, can be represented as:

$$\mu = \gamma_w m z \cos \alpha \cos \alpha \dots\dots\dots 11$$

Where γ_w is the unit weight of water and m is the vertical height of the water table above the slip plane, expressed as a fraction of the total thickness = z/z_w . The slope-parallel component of gravity is the shear stress τ :

$$\tau = \gamma z \cos \alpha \sin \alpha \dots\dots\dots 12$$

The safety factor (FS) is defined as the ratio between resisting and driving forces (Ritter, 2004) and in the case of the infinite slope model has the form:

$$FS = \frac{\text{Resisting force}}{\text{Driving force}} = \frac{\text{Shear strength (S)}}{\text{Shear stress } (\tau)} \dots\dots\dots 13$$

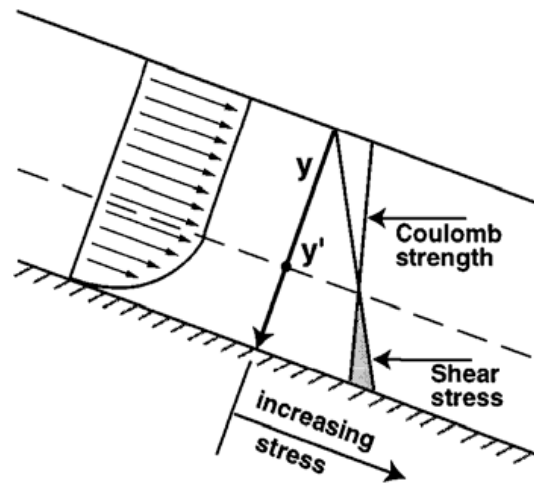


Figure I.3: Bingham model on infinite slope (from Iverson et al. 1997).

$$FS = \frac{c + (y - my_w)z \cos a \cos a \tan \phi}{yz \sin a \cos a} \dots\dots\dots 14$$

If the shear strength is greater than the shear stress, the safety factor has a value greater than 1 and the slope can be considered stable. If instead the shear strength is less than the shear stress, the safety factor has a value less than 1 and the slope should be considered unstable.

10. Slope stability models for shallow landslides

Many models have been proposed to explain the initiation of shallow landslides and debris flows. These models usually focus on the failure and the triggering of an infinite slope of an isotropic and homogeneous soil. One of the best-known hypotheses for the mobilization of debris flows and shallow landslides is that proposed by Johnson & Rodine (1984) and known as the Bingham model. This model assumes that triggering can only occur when the shear stress exceeds the Coulomb strength defined by Equation 3 and 1.

It is believed that strength or yield stress is an intrinsic material property and does not change dynamically with the other soil properties. The main assumption of the Bingham model is that failure can only occur when a soil with given water content exceeds a critical thickness. In this case, the shear stress at the foot of the slope is higher than the yield point (fig.3).

Below the failure plane, the Bingham model assumes that the yield stress is not fixed but varies depending on variables such as pore pressure and angle of friction (Iverson et al., 1997).

An alternative hypothesis for shallow landslide mobilization was proposed by Takahashi (1978). This model is based on Bagnolds' (1954) dispersive stress concept, but is essentially a

Coulomb failure model for a fully saturated and cohesionless soil with slope-parallel infiltration. This model assumes that the soil is fully saturated and water flows over the slope and over the slope surface (Figure 04). The presence of surface water allows failure at any bottom depth and on slopes of varying steepness.

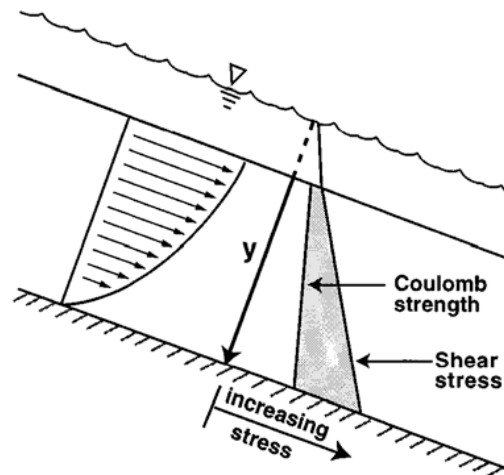


Figure I.4: Takahashi model on an infinite slope (from Iverson et al. 1997).

Other models consider the debris flows as a two-phase mixture of solid and liquid and assume that debris flows are triggered by the increase in pore pressure above hydrostatic values. According to some authors, groundwater flow can increase pore pressure to the point of soil liquefaction when Coulomb failure occurs and cohesive bonds break (Denlinger & Iverson, 1990). Others postulate that debris flow mobilization can only occur if the contraction of the loose soil during quasi-static failure increases the pore pressure to a critical state (Casagrande, 1979; Sassa, 1984), with behavior similar to that of undrained laboratory tests of cells resembles. It is very important to consider how quickly porosity can change during soil contraction compared to the variation in pore pressure. If this change is slow, the pore pressure can change and offset the new porosity. However, if the porosity change occurs too quickly, the increase in pore pressure can lead to soil liquefaction.

There models consider the debris flows as a two-phase mixture of solid and liquid and assume that debris flows are triggered by the increase in pore pressure above hydrostatic values. According to some authors, groundwater flow can increase pore pressure to the point of soil liquefaction when Coulomb failure occurs and cohesive bonds break (Denlinger & Iverson, 1990). Others postulate that debris flow mobilization can only occur if the contraction of the loose soil during quasi-static failure increases the pore pressure to a critical state (Casagrande, 1979; Sassa, 1984), with behavior similar to that of undrained laboratory tests of cells resembles. It is very important to consider how quickly porosity can change during soil contraction compared to the variation in pore pressure. If this change is slow, the

pore pressure can change and offset the new porosity. However, if the porosity change occurs too quickly, the increase in pore pressure can lead to soil liquefaction.

As already mentioned in the introduction, the main trigger for shallow landslides and debris flows is the increase in pore pressure during infiltration during heavy rain. At the same time, water intrusion increases weight, which plays a mechanical role, particularly where cohesion is a major contributor to soil Coulomb strength (Iverson et al., 1997). The pore pressure in a slope can be increased in two ways: through direct water ingress at the slope surface and through groundwater runoff from adjacent slope sections

Direct infiltration is usually a vertical flow from the surface to the deepest part of the ground, while groundwater flow is usually directed from a saturated area to the nearest materials. An increase in soil pore pressure can also be achieved by penetrating or flowing water raising the regional water table to a shallow soil level. Typically, the groundwater flow models used for distributed slope stability analyzes treat soils and rocks as continuous porous media that obey Darcy's law, although field experiments suggest that the flow distribution in natural slopes can be influenced by rock fractures, root canals, and animal burrows (Pierson, 1983)

11. Rainfall triggered shallow landslides (Iverson's model)

The Montgomery and Dietrich model has been used to estimate landslide risk but not to predict it over time. The main reason is that the subsurface flow is treated as a stationary process and therefore it is not possible to represent the transient flow of water due to short and heavy rains. Iverson (2000) found that the stationary approximation is only valid for very long precipitation durations, very low precipitation intensity, shallow soil depth and strongly anisotropic conductivity. Therefore, it is not possible with this approach to capture the effects of high-intensity precipitation in the short periods that often trigger shallow landslides and debris flows

The model proposed by Iverson (2000) uses Richards' equation (1931) to predict precipitation-induced pore pressure and its temporal and spatial response. This eliminates the need to assume steady-state conditions in the subsurface flow, and it is possible to describe transient conditions and infiltrations due to complex and high-intensity precipitation events.

12. Hydrological processes

Hydrological processes are the main cause of soil shear strength loss in precipitation-induced shallow landslides (SLs). These effects depend on pre-event water content and seasonal evapotranspiration processes and are therefore time dependent. For this reason it is

important to consider these dynamics in slope stability models in order to quantify the safety factor. The development of groundwater movement, positive pore water pressure, and a reduction in negative pore water pressure are all effects of increased soil water content.

Rainwater infiltration leads to changes in soil moisture, which is strongly influenced by environmental variables such as soil porosity or permeability. Changes in soil moisture affect the rate of infiltration and the movement of water through the soil. Water always flows in the negative pressure gradient, both in the unsaturated and saturated states, but in the particular case of saturated soils, water movement is mainly due to gravity.

Soil saturation is achieved by subsurface flows, which are divided into matrix and preferential flow paths. The unsaturated diffuse flow consists of the movement of water between the pores, resulting in a uniform moisture state throughout the soil. Gravity and matric pressure gradients are the driving factors and their effects depend on soil properties. An additional water supply promotes water movement through overland currents or preferential currents that arise in the macropores and spaces of the pedofauna and plant roots. Nimmo (2009) pointed out the existence of three basic modes of preferential flow: flow through macropores, funnel flow, and transient conductive flow.

In some cases, preferential flow promotes soil drainage by limiting the development of pore pressure during storms. The development of the preferred flow is essential for SL initiation processes. Studies have shown that flows developing in the presence of shallow bedrock fractures play a key role. Exfiltration is the process by which the connection of some bedrock fractures with areas of hydraulic backfill creates high pressure at the soil-bedrock interface. This process is influenced by precipitation duration and intensity, morphological and geological characteristics of the area, and differences in timing and mode of SL initiation in topographically similar areas. Water infiltration leads to an increase in the weight of the soil, which is considered a mechanical load. Pore-water develops an overpressure, which is known to be the main effect of precipitation-induced SLs. The main consequence of this is the reduction of effective stresses in the soil, leading to a reduction in shear strength. Lehman et al. (2013) found that hydrological connectivity is also a crucial process that can promote the formation of SLs in large interconnected areas.

Hydrological processes are influenced by soil depth, which is an important control parameter in assessing how saturated conditions can be achieved. To solve this problem, hydrological models calculate discharges considering the surface topography and develop terrain indices based on the digital terrain model. The topographic wetness index, introduced by Kirkby and Weyman (1972), is most commonly used to model slope stability. The assessment of hydrological processes, in particular the prediction of how pore water pressure

changes in response to precipitation events, is fundamental to estimate their influence on mechanical processes and to calculate the probability of the SL event (Ilenia Murgia et al 2022).

13. Slope stability analysis software

Distributed slope stability models provide algorithms and equations that can be applied to any cell or pixel of an extended region. To solve this problem, software programs have been developed that facilitate the application of large-scale stability models and the visualization of the results in many ways. These software programs are based on codes that introduce some sort of simplifying hypothesis into the general forms of equations:

- 1- SHALSTAB is distributed slope stability analysis software that uses a distributed steady-state description of hydrological flows and infinite slope analysis.
- 2- SINMAP and SINMAP2 are additional tools for ESRI ArcGIS software based on the infinite slope stability model with groundwater pore pressures derived from a topographically based steady-state model of hydrology. Input information is obtained from digital elevation models (DEMs).
- 3- SINMAP is an interactive visual technique that adjusts variables based on observed landslides and allows for uncertainty by specifying lower and upper bounds to define uniform probability distributions.
- 4- SEEP/W is finite element software that evaluates the Richards equations solves to account for transient groundwater flow within a slope. It analyzes groundwater infiltration and excess porewater runoff in porous materials and can model both saturated and unsaturated flows. It is very proficient at solving saturated-unsaturated and time-dependent problems. SEEP/W results are used by SLOPE/W software to perform slope stability analysis using the limit equilibrium method, which is suitable for single slope stability analysis but not for distributed analysis.
- 5- TRIGRS (Transient Rainfall Infiltration and Grid based Regional Slope Stability Model) is a software developed to calculate the transient pore pressure distribution due to precipitation infiltration. It is a FORTRAN program that gives the distributed safety factor map as the end result. It is widely used for regional landslide risk assessment and assumes a near-saturated bottom, a flow field, and isotropic, homogeneous hydrological properties. However, if the initial water table depth is not adequately constrained, questionable results may occur.
- 6- GEOtop-FS is an advanced distributed slope stability model developed by Simoni et al. was developed. (2008). It uses the GEOtop hydrological distributed model (Rigon

et al., 2006) to calculate the pore pressure distribution and an infinite slope stability analysis to calculate the distributed safety factor. The main novelty of GEOtop-FS is that the safety factor is calculated using a probabilistic approach that assigns statistical distributions to the soil parameters instead of a single deterministic value

14. Conclusion

In this chapter, we have shown that most of the landslides in the study area are shallow landslides . Superficial landslides occur when rainfall, infiltration, soil type, and topographical conditions are favorable. The complex geomorphological context of the Souk Ahras areas makes the diagnosis of these phenomena very delicate. The causes of these gravitational movements are generally related to the combination of excess water, fine rock and steep slopes. Anthropogenic factors can also play a role as triggers. The stability assessment of the slopes in the study area can be performed using various software programs, including Geoslope GeoStudio.

CHAPTER II:

Presentation of The Souk Ahras Region

1. Introduction:

The wilaya of Souk Ahras is located in a mountainous region in northeastern Algeria. Due to the mountainous and hilly nature of the landscape and the nature of the geological formations, landslide activity is highly active. They affect practically a large part of the natural slopes. To better understand the formation process of this natural phenomenon, it seems important to place the region in its context (geological, geomorphological, structural, tectonic, seismic, etc.) and to know that the data cited in this chapter are the result of a bibliographical synthesis of previous works.

2. The study area:

Souk Ahras is a region where landslides are very spectacular; it is located in the North East of Algeria between longitude $7^{\circ}52'06,53''$ and $8^{\circ}12'03,42''$ E and latitude $35^{\circ}59'31,05''$ and $36^{\circ}19'09,34''$ N, it covers an area of 812 Km² and the density 191 in hab/km². It is limited by Tunisia to the east, Wilaya of Taref and Guelma to the north and north-west, Tebessa and Oum Bouaghi to the south-west (fig.1). Almost the entire city is located on a diapir of triassic material with all the instability problems that may occur in this type of geological materials (fig.6). Three areas within the region of Souk Ahras have been chosen for this study. They are Zaarouria, Mechrouha and Hammam Tassa. Their respective coordinates are:

- Mechrouha ($36^{\circ}21'23.50''$ N, $7^{\circ}50'7.93''$ E)
- Zaarouria ($36^{\circ}13'37.66''$ N, $7^{\circ}57'28.09''$ E)
- Hammam Tassa ($36^{\circ}14'17.49''$ N, $8^{\circ}02'33.51''$ E).

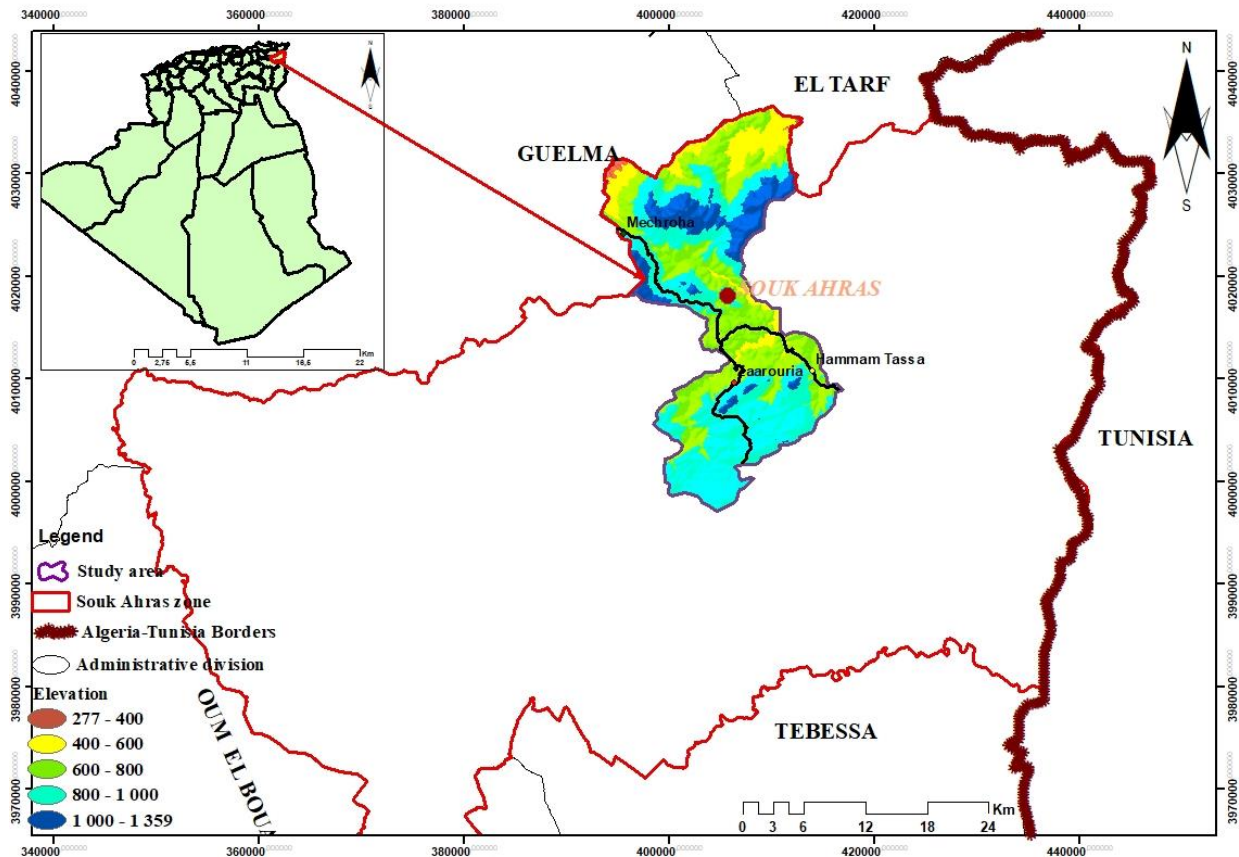


Figure II.1: Geographical location of the study area.

3. Socioeconomic context

Souk Ahras area is dominantly a mountainous area with high picks and deep valleys. It is primarily characterized by its mining and agricultural activities. A variety of crops such as cereals where wheat, barley, and oats are the main products. Horticulture and arboriculture are not uncommon along with milk production. Mining activities are also quiet frequent along with some industrial plants such as ceramics, bricks and food transformation plants. It has carried out several public investment projects during the various development programs, the basic infrastructure has been remarkably improved. It is crossed by national roads (N 16, 81, 82, 80 and 20) and the main railway line that ensures the transport of iron ore and phosphate (from Dj. Onk, Ouenza and Boukhadra). Fig.2.

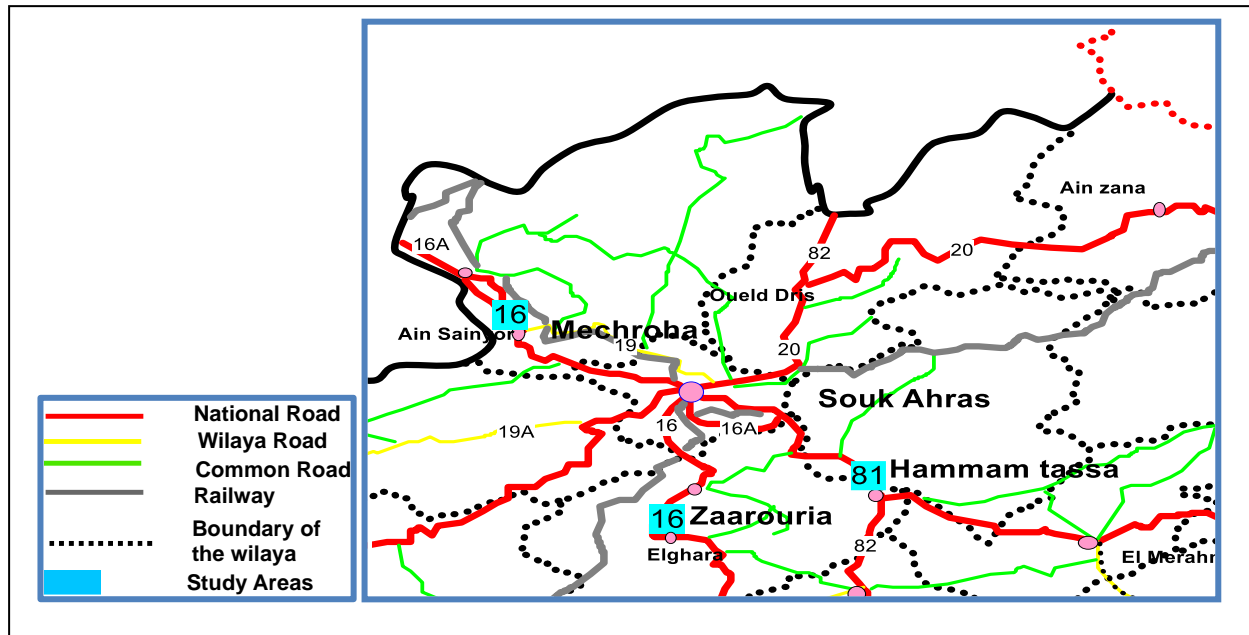


Figure II.2: The main railway line and road map of the study area (modify by a surfer).

4. Plant cover

The vegetation cover of this mountainous region consists of 43,625 ha of Aleppo pine, 23,431 ha of cork oak and 21,878 ha of holm oak, eucalyptus and scrub. concentrated mainly in the communes of Mechroha (75.48%), Ouled Moumen (50.01%), Ain Zana (52.98%) and Zaarouria (49.53%) (in H. Djaba, 2010)(*Djazairiss : Réaménagement Des Forêts de Chêne-Liège à Souk Ahras*, n.d.).

The part of the study area where the hills and ridges dominate is characterized by significant rainfall and dense forests of cork oaks, Zeen oaks and Afers oaks that form a real maquis, especially in Dj. Regune, Dj. Kelia and Djebel Zaarouria.

The vegetation helps stabilize forested slopes by providing root strength and altering the soil's saturated water balance. Plant roots can anchor through the soil mass in bedrock fractures making it more stable. Moreover, the dry summers and the wet winters and the water level variation usually play an important role in mass wasting and road side slope failure. After trees are removed, the frequency of landslides usually increases (Ziemer, 1981).fig (03)

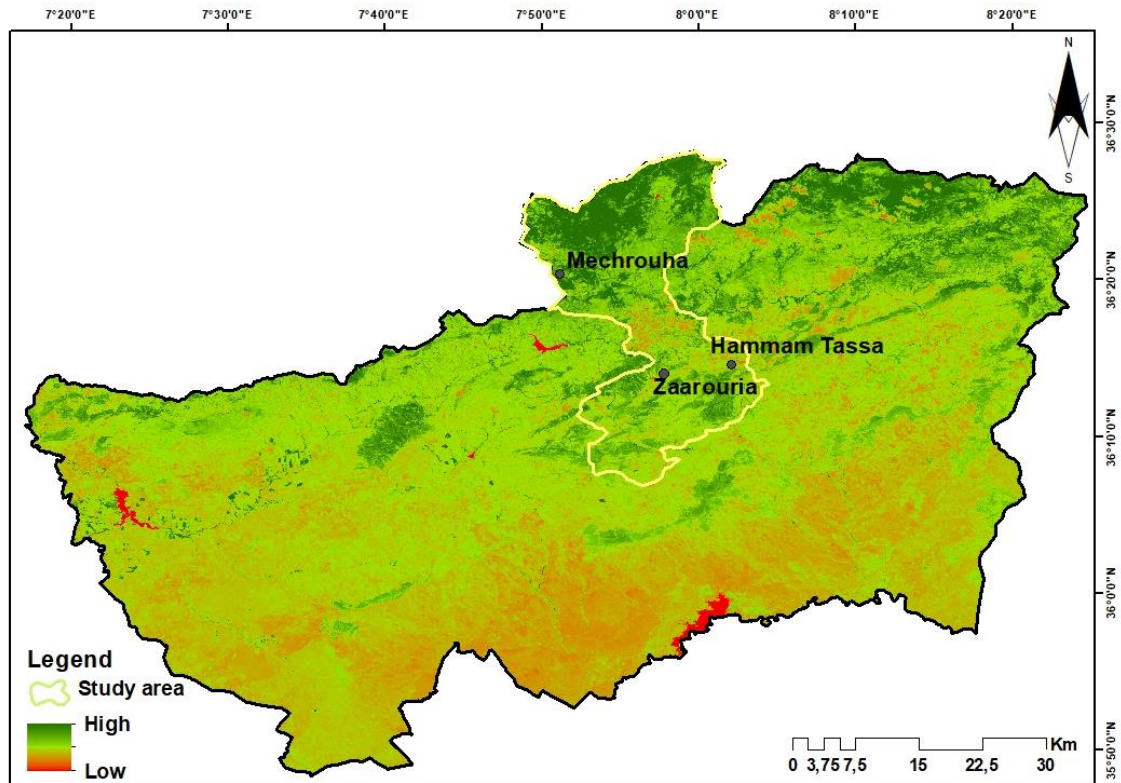


Figure II.3: NDVI map of study area.

5. The seismic context

Seismological studies have shown that seismic activity is mainly concentrated in the north of the country. The inner regions are characterized by diffuse seismicity. The measuring network recorded almost 50 tremors per month. Most of this activity is hardly felt due to the low intensity and takes place far from urban centers. The Algerian seismic zone distribution according to the Paraseismic Regulations of Algeria (R.P.A., Version 2003) divides the national territory into five (05) zones with increasing seismicity (Fig.04). This map shows that the zones of seismic activity are localized in the north and north-east of Algeria along the coastal mountain range between Oran and Annaba and in the Hodna and Aures regions. According to the R.P.A., Souk Ahras is in Zone I. with magnitudes 3 to 5.

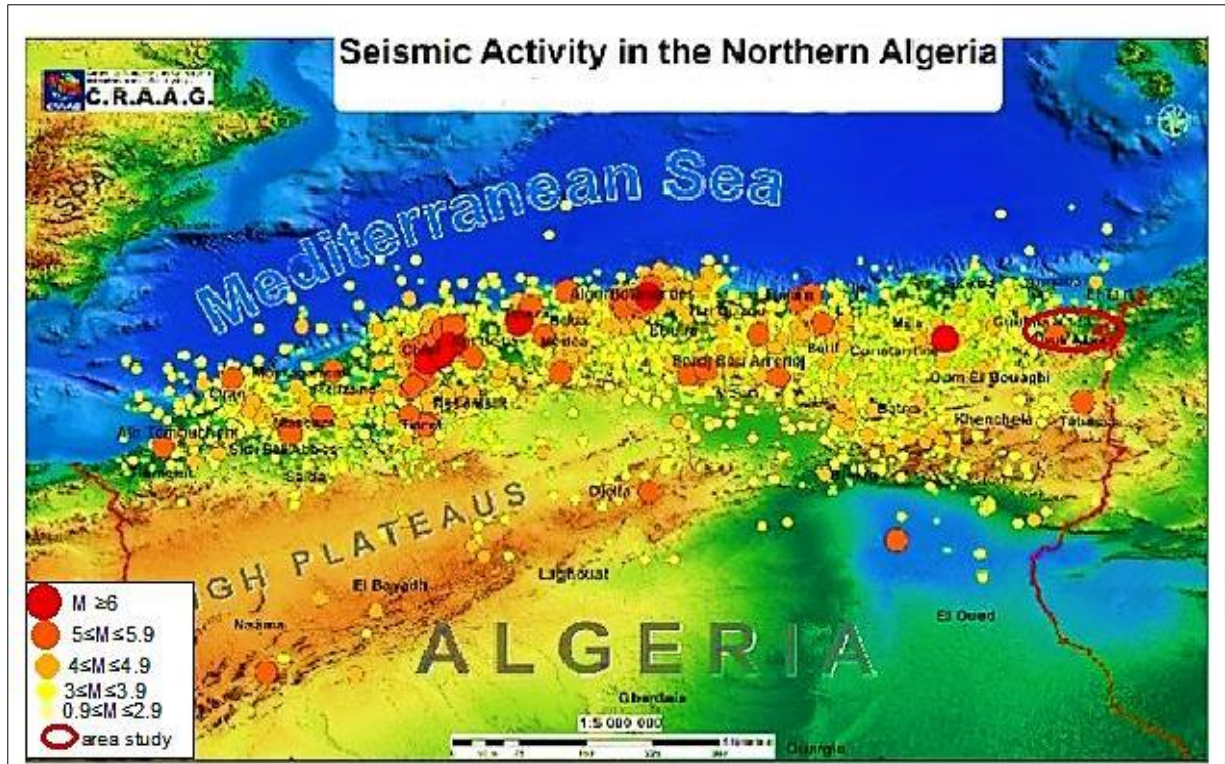


Figure II.4: Seismicity in northern Algeria from the CRAAG database.

6. Geological setting

From the work carried out by a number of researchers such as (Durand-Delga, 1969; Vila, 1980; Bouillin, 1986; Chouabi, 1987; L. David, 1956), Northern Algeria belongs to the well-known Maghrebide basin. It extends over 2000 km from Gibraltar to Calabria, Italy and represents a section of the alpine system of the western Mediterranean. It includes the Moroccan Rif to the west and the Algerian and Tunisian Tellian Atlas Kroumirie-Nefza. Villa (1980) and Wildi (1983) subdivided North Algeria into three paleogeographic paleo-domains which are from North to South, the internal, the external and the flysh domain (fig. 05).

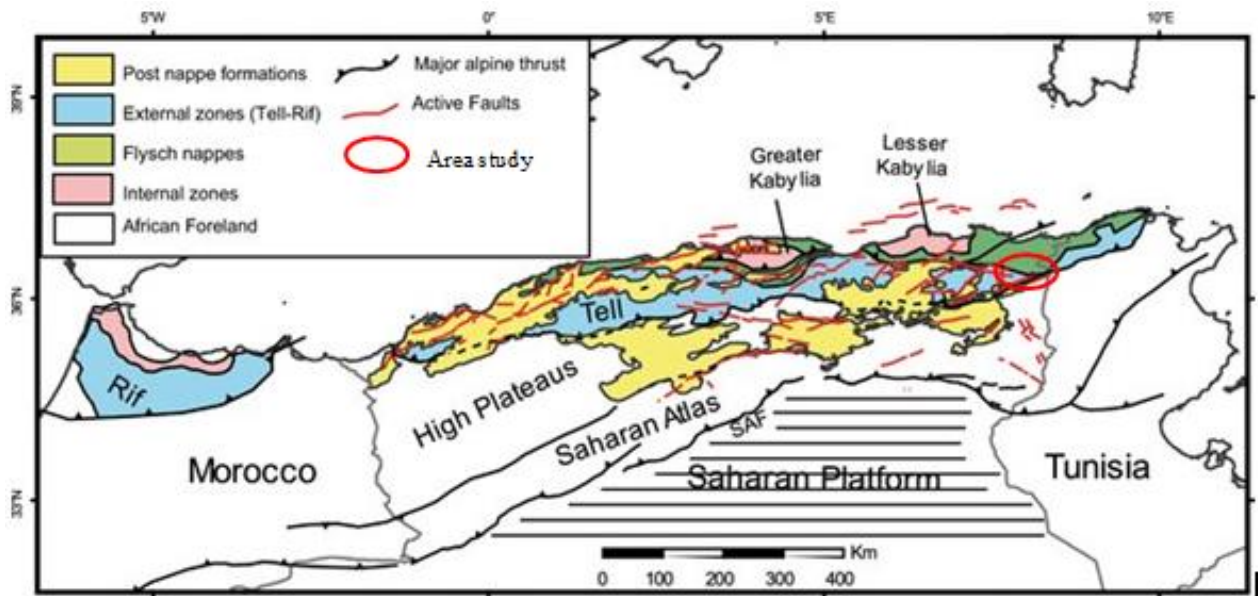


Figure II.5: The major structural domains and tectonic map of northern Algeria (Abdelkarim Yelles, et al. 2022).

6.1. The internal domain:

The internal domain consists of an ancient paleozoic metamorphique basement of variable nature. From the Triassic to the Upper Oligocene, the massifs of the inner Maghreb represented a common high zone. They form a series of coastal massifs bounded to the south by their sedimentary cover composed mainly of secondary and tertiary carbonate rocks called Dorsal Kabyle. This heavily scaled limestone ridge stretches from Sicily in the east to the Betic Cordilleras in the west and bisects the North Rif (Rihab, 2013).

6.2. The Flysch domain:

This domain is characterized by flysch-like sediments ranging from the Lower Cretaceous to the Oligo-Miocene. These are deep-sea deposits formed by turbidity currents, generally below the lysocline. They appear to be mainly abyssal plain formations (Bouillin, 1986).

From north to south of the flysch basin, a distinction is made: the Mauritanian flysch and the Massylian flysch, which differ from each other in their original habitat and source material. The whole is crowned by the Numidium of the Oligocene to the lower Burdigal Period. The latter filled a depression inherited from the Whale-Paleogene Flysch Basin (Rihab, 2013).

6.3. The external domain:

It is located south of the flysch domain and corresponds to the formations of the northern margin of the African plate. The bedrock of the Tellian domain is not exposed anywhere, it is probably of continental crust type. Some authors (Vila, 1980) consider the Edough massif to be the bedrock of the outer domain. The outer domain includes the Tellian units and the Tellian Foreland units (CHABBI Abdallah, 2017).

In souk Ahras area, only the formations of the external paleo-domaine can be found, they belong to the Tellian atlas and the Saharan Atlas.

7. The structural setting of Souk Ahras region

Souk Ahras region forms a transition zone between two distinct structural domains, namely the Tellian Atlas to the north and the Sahara Atlas to the south. The Saharan Atlas displays a folded structure with a dominant northeast-southwest orientation. This so-called Jurassic structure consists of a series of wide troughs and narrower anticlines that date back to the Cretaceous. Their shell is generally thin, at most a few thousand meters thick. To the north, towards the tell, the folds assume a westerly orientation, taking into account the tangential thrusts coming from the north. This so-called Numidian orientation is particularly visible in the north-western zone.

This lateral compression reduced the size of any wrinkles, resulting in sagging troughs that were defective in most cases. A progressive transition from the Atlas structure to the Tellian structure, which the Tellian zone knew, is therefore noted. Also, the presence of the transverse fractures responsible for the collapse basins (Taoura) caused the folds on the Tunisian border side to experience a slight northward torsion. The Triassic, on the other hand, reacts on its own account. He is always responsible for some complications like our zone. It is in an anomalous (mismatched) stratigraphic position. Its great plasticity allows it to shine through the terrain below (O.R.G.M., 2002). It is noticed in the anticlines, in the large fractures or in the massifs (the massifs of Souk Ahras). The establishment of this structure took place in many orogenic phases, as was the case for the entire north-eastern mountain range (Rouaibia, 2018).

8. Litho-stratigraphy

According to this litho-stratigraphic assemblage covering the study area, fig .7: are the Numidian and Tellian layers, the scaled series of the Sellaoua. The formations occupying the ground in the study region can be described as follows:

8.1. Allochthonous units

○ The Numidian formations (or Numidian flysch)

They are represented in the northern part of the study area and are unconformably lying on the Tellian bedrock from west to east. They are a thick turbidite series of Upper Oligocene to Lower Miocene age. They are composed of quartzitic sandstone with vertical grading and a cemented with red clays and silica.

They covered Djebel Rezgoune, El Kelakh, Boubakhouch, Koudiet bin Ahmed, Neb Hallouf, Medjene, M'Cid and up to the Algerian-Tunisian border, via Dj. Ain Zana. There are a few isolated outcrops, forming Dj's clips. Guern Djedi and Dj. El Amara.

○ The Tellian sheet

The Tellian sheet appeared in the east of the study region and in the South of the Medjerda valley, between Dj. El Kalakh in the West to Kef Dardja in the East. Its age extend from the lower pleocene to the upper eocene:

- The Paleocene with black clayey marls and black marl-limestones with light gray patina;
- The lower and middle Eocene with black clayey marls, yellow limestone kidneys;
- The Upper Eocene is composed of black and brown bituminous limestones with Globigerines, and black marl-limestones.

○ The Chebkat Sellaoua series

The Chebkat Sellaoua series belong to the allochthonous foreland organizations. They are represented by a thick series of Cretaceous marls and limestones that are more benthic than those of the native Atlas. They extend from Djebel Boualek and Djebel Boubakouch to NW of Souk Ahras (Vila, 1980; Kriviakine et al., 1986b; Chabbi et al. 2016, Fatna).

8.2- Atlas para autochthonous and autochthonous units

8.2-1. The Paleozoic:

The Permo-Carboniferous with multicolored mica sandstones rich in calamites and argillites constitute the oldest lands, they outcrop 3km south of the town of Souk Ahras on the plains of Oued Medjerda and Koudiet Hammouda (Oued Mougras). (Bouhafs Fatma ,2021)

8.2.2- The Mesozoic:

➤ The Trias

Triassic outcrops are located in the center of the massif, around the town of Souk-Ahras. To the north of our study area, the Triassic outcrops widely in Mechroha-Nador-N'Bails massif. The Triassic materials are found under and in front of the Tellian sheets, they serve as a sole upon which the above sheets slide as is probably the case in Zaarouria.

In general, the Triassic terrains are discordant with the overlying formations (Thibiéroz and Madre, 1976). The particularity of the Triassic terrains, intensely deformed and crushed, is the heterogeneity of their composition. It is a tectonic breccia, called "mixture", made up of elements, limestone blocks, sandstone, dolomites, all cemented by a sandstone-gypso-clayey matrix containing small fragments of these same rocks.

➤ The Lower Cretaceous

It is dominantly represented by Aptian outcrops in Sidi-Ameur and Ras El Guema mountains. It is mainly composed of marls, limestones and sandstones. Albo-Cenomanian formations are mainly Marls, siltstones and marl-limestones. They outcrop to the extreme NE near the boundary at Koudiet El Hemimib.

➤ Lower and Middle Cretaceous

The Albo-Cenomanian formation is composed of marls, siltstones, and limestones. It outcrops to the north in Oued Mougras anticline (Sidi el Hemessi, Djebel Graouet and Bourzine) and extends to the Tunisian border. It is also encountered in Djebel Ladjbel anticline at the edge of the El Ouasta Triassic diapir near the Tunisian border (O.R.G.M., 1997-2000).

➤ The Upper Cretaceous (Turonien–Sénonien)

The Turonian consists essentially of limestones. The ratio of limestone to marl is variable. It forms Koudiet Henchir Ellouz and Koudiet el Msala in Oued Mougras. They are also found in Djebels Shrachif Messaouda, Sahaba and Ouasta. The Turonian in the north exceeds 200 m, while in the south it does not exceed 100 m.

The Coniacian are marl, marl-limestone and limestone-marl, in the north-east, on the borders of Algeria and Tunisia. The lower Santonian outcrops in the form of isolated outcrops, limestones and marls. The Upper Santonian-Lower Campanian: consists of marl with few layers of limestone, clayey with gray or dark grey tint, with bluish or greenish hues, of variable compactness, from soft to very compact, often with confused stratification and scrubby flow (and outcrop in the djebles of el Ogla, Baba Embarek, zellez and Kef Ellouz; Kriviakine et al., 1989b, Fatna 2018, Hadji 2013)

The Upper Campanian consists of a grey limestone with 80 to 100 m thick layers of marl that outcrop on the southern flanks of the Djebels, Boussessou, Ogla and Baba Embarek. Scattered peaks are observed along the wadis El Hammam, Boudrhis and Guelib Hachem and appear at Djebels Serrou and Cherif.

The Maastrichtian begins near the top of the intermediate marl. It essentially includes the second limestone bar and the upper marl. It should be noted that Cretaceous limestones are found in the Ain Soltane Mountains, as well as on the flanks of the Dra-Taoura-Mrahna synclines and Bordj M'Raou, where they are covered by Miocene sandstone and Quaternary alluvia. Thicknesses can reach 300 m.

8.2.3- The Cenozoic

➤ Paleocene

The paleocene formations outcrop southeast of M'Daourouch, Djebel Sessou, Ain Hallouf, Mehars and Ogla. It is mainly a marle limestone with a thickness varying between 80 to 200m.

➤ Eocene

From a geographic distribution point of view, the Eocene is scarcely observed in Souk Ahras area. It occurs only in the northern region in the form of shreds. It occurs at Djebel Dekma north of Djebel M'sid, at Djebel Boukebch and near Oued Mougras station. It consists of Priabonian calcareous marls and lumachelles overlain by Nummulitic limestones and Ypresian-Lutecian marls. These deposits are moderately thick (25 to 30 m) and outcrop mainly northeast of Taoura.

➤ Miocene

The Miocene formations form a thick series of 700 to 1200 m. It occupies quite a large areas of the study region. The lower Miocene covers a vast area of souk ahras. It is observed in the center of the synclines. It emerges along the Medjerda Valley to the Tunisian border. It

is also found in Djebel Serrou, Oued Chouk and in the Merahna Depression (O.R.G.M, 2002). It includes continental deposits, sandstones, marl conglomerates and mudstones.

The Lower and Middle Miocene consist of sandstones, conglomerates, marls and mudstones; Outcrops south of Zaarouria and east of Taoura. The middle and upper Miocene contains heterogeneous deposits such as marls, clays, sandstones, and clayey sandstones. It only outcrops along Oued Medjerda on the north coast around the Oued Mougras area.

➤ **The Oligocene**

The Oligocene presents as an east-west band north of the zone passing through, Oued Mougras, Sidi El Hemissi and Mechrouha. It occurs in the form of Numidian sandstone, sometimes separated by schistose clays or thin grey marls with thin beds of limestone.

➤ **The Pliocene**

The Pliocene consists of red clays, sandstones, custard stones, marls and sea limestones. The series is represented by dissonant continental terrains overlying Triassic, Cretaceous, and Miocene formations. Its lower part, 150-200 m thick, is made up of conglomerates, micropudding stones, sandstone with layers of clay and red clay marl.

8.2.4- Quaternary

In Souk-Ahras, the Quaternary extends over large areas. It is present in virtually all geological strata covering the wilaya. It generally consists of continental formations such as colluvium, river terraces, boulders and silts, which have been classified into three (03) groups according to their characteristics:

➤ **Old formations:**

They correspond to two types of deposits:

The limestone crust consists of white, yellowish and pink carbonate rocks. It's grainy earthy and dusty. It is located on the southern back of the Medjerda Mountains. The pebbles are found south of Souk-Ahras in the Triassic at elevations of 660–700 m, thus belonging to Quaternary formations.

➤ **Recent formations:**

These formations are represented by gravity deposits which are mainly represented by material coming from landslides, debris flow and deposited along the slopes or at their foots. They are heterogeneous in nature and contain clay, silts, loam, and colluvium of all sorts. Djebel Guenbuita, Zaarouria and Djebel Ladjbel are mostly covered by fine colluvium materials.

➤ **Current formations:**

Alluvial material which is found around water streams are mainly pebbles, gravel, sand, sandy or loamy silt. These sediments are developed in the valleys of Oueds Medjerda, Hammam, Tiffech and other smaller rivers. Larger blocks or clusters of blocks are found in the bed and in the flooded plains of the wadis. Some valley trails currently have consolidated and compact gravel cemented with a muddy or aerated material

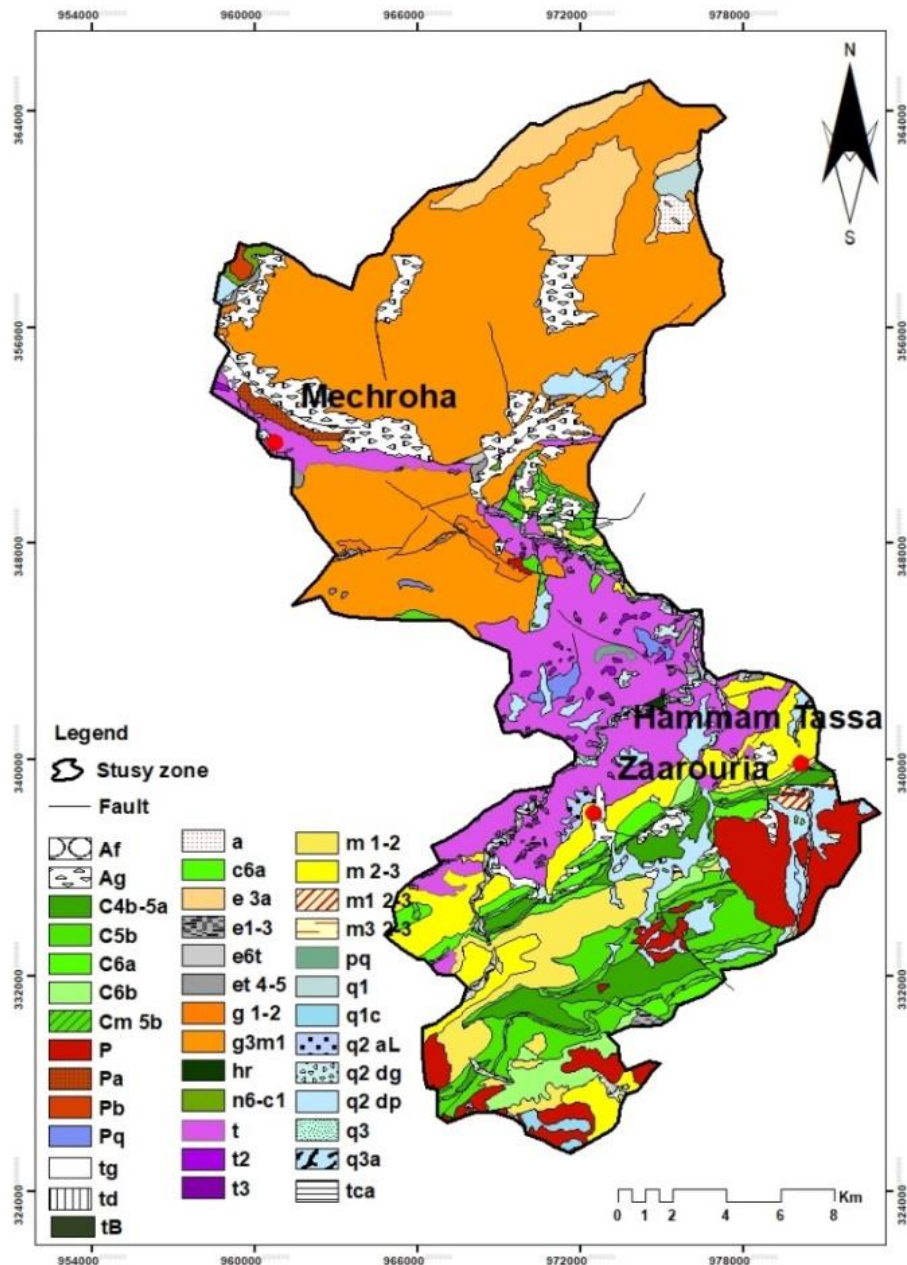


Figure II.6: Geological map of the study area.

m1-2: Lower-Middle Miocene. Sandstone, marl, conglomerates. **e1-2:** paleocene. marls, clays, marl-limestones. **C6a:** super cretaceous, Maestrichtian under lower level. Chalky white limestone, marly limestone, gray marl. **C6b:** super cretaceous, Maestrichtian under upper level. Chalky white limestone, marly limestone, gray marl. **C5b m:** Upper Campanian Clayey marl,

limestone marl. **C5b**: Upper Campanian limestones, sandstone limestones, marl-limestone. **C4b-5a**: Superior Santonian - Lower Campanian, Gray marl and clayey marl and marl-limestone. **G3 -m1**: Oligocene superior -miocene inferior. Quartz grate with red patina, gray clays. **G1-2**: Oligocene upper -middle. Greenish clays. **Pb**: Pliocene, Red clays, sandstone, intercalation of marl, lake limestone. **Af**: Current fluvial alluvium of submersible lands, low terraces; pebbles, gravel, sands, sandy loams, silts. **Ag**: gravitational formations - scree: blocks, abatis, sand silts. **q³**: Quaternary Recent, alluvium from the middle terraces: pebbles, gravel, sand. **q² al**: alluvium from conglomerate lands, sand, silt. **q² dp**: deluvial-proluvial formations covered with gravel, sand, silt. **q² dg**: deluvio-gravitational formations - slope scree: breccias, gravel, sand, silt. **q 1t**: travertines. **Pq**: plioquaternaire, villafranchien. conglomerate, sandstone, clays. **N6-C1**: Lower-Upper Cretaceous, Albian -Cenomanian, Black clayey marls. **T**: Trias, argilo-gypsum formations with fragments and blocks of rock poured out. **Tca**: Trias, gray and black limestones in platelets with rare intercalations of yellow dolomites. **Td**: Trias, dolomites and gray dolomitic breccia, cagneules. **Tgy**: Trias, pure gypsum **Tb**: diabases. **T3**: Upper Triassic Alternation of sandstones, argillites and bluish red marls. **T2**: Middle Triassic, dark gray limestones to modiala, miophoria, marls, dolomites. **Hr**: Permocarboneous, versicolored micaceous sandstone with calamites, argillites **P**: pliocene, conglomerates, gravelines, sandstones, clays and marls **q 1c**: quaternaire ancient **m 2-3**: Middle-Upper Miocene. Clays, marls, siltstones intercalation of sandstones **q c1**: Quaternary ancient limestone crust. **e¹⁻³**: Paleocene. marls with rare intercalations of limestones. **E_t 4-5**: Eocene priabonien. marnes a intercalations de lumachelles (Eocene priabonien. Marnes with intercalations of lumachelles). **Q1**: Alluvions de la moyenn terrasse (115m). (Alluvium from the middle terrace (115m)). **Q2 dp**: middle quaternary, deluvio-proluvial cover formation: gravel, sands, silts. **q² dg**: middle quaternary, deluvio-gravitational formation-scrée of slopes: breccias, gravel, sands, silts. **q² aL**: middle quaternary, alluvium from high terraces: conglomerates, sands, silts. **Ag**: current gravitational scree formation: blocks, abatis, sands, silts **Af**: current, fluvial alluvium of submersible lands, low terraces: pebbles, gravels, sands, sandy silts, silts **E1-3**: Paleocene. marls with rare intercalations of limestones. **A**: eboulis de pentes. **E6 t**: Lower-middle Eocene. Black clayey marls with yellow limestone kidneys. **Pa**: Pliocene, clayey marls, conglomerates, gravelines. **M1 2-3**: miocene, Argiles, marnes, grés glauconieux **M3 2-3**: miocene moyen superieur. marnes, argiles, grés. **M3 2-3**: upper middle Miocene. Marls, clays, sandstones. **M1 2-3**: miocene, Clays, marls, glauconious sandstone. **Q3a**: recent quaternary, alluvium from the middle terraces: pebbles, gravel, sand, silt. **Tb**: diabases

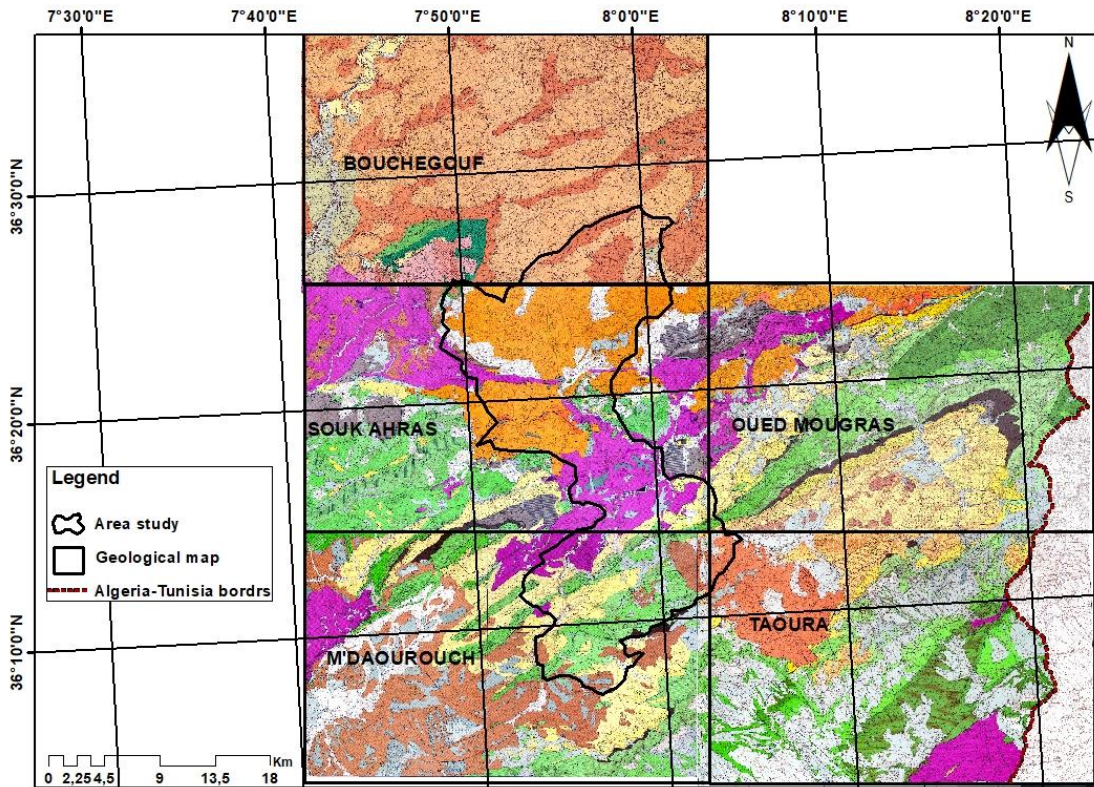


Figure II.7: Compilation of geological maps (1/50.000).

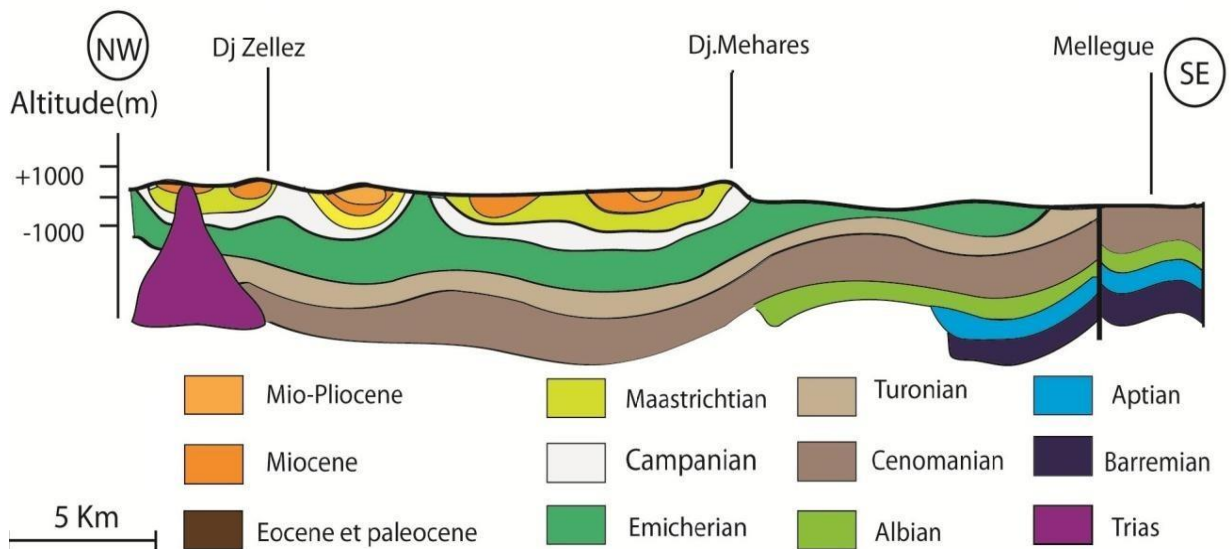


Figure II.8: Geological section in the study area (Hadji et al. 2012).

9. Tectonic setting

The tectonics is characterized by the dominance of a series of NE-SW trending faults with other vertical NW-SE faults. The presence of these fault networks facilitated the displacement and upwelling of the region's Triassic salt complex. With its heterogeneous composition, the latter accounts for the majority of the outcrops in the north of the study area fig (9). This complex geological context favors the initiation of gravitational movements of different types. From this we can see that landslides have evolved as a geomorphological process characteristic of the region.

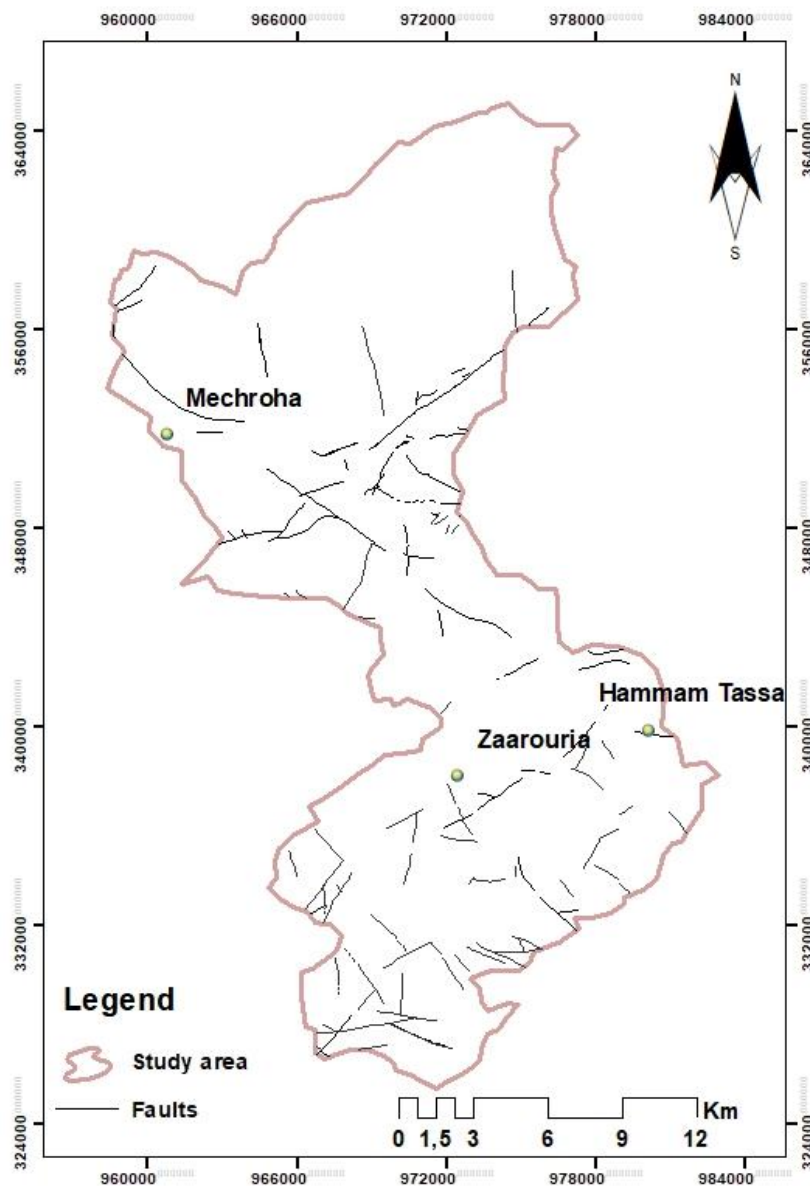


Figure II.9: Fault map of the study area.

10. Conclusion

In this chapter we have made the first remarks on the geological context of the study area. The Souk Ahras region is characterized by Triassic to Quaternary sedimentary formations, generally composed of limestone, sandstone, clay, marle, gravels and alluvium. The Oligocene areas north of Mechrouha and the Plio-Quaternary areas occupy the central part of the study area, thus separating the Triassic areas north of Zaarouria and the Cretaceous areas to the south, and the Miocene areas north of Hammam Tassa.

The structural analysis shows the dominance of NE-SW faults with other vertical NW-SE faults. It consists mainly of sedimentary formations from the Upper Cretaceous to the Quaternary. This complex geological context favors the initiation of gravitational movements of different types.

Chapter III: **Climatology**

1. Introduction

In the area of landslides and mass waste, climate plays an important role as it influences material behavior and transport. Studies have shown a strong association between climatic factors and mass wastage (slope instability) (Beatty, 1972; Tricart and Cailleux, 1972; Toy, 1977; Churchill, 1981; Budel, 1982). The climate directly affects the physical-mechanical properties of soils. In fact, it is a key factor in landscape design and development (Tricart and Cailleux, 1972; Sugden, 1973; Doornkamp, 1986, p. 10).

In this study, the climatological data are taken from the Google Earth Engine (GEE) platform; This is currently the most advanced cloud-based spatial data processing platform in the world. Earth Engine's goals include conducting highly interactive algorithm development on a global scale, pushing the boundaries of big data in remote sensing, enabling impactful data-driven science, and making substantive advances in the global challenges associated with large geospatial datasets.

In this chapter, we will be interested in evaluating those climatic parameters considered important: precipitation, maximum temperature, minimum temperature, evapotranspiration, wind and humidity in order to explain some of the factors affecting landslides.

2. The climatic evolution of northern Algeria

Over the past 50 years, numerous scientific studies have shown that climate change is one of the biggest problems facing the world at local, regional and even international level. In the last three decades, Algeria has experienced a remarkable climate change that has amplified extreme hydrological events (heavy rainfall, floods, droughts...) due to several factors including: The first is man through his actions, the complex geomorphological features that Mountain ridges surrounding the Mediterranean Basin and the influence of diversity and tropical atmospheric circulation patterns result in a decidedly complex climate.

Algeria is one of the largest countries in Africa (arid and semi-arid zones) which are vulnerable and suffer from chronic droughts.

The last studies expect envisage the accentuation of this calamity, from which major climatic upheavals are expected during this century throughout the Mediterranean basin (Fig 01).

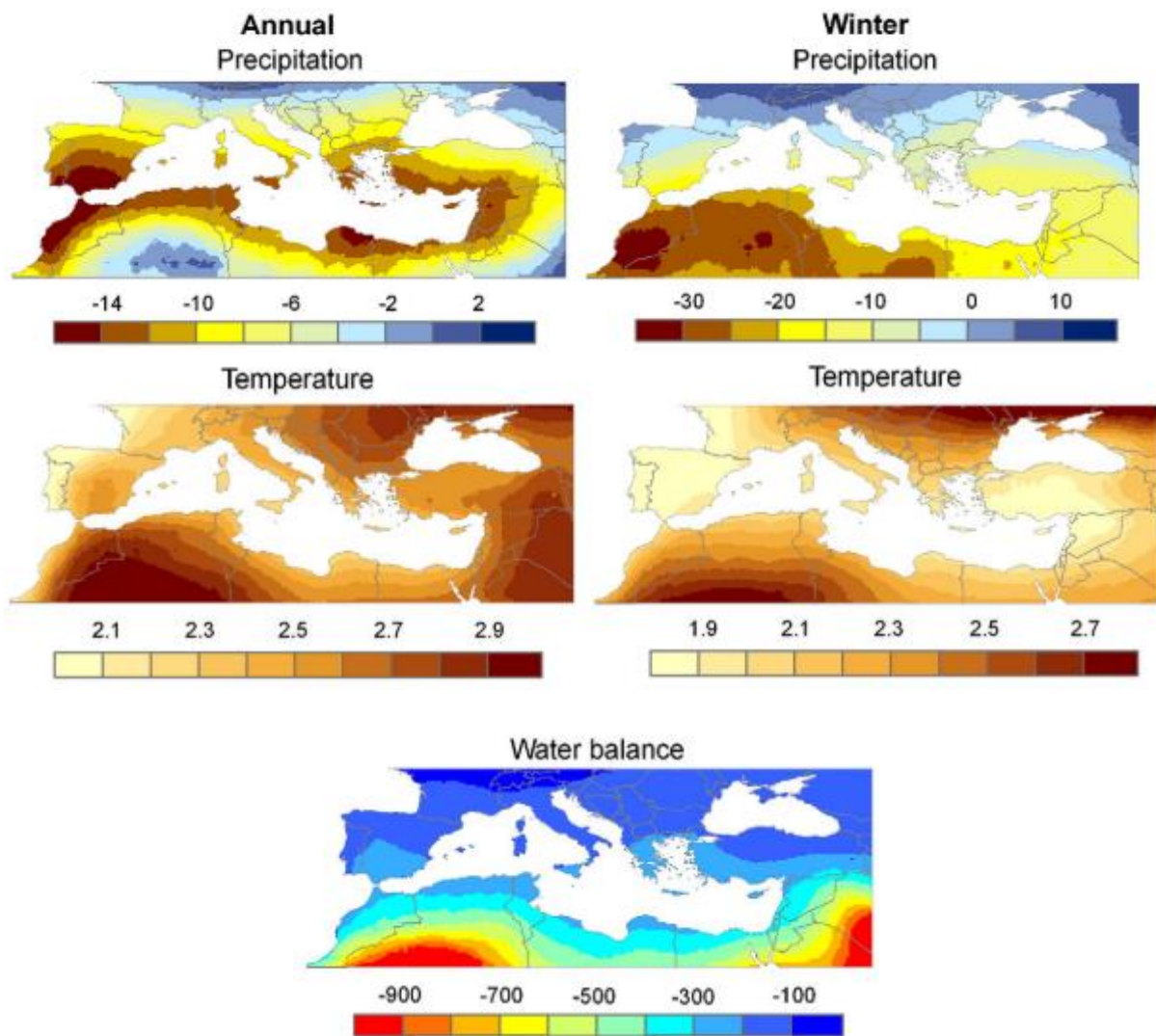


Figure III.1: Mean annual and winter climate changes, precipitation (P, %), temperature (T, C), and water balance (PT, mm) projected for the Mediterranean basin between 2040 and 2070 compared to 1960-1990 by nine general circulation models. (García-Ruiz et al., 2011)

3. Climatological characteristics of the study area

The Souk Ahras region is characterized by a transitional position between the Tellian Atlas in the north and a semi-humid, cold and rainy climate. Most of the meteorological and hydrological factors depend on the altitude and the study area is a complex relief with an altitude of more than 1400 m in the north to 500 m in the south, giving the area of Souk Ahras a basin surrounded by mountains (Fig. 02). Its northern part is humid with a rainfall of 1200 mm in the municipality of El Machrouha, the central part of the region is considered semi-humid, while the southernmost part is dry with a rainfall of 300 mm in Oued Kabarit.

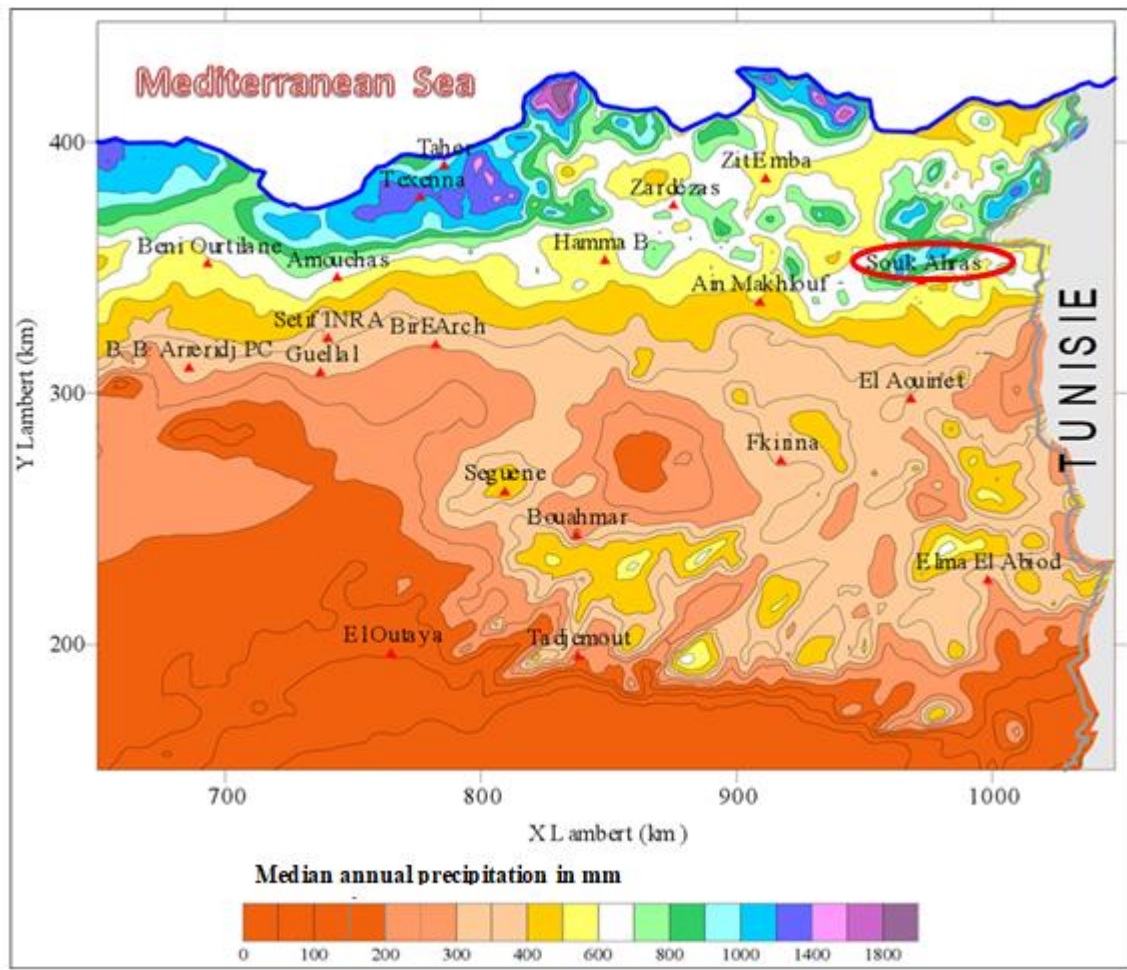


Figure III.2: Map showing the average annual rainfall in Eastern Algeria (period: 1972/73-1983/84)(ref carte pluvio).

4. Analysis of climatic factors

Climatic factors play a determining role in the occurrence of landslides through infiltration the latter depends directly on the rate of rainfall in the region.

4.1- Rainfall:

The total amount of meteoric water, whether liquid or solid, that falls over a defined horizontal area, called the precipitation section. Rain is an important climate element that influences seasonal water flow and thus rivers and groundwater regimes. Precipitation is the most effective factor affecting soil structure properties, often leading to landslides.

The data collected by Google Earth Engine platform (GEE) over a period of 20 years (2000-2019) of precipitation are summarized in the following table:

Table III.1: Monthly averages of precipitation in the study area, (period: 2000-2019).

	Sept	Oct	Nov	Dec	Jan	Feb	Mar	Apr	May	Jun	Jul	Aout	Interannual average (2000-2019) 639.2 mm
Average	40,9	50,4	67,0	89,6	98,9	78,9	69,2	54,8	52,2	15,4	7,5	14,4	
Avg. Seas	Autumn			Winter			Spring			Summer			
mm %	158.3	24.7	267.4	41.83	176.2	27.56	37.3	5.84					

The analysis of the curve of the monthly variations of the precipitation over a period of 20 years for the Souk Ahras region (fig 03), shows that:

- ✓ The wettest month is January with an average monthly precipitation of 98,9 mm.
- ✓ The least wet month is July with an average monthly precipitation equal to 7,5 mm.



Figure III.3: Variation in average monthly rainfall in the study region.

4.1-1. Seasonal variations in precipitation:

According to table (01), we notice that for Souk Ahras area, the winter is the rainiest; it receives up to 267.4 mm on average. For autumn and spring, the recorded rainfall reaches 158.3 mm and 176.2 mm respectively. Summer remains the driest season where rainfall is at its lowest, it is around 37.3 mm (fig. 04).

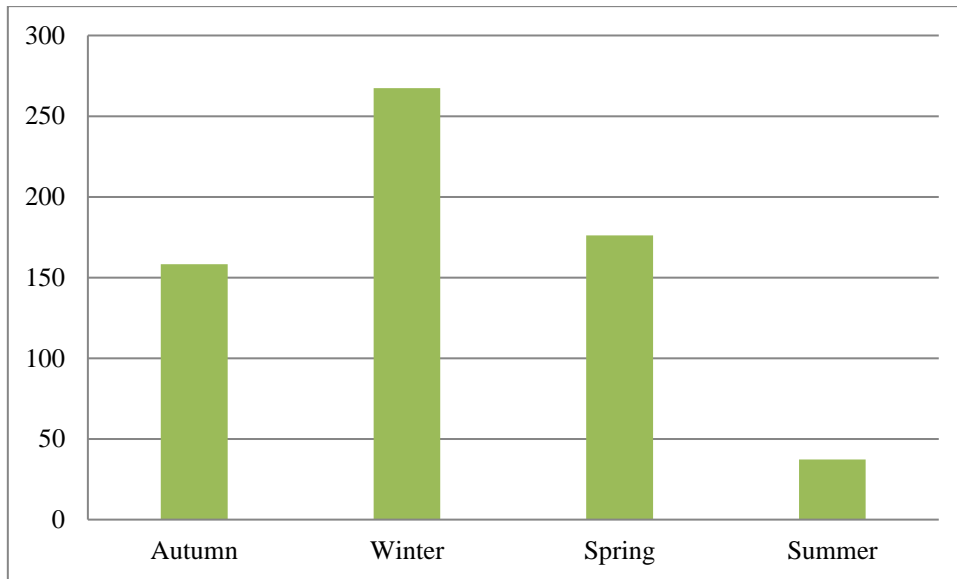


Figure III.4: Variation of seasonal rainfall in the study area.

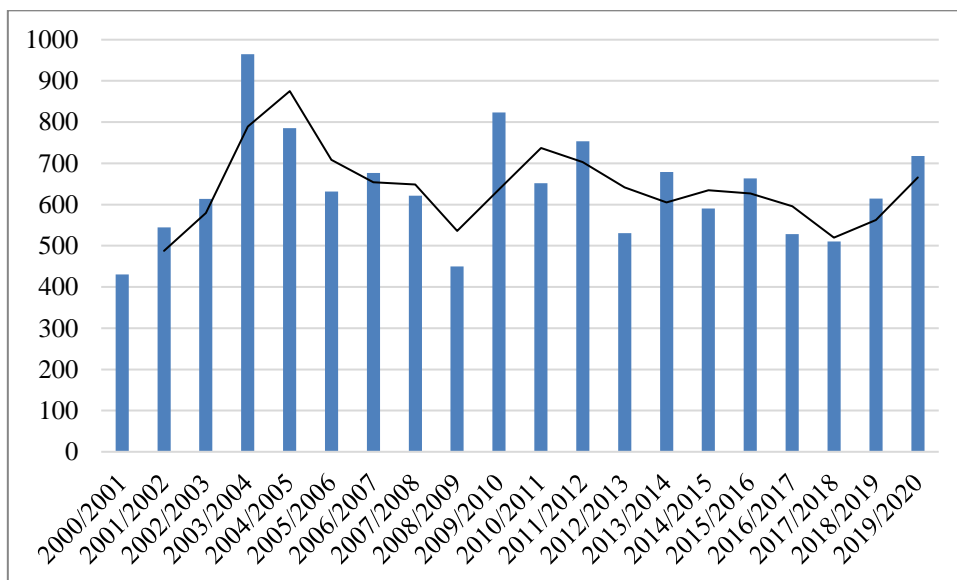


Figure III.5: Variation in average annual precipitation (2000-2019).

4.2- Temperature

Temperature is a major factor in conditioning the climate of a region. It has a great influence on the evaporation, evapotranspiration, and hence the water balances in the watershed. To carry out our work, we used data collected from (GEE).

Table III.2: Monthly average temperatures of Souk Ahras (period 2000-2019).

	Jan	Feb	Mar	Apr	May	Jun	Jul	Aug	Sep	Oct	Nov	Dec
Tmin	1,8	2,0	4,6	7,4	11,0	14,7	18,1	17,8	15,1	12,1	7,1	3,1
Tmax	11,5	12,5	16,6	20,7	24,6	30,9	35,2	34,2	28,8	23,7	17,0	12,5
moy	6,7	7,2	10,6	14,1	17,8	22,8	26,7	26,0	22,0	17,9	12,0	7,8

The study of the monthly average thermometric measurements of the Souk Ahras station data for a 20-year period from 2000 to 2019 allows the following results:

- 1- The variation of the monthly average temperatures shows a maximum of about 35.2 °C observed in July a minimum of 1.8 °C characterizes the month of January. July and August were the hottest months with a monthly average of 26.7°C and 26°C respectively. While January and February were the coldest months, with monthly averages of 6.7°C and 7.2°C respectively.

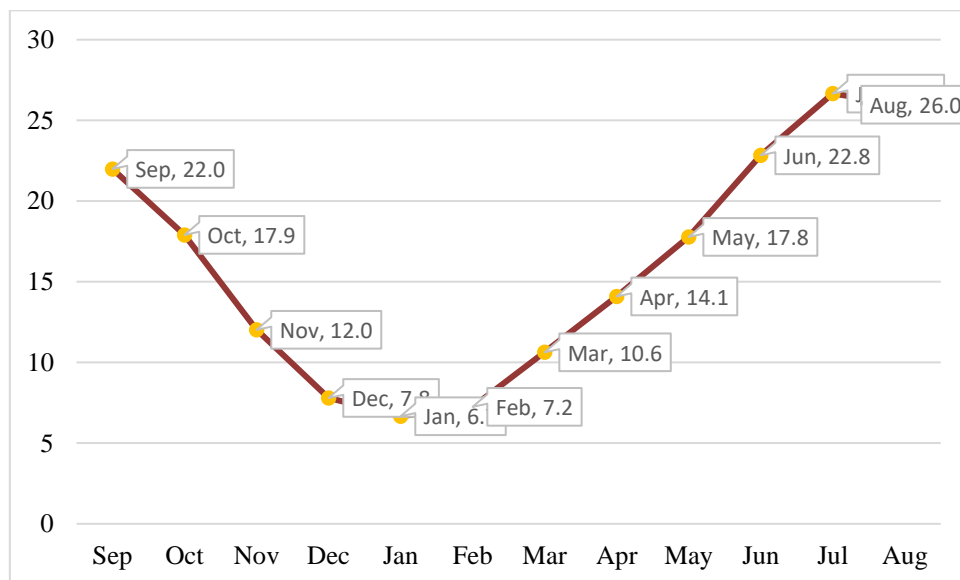


Figure III.6: Variation of monthly average temperatures (2000-2019).

4.2-1. Seasonal variations in temperature

According to table (02), we notice that for Souk Ahras area, the average seasonal temperature variation from one season to another shows that summer is the hottest season with an average of 25.2°C is; the coldest season is winter with an average of 7.23 °C. (fig. 7).

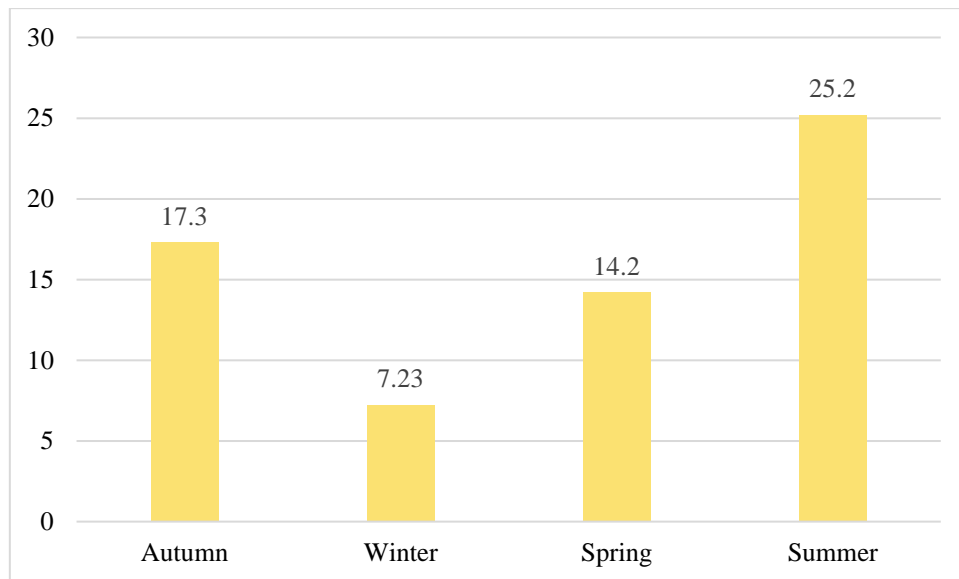


Figure III.7: Variation in seasonal mean temperatures (2000-2019).

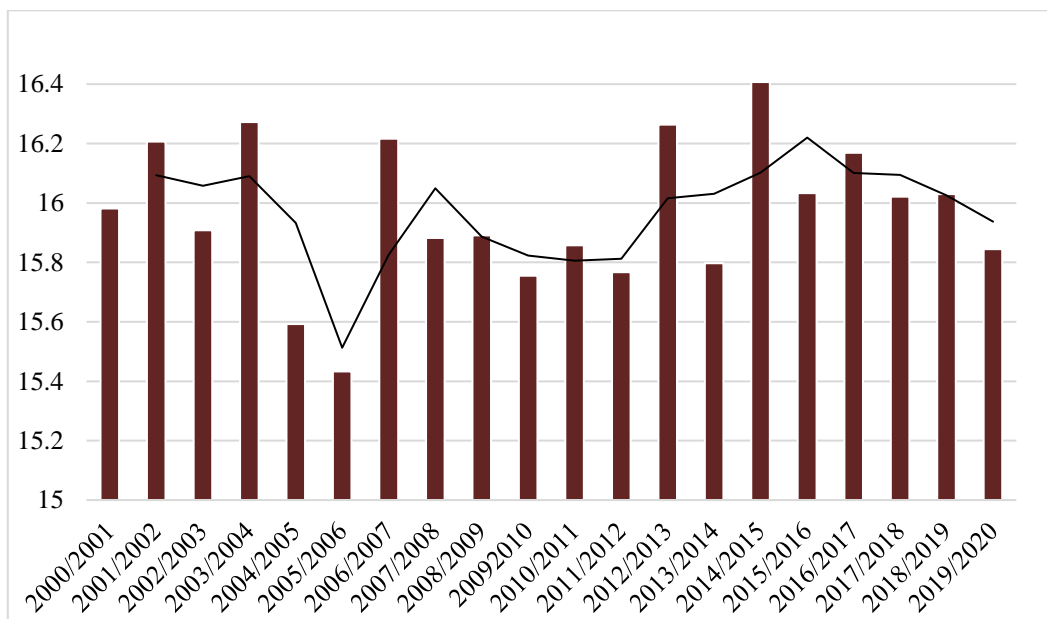


Figure III.8: Variation in average annual temperature (2000-2019).

4.3- Temperature-Precipitation Relationship (Umbro-Thermal Diagram)

Through the Google Earth platform in the Souk Ahras study area, the values of precipitation and temperature over a period of 20 years (2000-2019), allowed the establishment of an ombro-thermic diagram fig 9. It is a graphical representation of the average monthly temperatures and precipitation amounts at a given location where: $P = 2T$.

It shows the succession of two seasons, one dry and the other wet. A month is said to be dry when the total monthly precipitation in mm is equal to or less than twice the recorded temperatures in degrees Celsius.

The ombro-thermic diagram of our study area shows that the area is characterized by eight wet months during the year, October to May, and 4 dry months from end of May to early October.

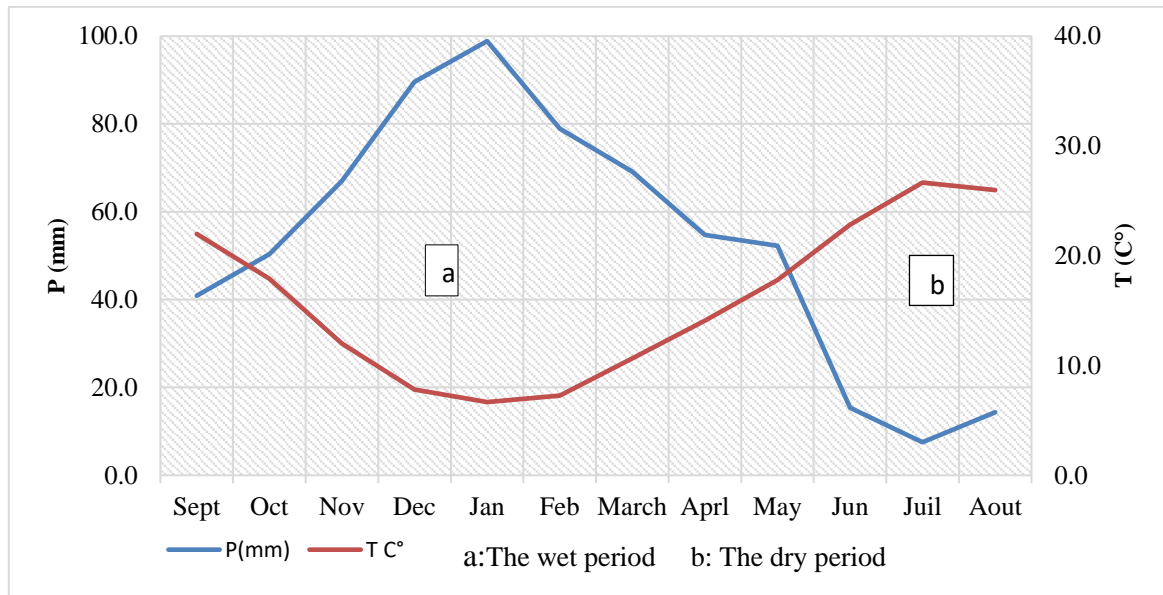


Figure III.9: Rainfall-thermal diagram of the study area.

5. Determination of climatic indices

5.1- Emberger climagram

In order to determine the climate types in the Mediterranean region, L. Emberger suggested determining a precipitation quotient Q . This quotient depends on the average annual precipitation and the average minimum and maximum temperatures of the coldest and hottest month.

$$Q = \frac{P}{\frac{M + m}{2} (M - m)} \cdot 100$$

With P: The average annual precipitation (in mm);

M: average of the maxima of the hottest month (degrees/kelvin);

m: average minima of the coldest month (degrees/kelvin).

According to Emberger's climagram fig. 10 the study area has a semi-arid climate.

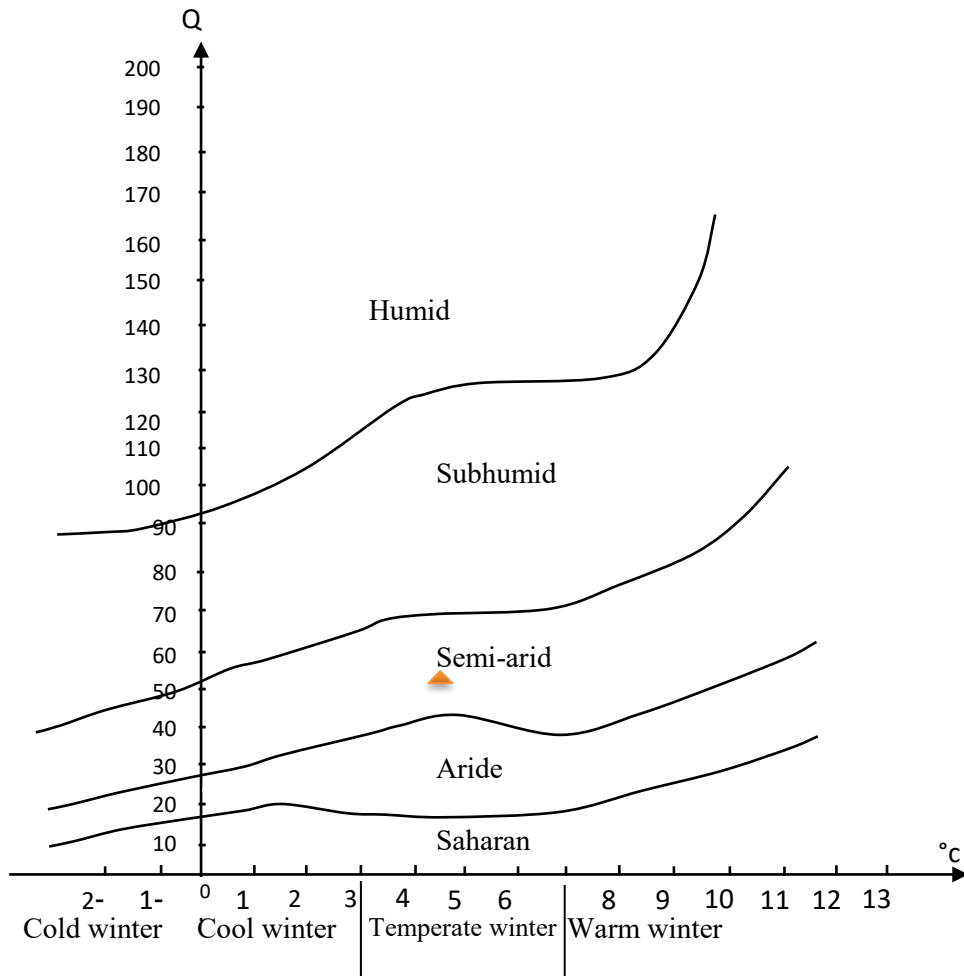


Figure III.10: representation of the climate of the study area on the Emberger climagram.

The aridity index (I) is a quantitative indicator of the degree of water scarcity in a given location (Oliver, 2006). This index takes into account the average annual precipitation and the average annual temperature. It is calculated using Martinne's (1923) formula:

$$\text{Aridity index} : I = \frac{P}{T+10}$$

P: average annual precipitation (mm). T: Average annual temperature (°C).

Table III.3: Martonne classification of climate type, according to the values of "I"

$I < 5$: Hyperarid climate
$5 < I < 7,5$: Desert climate
$7,5 < I < 10$: Steppe climate
$10 < I < 20$: Semi-arid climate
$20 < I < 30$: Temperate climate.

Through climatological data $P=704.8$ mm and $T= 16$ °C=>ce which gives $I= 27.10$.

Consequently $20 < I < 30$ the study area is characterized by a temperate climate.

According to this classification, the climate is temperate for the station:

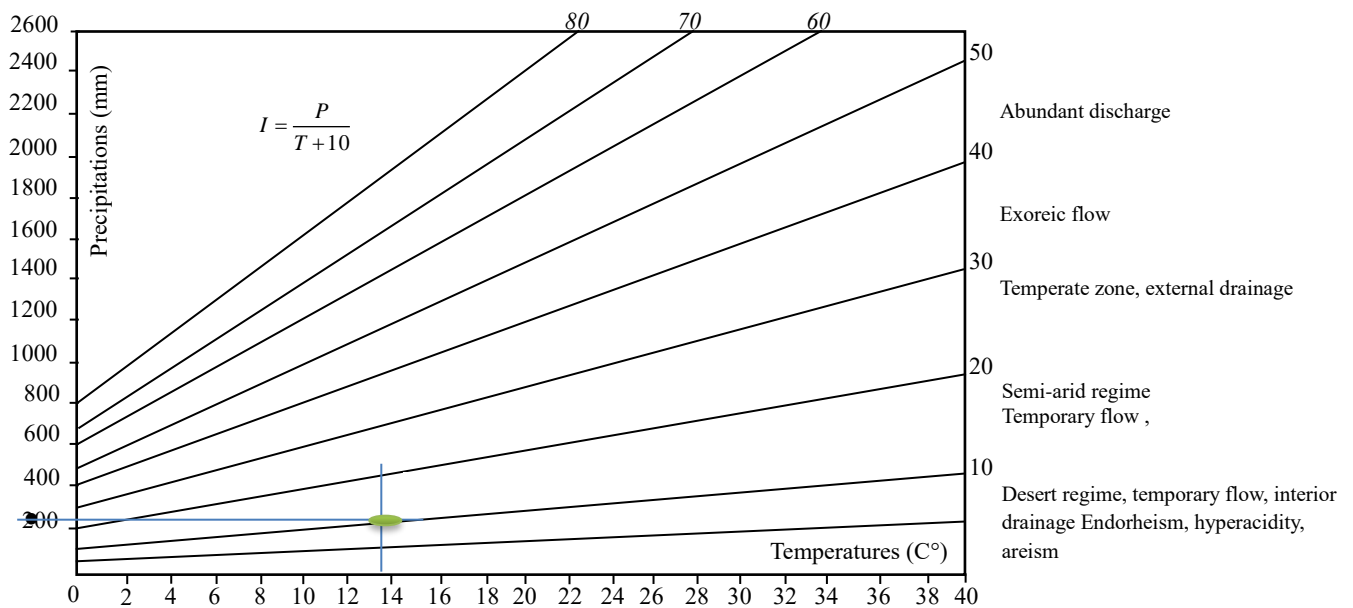


Figure III.11: Representation of the study area on the Martonne Aridity Index abacus (1923).

(HR).

5.2- Soil moisture

Soil moisture is the result of the intrusion of water in its various forms into the pore spaces of the soil. The water can come directly from rain or snow or hail, or the condensation of atmospheric vapor on the soil surface, as well as the vapor phase in the soil. It is expressed as a percentage of the mass of water in the soil to the mass of dry soil. It therefore plays a key role in the differentiated assessment of water and energy balances. Using soil moisture information to define hydro-meteorological thresholds is a possible avenue for improvement.

Soil moisture is one of the most important determinants of health or stress in terrestrial surface ecosystems and managed systems such as agriculture. Soil moisture monitoring provides the data needed to develop and implement plans to mitigate damage from rainfall scarcity, identify methods to improve soil moisture, and optimally manage natural ecosystems under the threat of climate change. (Monitoring, observations and global dimensions of remote sensing).

From a geotechnical point of view, soil moisture plays a crucial role as increased pore water pressure decreases soil strength and increases overall stress. (Relationships between remotely sensed soil moisture, precipitation and landslide events)

Table III.4: Monthly averages of soil moisture in the study area, (period: 2000-2019).

	Sept	Oct	Nov	Dec	Jan	Feb	Mar	Apr	May	Jun	Jul	Aout	interannual
Average	17.9	18.4	37.1	76.92	127.2	108.8	77.9	54.8	45.7	31.6	24.4	20.1	average (2000-2019) 53,4 mm
Avg. Seas	Autumn			Winter			Spring			Summer			
mm %	24.4		11.45	104.30		48.83	59.47		27.84	25.37	11.88		

Analysis of the data in Table 04 and Figures 10 and 11 shows that the relative soil moisture content in the Souk Ahras region varies from a minimum of 17.9% in September to a maximum of 127.2% in January with an annual average of 53.4 mm. The driest season is autumn with an average relative humidity of 11%. While the wettest season is winter, relative humidity reaches 49%.

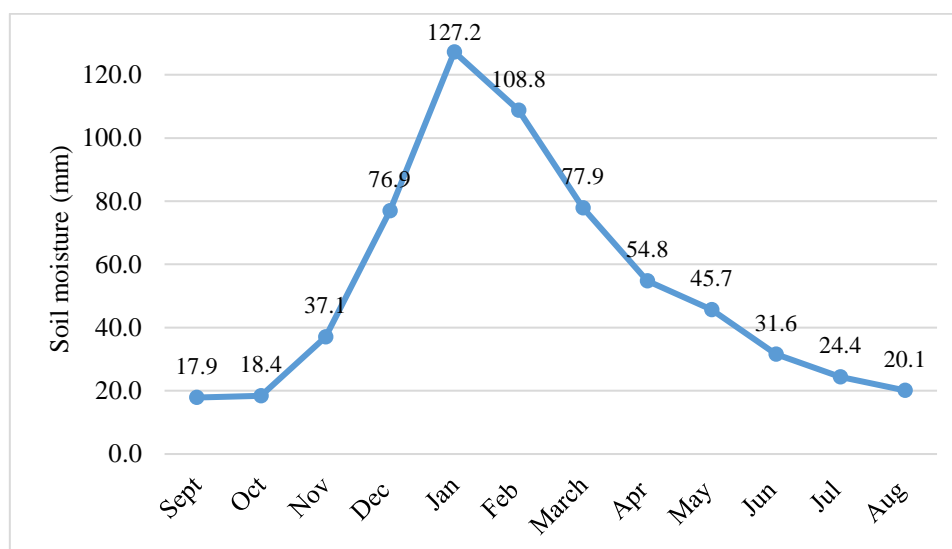


Figure III.12: Variation of monthly average soil moisture (mm) (2000-2019).

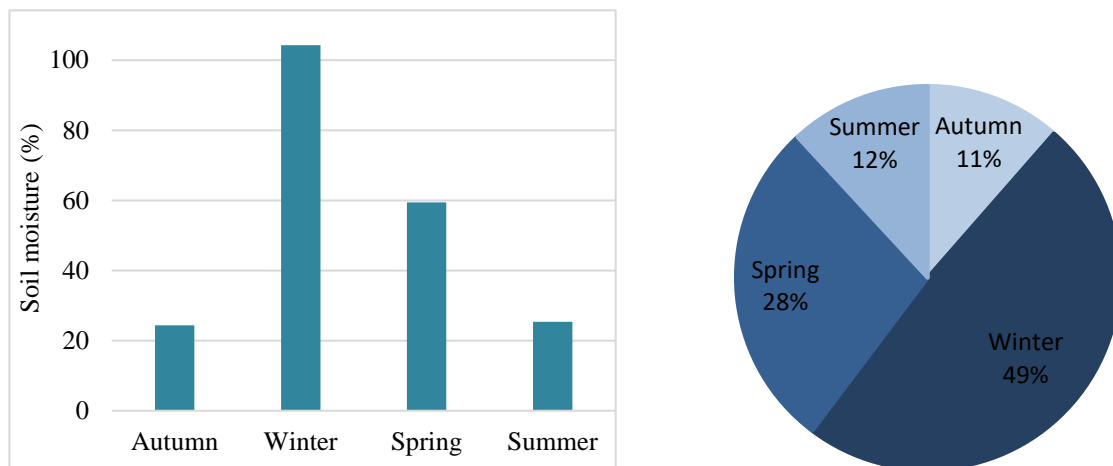


Figure III.13: Variation in monthly average relative soil moisture (%) (2000-2019).

5.3- Water balance

The water balance expresses the process followed by a quantity of water arriving on the ground by precipitation or snow before returning to the atmosphere.

The natural water balance can be calculated using the following formula:

$$P = ETR + R + I$$

- ETR: Average evapotranspiration (mm).

- I: Infiltration.

- P: Precipitation.

- R: Runoff.

5.4- Evapotranspiration

Evapotranspiration is a result of two phenomena: evaporation (physical) and transpiration (biological) and depends on several factors (temperature, humidity, plant cover etc) and also play a very important role in the water cycle.

This term includes both the evaporation of moisture soils and the transpiration of plants and animals. We can distinguish Actual evapotranspiration ETR and potential evapotranspiration ETP.

5.4-1. Actual evapotranspiration ETR

Actual evaporation ETR is the amount of water evaporated from the ground, open water surfaces, or transpired by plants. At some specific humidity of the soil, and when the plants are at a stage of real physiological and sanitary development the ETR is greater than or equal to the soil water storage (RFU)

Turk's formula expresses the actual annual evapotranspiration as a function of the annual precipitation and the annual mean temperature.

$$ETR = \frac{P}{\sqrt{0.9 + \frac{P^2}{L^2}}}$$

P: Average annual precipitation in (mm)

$L = 300 + 25t + 0.05t^3$, which T is the average annual temperature in (°C).

5.4-2. Potential evapotranspiration ETP

Potential evapotranspiration is the evapotranspiration from a surface that would be sufficiently supplied with water. It correspond to the maximum possible amount of water allowed to evapotraspirate in a given climatic conditions.

The uncorrected potential evapotranspiration is given by G.W. Thornthwaite Formula:

$$ETP = 16 \cdot (10T/I)^a \cdot F(\lambda)$$

$$a = (16/100) I + 0,5 \quad I = \sum_{i=1}^{12} i \quad \text{which} \quad i = (T/5)^{1.514}$$

T: average monthly temperatures in (°C);

I: annual thermal index;

i: monthly thermal index;

F (λ): correction factor integrating the duration of insolation and the number of days of the month.

The corrected potential evapotranspiration is obtained by multiplying Thornthwaite's formula by the correction coefficient k which depends on the latitude.

5.5- Runoff

In hydrology, the Runoff includes the quantity of rainwater that cannot gain entrance into the soil and cannot go into the atmosphere via evapotranspiration. It is the amount of water that flow by gravity in the streams.

Table III.5: Monthly averages of Runoff in the study area, (period: 2000-2019).

	Sept	Oct	Nov	Dec	Jan	Feb	Mar	Apr	May	Jun	Jul	Aout	Interannual average (2000-2019) 639.2 mm
Average	2	2.5	3.4	12.4	33.8	26.7	10.4	3.9	2.7	0.7	0.3	0.7	
Avg. Seas	Autumn			Winter			Spring			Summer			
mm	%	2.6	7.93	24.3	73.27	5.67	17.08	0.567	0.71				

GEE climate data base was used to extract runoff values for the period (2000-2019) for the study area .table 05 summarizes the runoff for the different seasons , it is maximan in winter with a value 24.3 mm and a minima with a value 0.56 mm in the summer . The total runoff average value over the years is 639.2 mm.

The value of the runoff estimated by the TEXIRON-BERKALOFF formula:

$$R = \frac{P^3}{3ETP^2}$$

For our area study, runoff is estimated at:

P: 639,2 mm , ETP = 846,8 mm ,

R=(639.2)³/3(846.8)²= 121.40 mm

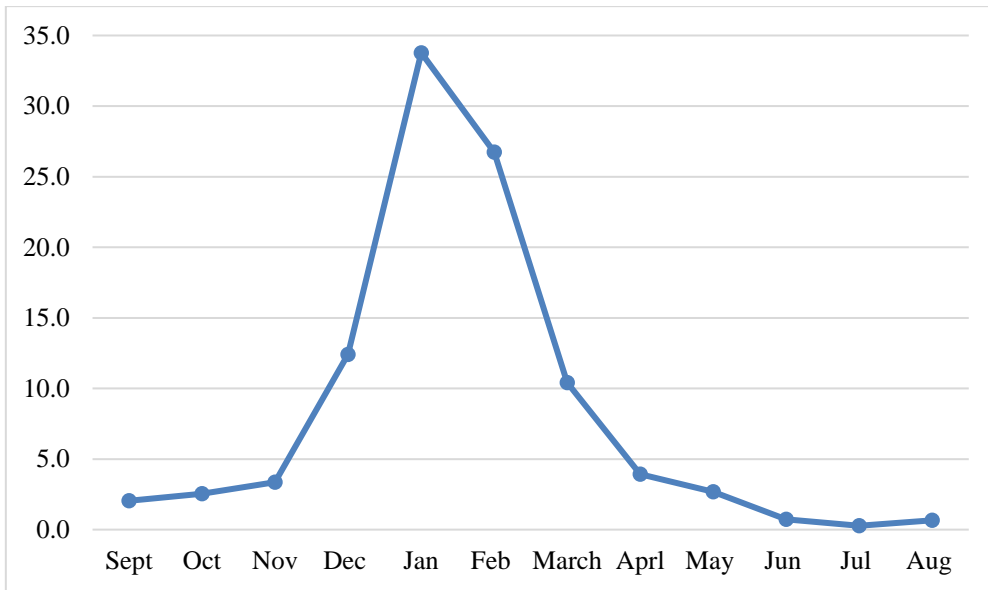


Figure III.14: Variation of monthly average runoff (mm) (2000-2019).

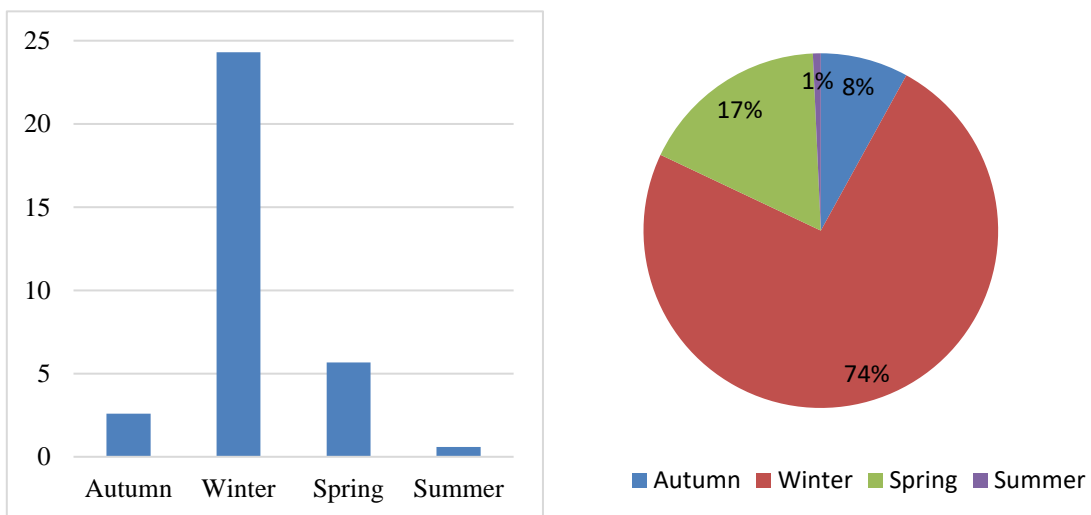


Figure III.15: Variation in monthly average relative runoff (%) (2000-2019).

5.6- Water infiltration calculation

Water infiltration correspond to the amount of water that passes from the surface into the of the soil interior, thus supplying reserves of groundwater.

It is calculated by the following formula: $I = P - (R + ETR)$

P=639,2 mm, ETR= 426,5 mm, R= 121.40 mm

Which give: I = 91.3 mm, I%=I/Px100 = 14.28%

The water balance for the area of study for the period between 2000 and 2019 is presented in table (06). It allows seeing the extent of the drought period which extends over a good part of the year.

Table III.06: showing the water balance of Souk Ahras region.

	T	IT	CL	ETP_c	P	BH	CH	VR	RFU	ETR	Def	Exc
S	22	9,4	1,03	102,8	40,9	-61,9	-0,6	0,0	0,0	40,9	61,9	0,0
O	17,9	6,9	0,97	66,0	50,4	-15,6	-0,2	0,0	0,0	50,4	15,6	0,0
N	12	3,8	0,86	30,7	67	36,3	1,2	36,3	36,3	30,7	0,0	0,0
D	7,8	2,0	0,81	15,3	89,6	74,3	4,8	63,7	100,0	15,3	0,0	10,6
J	6,7	1,6	0,87	11,2	98,9	87,7	7,9	0,0	100,0	11,2	0,0	87,7
F	7,2	1,7	0,85	12,7	78,9	66,2	5,2	0,0	100,0	12,7	0,0	66,2
M	10,6	3,1	1,03	29,8	69,2	39,4	1,3	0,0	100,0	29,8	0,0	39,4
A	14,1	4,8	1,10	46,0	54,8	8,8	0,2	0,0	100,0	46,0	0,0	8,8
M	17,8	6,8	1,21	84,3	52,2	-32,1	-0,4	-32,1	67,9	84,3	0,0	0,0
J	22,8	9,9	1,22	127,2	15,4	-111,8	-0,9	-67,9	0,0	83,3	43,9	0,0
J	26,7	12,6	1,24	167,1	7,5	-159,6	-1,0	0,0	0,0	7,5	159,6	0,0
A	26	12,1	1,16	153,7	14,4	-139,3	-0,9	0,0	0,0	14,4	139,3	0,0
Annuel	16,0	74,8		846,8	639,2	-207,6				426,5	420,3	212,7

T: monthly temperature in (° C); **P**: monthly precipitation in (mm); **IT**: thermal index **RFU**: easily usable reserves in (mm); **CL**: latitude coefficient; **ETR**: real evapotranspiration in (mm); **ETP** potential evapotranspiration in (mm); **Def.** : Agricultural deficit in (mm); **BH**: Water Balance; **Exc**: exceed in (mm).

6. Comments on the water balance

The water balance allows you to calculate the proportion of each hydrological parameter. We can take the following conclusions based on the findings:

- 1- In January, the amount of precipitation reaches its peak (98.9 mm) .
- 2- The evapotranspiration reaches its peak in July (167.1 mm), when precipitation is at its highest (7.5 mm). The stock is reconstituted in December, with the RFU reaching its maximum (100 mm) until April, then remaining at 67.6 mm until the exhaustion Tot in May, then decreasing until the exhaustion Tot in June.

- 3- The deficit period begins in June and ends in October of the following year with a reading of 159,6 mm in July and 15.6 mm in October. During this period, physical decomposition is significant; the soil is fatigued by the lack of water volume, which is manifested by the shrinkage of the clay and the appearance of cracks generated by the traction.
- 4- The surplus water is significant from December to April (10.6 mm - 8.8 mm), which is when stability is challenged and the risk of ground movement grows due to the increasing amount of water in the soil and foundation;

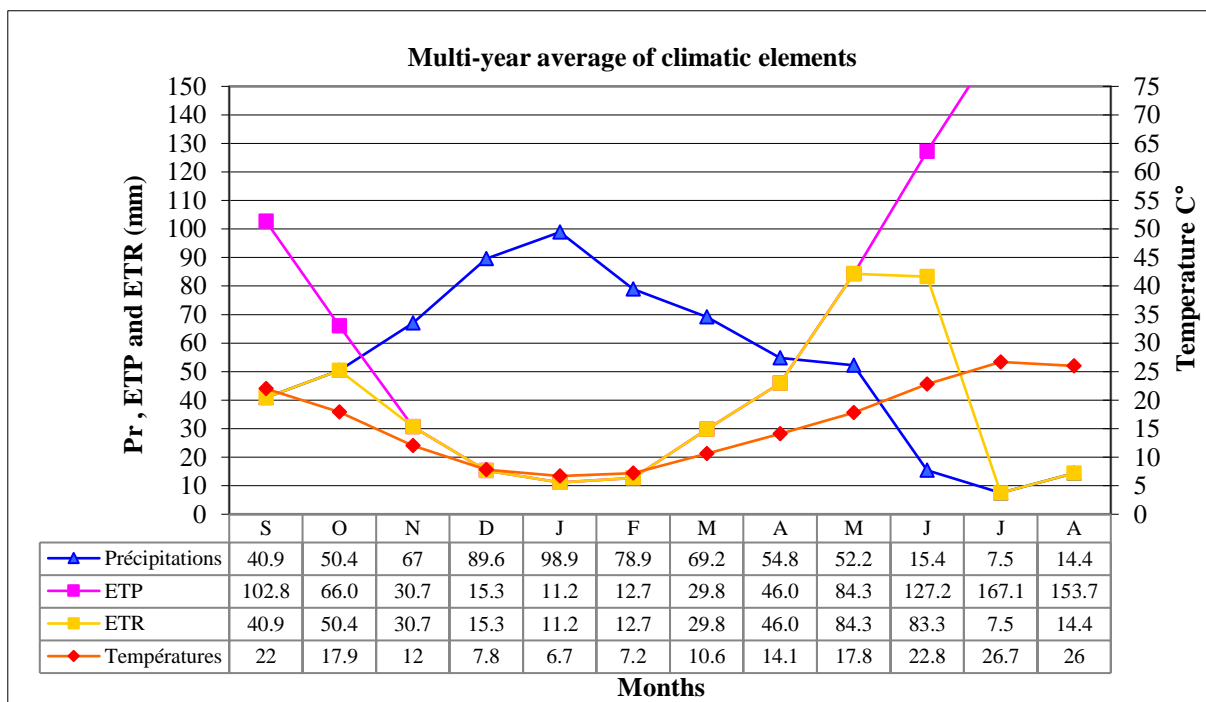


Figure III.16: Graphic representation of Thorn Thwaite's water balance sheet (Souk Ahras 2000-2019)

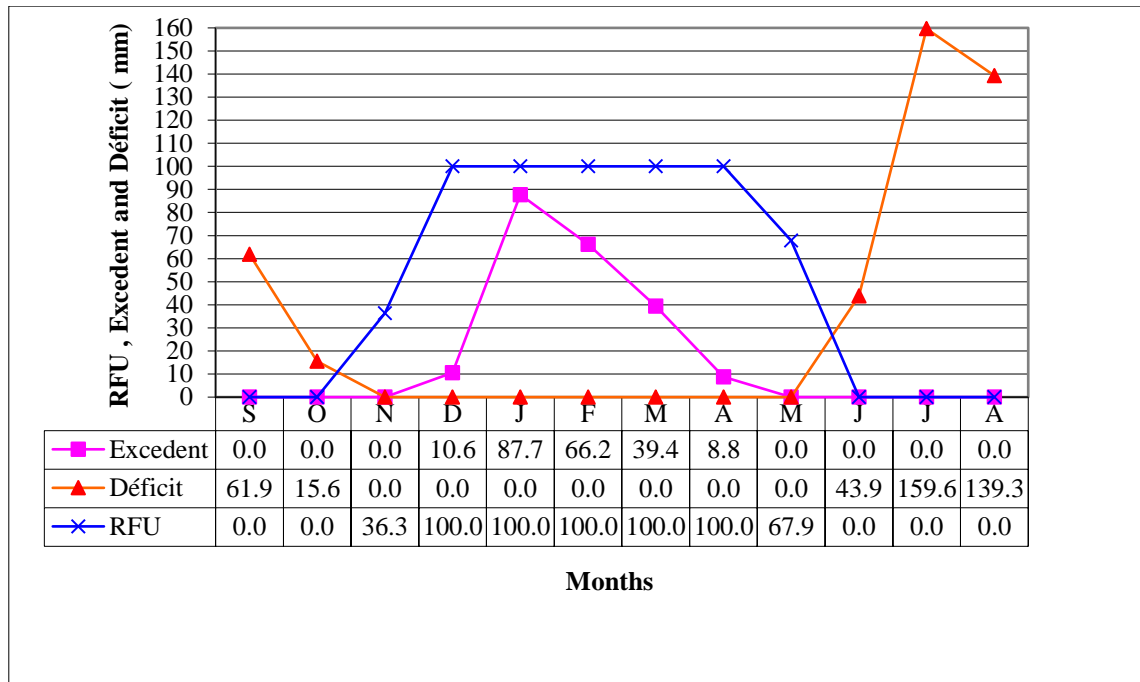


Figure III.17: Graphic representation of the hydrological balance (Souk Ahras 2000-2019).

7. Conclusion

The above bibliographic review enabled us to create an important database for studying the influence of various parameters on the formation of landslides in the Souk Ahras region. The hydroclimatic study of the study area shows more or less variable precipitation in terms of time and space; Temperatures are showing a slight gradual increase reflecting global warming. The hydro climatological investigations led to the conclusion that our study area is characterized by :

- A semi-arid climate confirmed by the Emberger climate chart.
- Precipitation is not homogeneous throughout the area; The average annual rainfall over a 20-year period (2000-2019) is estimated at 639,2 mm.
- The average annual temperature in the Souk Ahras precipitation station is about 16 °C.
- Actual evapotranspiration is estimated at 426, 5 mm or 64.04% of total precipitation.
- The runoff calculated using the Tixeront-Berkaloff formula is 121.40 mm.
- Infiltration is very important $I = 91.3$ mm or 14.28% of precipitation, as it plays a crucial role in triggering landslides.

**Chapter IV: Historical
Development of Unsaturated
Soil Mechanics**

1. Introduction

Throughout human history, man has always used earthly materials to create what he needs to survive. He built shelters, houses, bridges, fortified defenses, and water channels to protect himself, his family, and his tribe from predators of all kinds. Although these activities are of a primitive form, they require a high level of intelligence and skill in soil mechanics and civil engineering. In modern times, the need for large structures such as bridges for large traffic loads, high-rise buildings to accommodate thousands of people in one place, hospitals, large factories and large hydroelectric dams with the necessary safety standards has made resorting to soil mechanics of great interest. Although soil mechanics began in the dawn of mankind, it only became what it is in the late 20th century. Western Europe and the North of the USA were the first to tackle this area of research and application.

Soil mechanics went through several stages of development from the preclassic era to AD 1776, when Henri Gautier (1660–1737) began designing retaining walls on the same principles, resulting in a stable state of natural slope. Coulomb C. A. (1773) began using classical mechanics laws of friction and cohesion to soil media for determining the actual slip area behind retaining walls. Coulomb and Mohr jointly founded the so-called Coulomb theory of failure according to Mohr. Boussinesq J. (1842–1929) developed the theory of stress distribution within a mass of soil. Rankine W. (1820–1872) simplified Coulomb's earth pressure theory and Osborne Reynolds (1842–1912) demonstrated the phenomenon of dilatancy in sand.

2. Historic of soil mechanics

Soil mechanics has evolved greatly in three main phases. It mainly deals with pre-classical, classical and modern soil mechanics. Modern soil mechanics has been shaped by a number of important studies and publications on the mechanical behavior of clays. Albert Atterberg (1846–1916), a Swedish chemist and soil scientist, explained the consistency of cohesive soils by defining liquid, plasticity, and shrinkage limits. Arthur Bell (1874–1956), a civil engineer from England, developed relationships for lateral pressure and resistance in clay and the bearing capacity of shallow foundations in clay. Wolmar Fellenius (1876–1957), an engineer from Sweden, developed the circular method for analyzing slope stability.

Karl Terzaghi is generally considered the father of modern soil mechanics and geotechnics. With Terzaghi (1883–1963) modern soil mechanics took on their modern form. He defined soil mechanics as the application of the laws of mechanics and hydraulics to engineering

problems dealing with sediments and other unconsolidated accumulations of solid particles from mechanical and chemical decomposition of rocks, whether or not they contain an admixture of organic constituents. With his theories of consolidation, lateral earth pressure, load-bearing capacity and stability, he founded modern soil mechanics. His contributions have covered almost every topic in soil mechanics and geotechnics covered in textbooks: effective stress, elastic stress distribution, consolidation settlement, shear strength and in situ testing. His first book *Erdbaumechanik* appeared in German in 1925, which was later translated and published in 1926 under the title "Fundamentals of soil mechanics".

In his book *Theoretical Soil Mechanics* (1925), Karl Terzaghi introduced the principle of effective stress and found that the compressive stress in a saturated soil consists of two parts with very different mechanical actions. The first is the pressure of the water that does not produce any measurable compression or increase in shear stress. It is called the neutral stress (u_w). It is given by:

$$u_w = h_w \cdot \gamma_w$$

h_w : Can be positive or negative and as a result u_w can also be positive or negative.

3. The effective stress

In soil mechanics, the concept of effective stress introduced by Terzaghi (1925) was a breakthrough in understanding the behavior of saturated and unsaturated soils. It provided a rational framework for analyzing soil mechanical problems and allowed engineers to more accurately assess soil strength, settlement, and stability.

Since Terzaghi first introduced the concept, the understanding and application of effective stress has evolved significantly. Researchers and engineers have built on his work, refining theories and developing sophisticated models to analyze complex geotechnical problems. Nonetheless, Terzaghi's contributions remain central, and his concept of effective stress continues to be a fundamental principle in geotechnical engineering practice.

In a soil sample, the total stress is the sum of the weight of the soil particles and any externally applied loads. However, not all of this stress is transmitted between the soil particles.

$$\sigma' = \sigma - u_w$$

Where: σ' is the effective stress, σ is the total stress, u_w is the pore water pressure

The effective stress is of crucial importance as it determines the strength and deformation properties of soils. It determines the shear strength of the soil and influences

factors such as soil consolidation, slope stability and soil bearing capacity. It determines the shear strength of the soil and influences factors such as soil consolidation, slope stability and load-bearing capacity. When external loads act on a soil mass, they increase the overall stress. If the pore water pressure remains constant, the effective stress also increases, resulting in increased soil strength. Conversely, if the pore water pressure increases (e.g. due to groundwater rise or excessive pore water pressure developed during loading), the effective stress decreases, potentially leading to soil failure or instability.

Geotechnical engineers use the concept of effective stress extensively in analyzing soil behavior, designing foundations, assessing slope stability, and understanding the consolidation behavior of soils under applied loads.

4. Development of unsaturated soil mechanics

4.1. Definition:

The mechanics of unsaturated soils is a subfield of geotechnical engineering and soil mechanics that deals with the behavior and properties of soils that are not fully saturated with water. In unsaturated soils, also called partially saturated or moist soils, the voids between soil particles contain both air and water. In addition, the mechanics of unsaturated soils is important because many natural and engineered systems include unsaturated soils such as slopes, embankments, foundations, and agricultural land. Understanding the behavior of unsaturated soils is essential for predicting soil response, assessing stability and designing appropriate engineering structures.

The mechanics of unsaturated soils has its own theories, experimental techniques and modeling approaches to understand and predict the behavior of unsaturated soils. It complements the knowledge of the mechanics of saturated soils and promotes the understanding of soil behavior in different technical and ecological contexts.

The first international meeting on the behavior of unsaturated soils was organized in South Africa in 1957. The focus was on structural damage to buildings and other infrastructure. The colloquium will lead to a series of international discussions on the spacious floors. In the coming years; The conferences organized in London 1959, Colorado 1960 and Texas 1965 dealt with unsaturated soils but focused more on previous research, e.g. Terzaghi (1943), Hilf (1948), Seat (1948), Aitchison (1956), Aitchison and Donald (1956), Croney, Coleman & Black (1958) and Bishop (1959).

At the 1960 London Conference on Pore Pressure and Suction in Soils, 35% of the papers dealt with suction and the mechanics of unsaturated soils. At this conference Bishop

presented his famous four forms of the effective stress equation for unsaturated soils. The equations are as follows:

$$\text{Bishop: } \sigma^1 = (\sigma - u_a) + X(u_a - u_w) \quad (1.2b)$$

$$\text{Atchison: } \sigma^1 = \sigma + \psi P^{11} \quad \text{where } P^{11} = \text{pore water suction}, P^{11} = -u_w$$

$$\text{Cronney et al: } \sigma^1 = p - \beta^1 u$$

$$\text{Jennings: } \sigma^1 = \sigma + \beta P^{11}$$

where σ the total stress, and u_w the pore water pressure,

The Bishop equation had a more general application as it did not assume that the pore air was at zero (i.e. atmospheric) pressure. In the same year, 1960, a conference on the shear strength of cohesive soils was held in Boulder, Colorado, USA, with 11% of the work taking place on unsaturated soils. The concept of soil suction (osmotic or dissolved suction and matric suction) was clearly defined in a colloquium jointly organized by the Commonwealth Scientific and Industrial Research Organization, Australia, and the National Building Research Institute of Australia Scientific and Industrial Research Council, South Africa.

4.2- Matric suction:

In a triaxial apparatus, the matric suction is the quantity of water in the pore pressure measuring device that is isolated from the soil water by a water saturated porous stone instead of a semi-permeable membrane.

4.3- Solute (or osmotic) suction:

Solute (or osmotic) suction (Marshall, 1959) is the result of dissolved salts in the pore water creating an osmotic or dissolved pressure. Solute suction is defined as the negative pressure that must be exerted on a pool of pure, salt-free water to bring it into equilibrium with a pool containing a pore water-like solution across a semi-permeable membrane.

Bishop and Henkel (1957) published the first book, *The Measurement of Soil Properties in the Triaxial Test*, describing techniques for testing unsaturated soils. Later, Nelson and Miller (1992) published an important book called *Expansive Soils* and a second called *Problems and Practice in Foundation and Pavement Engineering*.

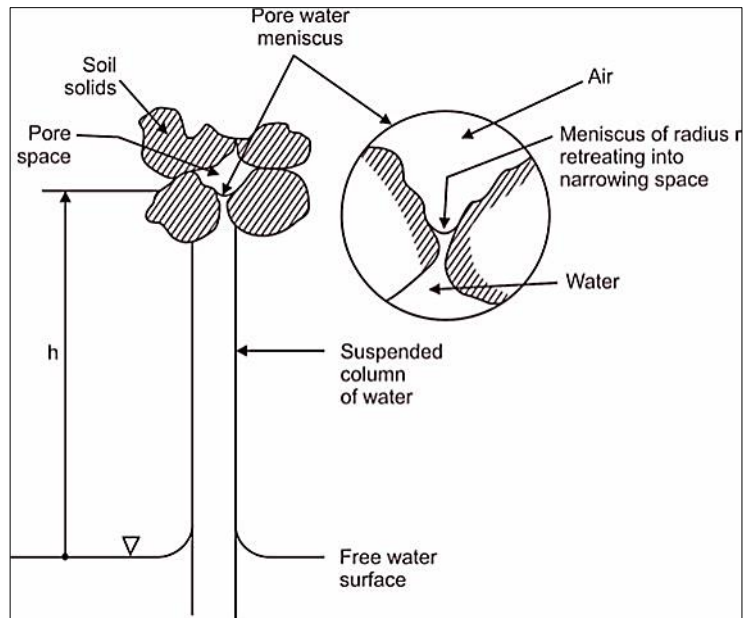


Figure IV.1: Capillary model of unsaturated soil.

In 1993 Fredlund & Rahardjo published a more detailed book on the theoretical aspect of unsaturated soil mechanics as a result of numerous experiments obtained through laboratory tests. Fredlund and Rahardjo defined unsaturated soil as a medium with four phases: solid, water, air, and contractile skin (air-water interface) (Fredlund and Morgenstern, 1993). Fredlund (1977) presented his equation for the change in volume in an unsaturated soil:

$$\Delta e = Ct \Delta \log(\sigma - u_a) + Cm \Delta \log(u_a - u_w)$$

e = void ratio, Ct = compression index in terms of $(\sigma - u_a)$, and Cm = suction index in terms of void ratio and matrix suction.

In simpler terms, C_i is the slope of the relationship e versus $(-u_a)$ and C_m is the slope of the relationship e versus $(u_a - u_w)$.

In addition, they introduced the following shear strength equation τ_f :

$$\tau_f = c^1 + (\sigma - u_a) \tan \varphi^1 + (u_a - u_w) \tan \varphi^b \dots\dots\dots 1$$

Where φ^b is the angle indicating the rate of increase in shear strength relative to the suction force $(u_a - u_w)$. This equation is similar to Bishop's:

$$\tau_f = c^1 + (\sigma - u_a) \tan \varphi^1 + X(u_a - u_w) \tan \varphi^1 \dots\dots\dots 2$$

In other words, there is no difference between two equations, $\tan \varphi^b = X \tan \varphi^1$, other than symbols used for the Fredlund and Bishop parameters.

There are a number of effective stress equations that have been proposed since 1958. Table 1.

Table IV.1: The search for a description of effective stress in an unsaturated soil.

Author(s)	Date	Equation for effective stress	Equivalency to Bishop equation
Cronley, Coleman & Black	1958	Volume change $\sigma' = \sigma - \beta' u_w$	Assumed $u_a = 0$. With $u_a \neq 0$, $\sigma' = (\sigma - u_a) + \beta'(u_a - u_w)$
Bishop	1959	$\sigma' = (\sigma - u_a) + x(u_a - u_w)$	Suggested \times approximated by S_r
Lambe	1960	$\sigma = \bar{\sigma} a_m + u_a a_a + u_w a_w + R - A$	$\bar{\sigma} a_m + R - A = \sigma'$ $a_w = S_r, a_a = 1 - S_r$ Hence $\sigma' = (\sigma - u_a) + S_r(u_a - u_w)$
Aitchison	1961	$\sigma' = \sigma + \psi p^u$	Assumed $u_a = 0$. Putting $p^u = (u_a - u_w)$
Jennings	1961	$\sigma' = \sigma + \beta p^u$	i.e. $\sigma' = (\sigma - u_a) + \psi(u_a - u_w)$
Richards	1966	$\sigma' = (\sigma - u_a) + x_m(u_a - u_w) + x_s p_s^u$	$(u_a - u_w) =$ matric suction $P_s^u =$ solute suction
Kassiff & Ben Shalom	1971	Volume change: $\alpha p_s^u = \Delta s - \Delta s_a$ $s =$ suction, $P_s^u = \Delta(\sigma - u_a)$	$\alpha = \frac{\Delta(u_a - u_w)}{\Delta(\sigma - u_a)}$ Hence $\sigma' = (\sigma - u_a) - 1/\alpha(u_a - u_w)$
Fredlund & Morgenstern	1977	Volume change $\epsilon_v = \theta_w + \theta_a$ $\theta_w = \frac{(\sigma_x + \sigma_y + \sigma_z - 3u_a)}{3H} + \frac{(u_a - u_w)}{R}$	For isotropic stress: $\theta_w = \frac{(\sigma - u_a)}{H} + \frac{(u_a - u_w)}{R}$ $\theta_w = \{1/H\}\{(\sigma - u_a) + H(u_a - u_w)/R\}$
Fredlund, et al.	1978	Shear strength $\tau = c' + (\sigma - u_a) \tan \varphi^l + (u_a - u_w) \tan \varphi^b$	$\tau = c' + \{(\sigma - u_a) + \frac{\tan \varphi^b}{\tan \varphi^l}(u_a - u_w)\} \tan \varphi^l$
2 Decades later:			
Oberg & Sallfors	1997	$\tau = c' + \{(\sigma - u_a) + S_r(u_a - u_w)\} \tan \varphi^l$	equivalent if $S_r = \chi$
Khalili & Khabbaz	1998	Bishop's eqn with $\chi = (s/s_a)^{-0.55}$ if $s \geq s_a$, $\chi = 1$ if $s < s_a$ & $s =$ existing suction, $s_a =$ air entry suction	completely equivalent with value for χ
Sheng, et al.	2002	$\sigma' = \sigma - \delta_3(S_r)u_w, u_a = 0$	$\sigma' = (\sigma - u_a) - \delta_3(S_r)(u_a - u_w)$
Lu, et al.	2010	$\sigma' = (\sigma - u_a) + s$, if $s \leq 0$ $\sigma' = (\sigma - u_a) + s/[1 + \infty s^n]^{(n-1)/n}$ $s =$ existing suction α & n are fitting constants	Completely equivalent with value for χ . See section 2.7

5. What Is an Unsaturated Soil?

In contrast to saturated soils, which are considered to be two-phase, unsaturated soils consider four phases: the solid grains, the air, the water, and the contractile skin (Fredlund and Morgenstern, 1977). In unsaturated soils, the pore water pressure is generally negative. The soil horizon, which is normally unsaturated and whose degree of saturation is less than 100%, is called the vadose zone (Fig. 02).

Accordingly, the approach to study unsaturated soils needs to be different from saturated soils, particularly with regard to fluid flow, compressibility, and shear strength. Unsaturated soils also have a number of physical applications, namely water flux (and storage), air flux (storage and compressibility), heat flux (and storage), volume-mass change, and shear strength.

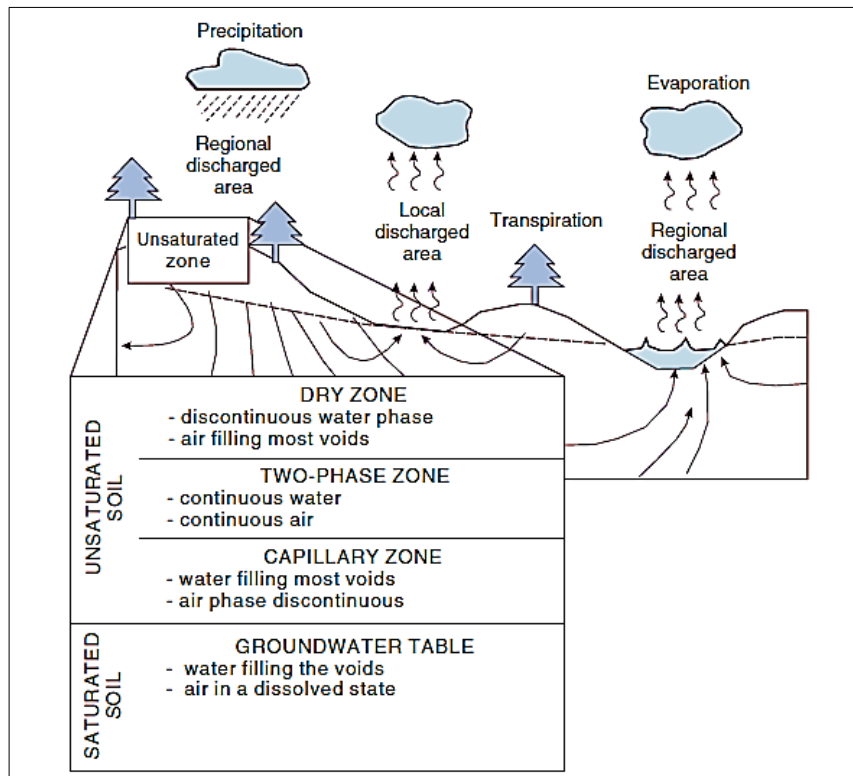


Figure IV.2: Subdivision of the unsaturated soil zone (vadose zone) at local and regional level (Fredlund et al 1993).

6. Typical profiles of unsaturated soils

The unsaturated state of a soil medium is highly dependent on the local climate. Soils that are unsaturated or have negative water pore pressure can be found in almost every geological deposit. They range from residual soils, lake deposits, bedrock formations to any other type of soil or rock. On the other hand, negative water pore pressures are often observed in certain geological soil types. For example, residual tropical soils are mostly in an unsaturated state due to their composition and the environment in which they are formed. The microstructure, which gradually changes with depth, is the most unique feature (Vargas, 1985; Brand, 1985). Figure 03 shows a typical deep tropical weathering profile (Little, 1969). The distinction between layers and changes in depth is rarely made. Many classification methods for residual soils have been developed, based primarily on weathering

and engineering characteristics (Deere and Patton, 1971; Tuncer and Lohnes, 1977; Brand, 1982). Saprolite is a term used to describe zones of fully or heavily weathered rock that contains soil particles but preserve the underlying rock structure. Laterite or residual soil is a deposit that bears little resemblance to the parent rock.

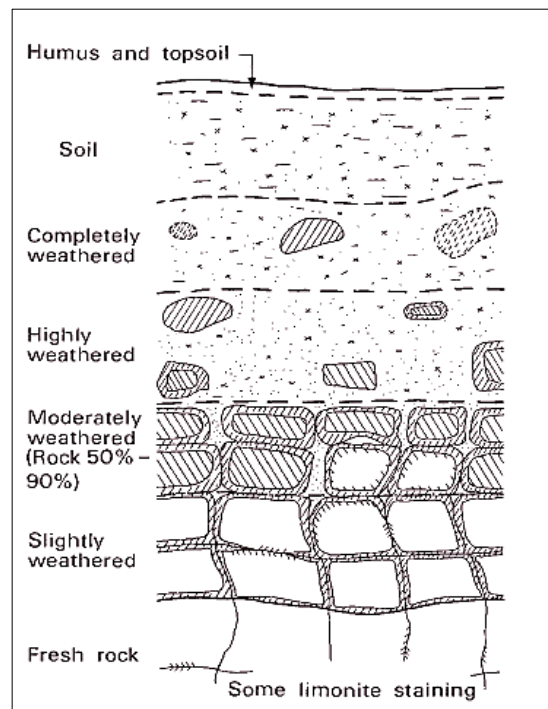


Figure IV.3: Schematic representation of the typical tropical residual soil profile (Little, 1969).

These soils tend to be problematic due to their volume changes during the transition from the unsaturated to the saturated state. The soil profile shown above is representative of conditions seen in many places around the world. The natural water content is always low and the pore water pressures are extremely negative. Soil expands and contracts in response to changes in net moisture flux at the soil surface during each season and from season to season. The possible expansion and contraction of the underlying soil is strongly influenced by climatic and man-made surface flow conditions at the soil surface.

7. Unsaturated soil properties determination

One of the fundamental differences in the behavior of saturated and unsaturated soils is the presence of suction pressure for the latter. This negative pressure has an enormous impact on the shear properties of the soil. Most unsaturated soil properties can now be measured in the laboratory. However, direct measurement of unsaturated soil parameters is time-consuming and expensive. As a result, research studies in different parts of the world

have produced a variety of methods for determining property functions of unsaturated soils (Fredlund, 2000a, Vanapalli et al., 1996a). The use of indirect methods has become standard practice in geotechnical engineering as direct laboratory testing of unsaturated soils has become prohibitively expensive for many engineering projects. However, they are only carried out in exceptional cases, for example for research purposes or in critical situations.

In the field of modelling, where both the permeability functions and the groundwater table are known, estimation techniques are enjoying increasing popularity. The estimation of unsaturated soil property functions provides a new philosophical framework for the implementation of unsaturated soil mechanics. The aim is to find out which estimation approach is better suited for characterizing unsaturated soil properties in a specific situation. Figure: 04 shows how the property functions of unsaturated soils can be determined using one of several methods. Testing unsaturated soils with soil suction measurements is the most direct application of unsaturated soil theories at the highest level. Compared to saturated soil tests, these tests are more demanding and time-consuming to perform.

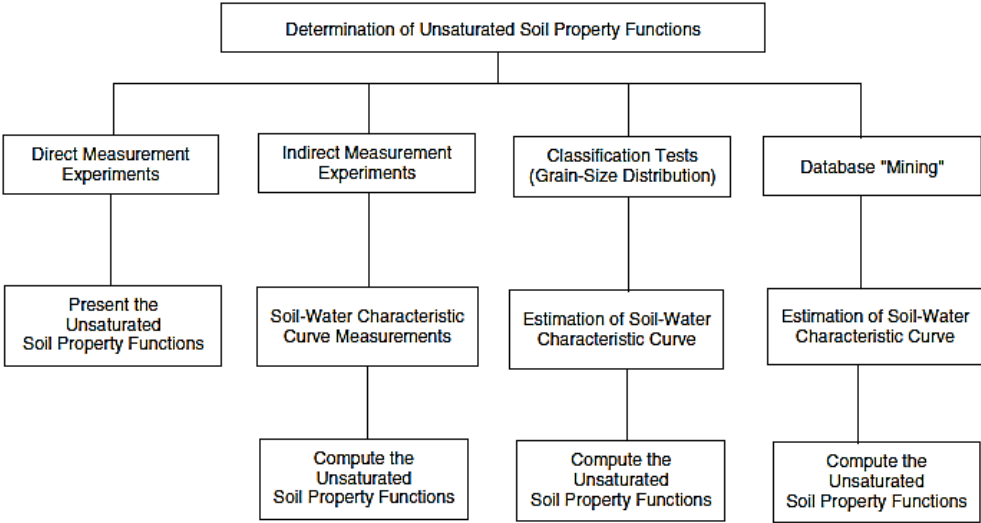


Figure IV.4: Methods for determining unsaturated soil property functions (Fredlund et al 2013).

Other methods of putting theories on unsaturated soils into practice have been proposed, such as using the SWCC in conjunction with saturated soil parameters to estimate unsaturated soil parameters. A SWCC can also be estimated using physical tests such as grain size distribution (Smith 1987) The approach is somehow similar to estimating the saturated hydraulic conductivity of a soil using the grain size distribution curve (Hazen, 1911).

8. Soil physical properties

Particle size distribution and plasticity are two laboratory tests commonly used in soil classification. With unsaturated soils, however, the categorization tests take on a whole new meaning. The particle size distribution curve shows the distribution of the solid particles and the percentage of each particle size. The distribution of solid particles and the distribution of pore diameters or cavities are related. The relationship between water content and soil suction power can be estimated from information about the pore size distribution. As a result, the particle size distribution becomes more important for understanding the behavior of unsaturated soils. The shrinkage curve shows that fundamental aspects of the behavior of unsaturated soils can be identified. It indicates the air intake value of the soil and the residual moisture condition.

8.1- Grain-size distribution curve

The particle size distribution of the soil is determined as a result of a test sieve analysis of the soil. The coarser fraction is that which is retained at a sieve size of 75 μm , while the finer fraction is less than 75 μm . For the coarser fraction we commonly use sieves, while for finer fractions we use the ASTM standard D422 sedimentometry technique. In other words, the particle size distribution curve provides information about the distribution of solid particle sizes in a soil and can be used to introduce concepts related to the behavior of unsaturated soils (Fredlund, 2000).

- **Equation for Grain-Size Distribution Curve**

Further investigations are based on a mathematical equation that maps the entire range of detected grain size particles. A particle size distribution equation gives you the flexibility to search databases for similar soils. The grain size equation gives you a continuous mathematical formula that you can use to calculate the SWCC. Most grain size distribution curves show a unimodal particle size distribution, while other soils show a bimodal particle size distribution. A mathematical equation can be used to describe both types of distributions. The use of a logarithmic normal equation has the disadvantage that a symmetrical particle size distribution is assumed. Grain size distribution curves, on the other hand, are often asymmetric and can be better fitted with other types of equations. A method is needed to more accurately describe bimodal or mottled soils. Well-graded soils, uniform soils, and gap-classified soils are the three types of grain size distributions (Holtz and Kovacs, 1981). Well sorted and uniform soils have a unimodal character, while incompletely sorted soils have a bimodal character.

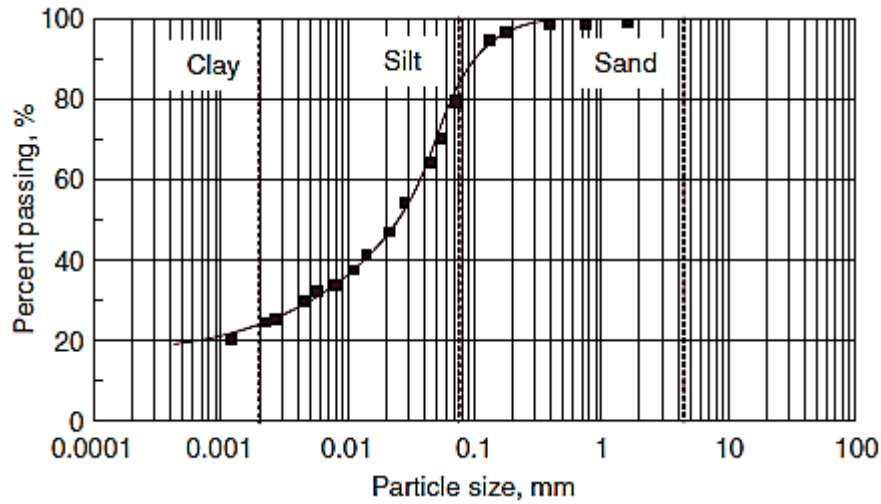


Figure IV.5: Grain size distribution curve data with unimodal fit for clay mud, best fit of grain size distribution data for clay mud (from M.D. Fredlund et al., 2000).

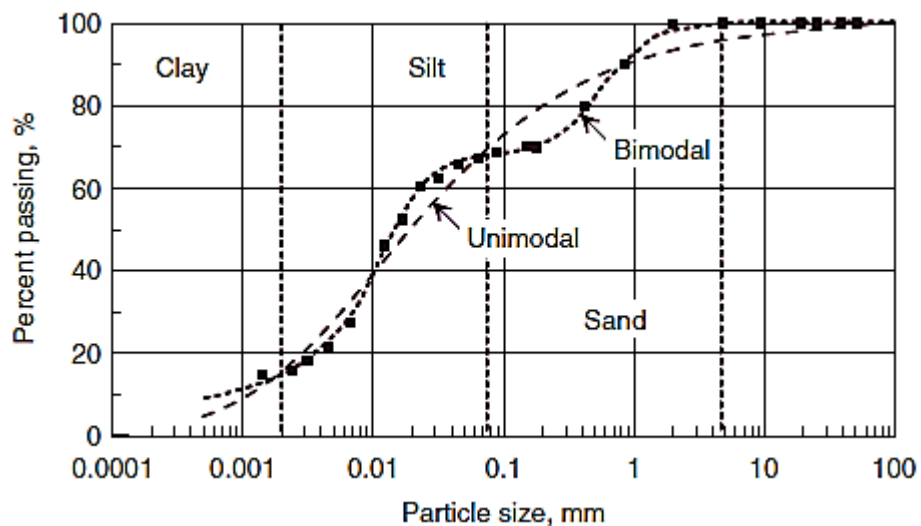


Figure IV.6: Gap bottom fit using the unimodal and bimodal grain size distribution equation (M.D. Fredlund et al., 2000).

- **Application of the particle size distribution function**

In geotechnics, a mathematical equation for grain size distribution data is very useful. First of all, the unimodal and bimodal grain size equations give the grain size distribution curve a continuous mathematical function. Second, equations that best fit the experimental data can be used to identify grain size distributions. Third, grain size distribution equations provide a consistent way to calculate physical indices such as % clay, % sand, and % silt, as well as particle diameter variables such like d_{10} , d_{20} , d_{30} , d_{50} , d_{60} , C_U and C_c . These parameters are defined as follows (Fig 7.): d = particle diameter, mm,

- ✚ % clay = percentage of clay-sized particles present in the soil (USCS definition is $d > 0.005$ mm),
- ✚ % silt = percentage of silt-sized particles present in the soil (USCS definition is $0.005 < d < 0.075$ mm),
- ✚ % sand = percentage of sand-sized particles present in the soil (USCS definition is $0.075 < d < 4.75$ mm),
- ❖ d_{10} = diameter at which 10% of the soil particles pass,
- ❖ d_{30} = diameter at which 30% of the soil particles pass,
- ❖ d_{60} = diameter at which 60% of the soil particles pass,
- ❖ C_u = Coefficient of uniformity, d_{60}/d_{10} and
- ❖ C_c = Coefficient of curvature, $d_{30}^2/(d_{10} \times d_{60})$

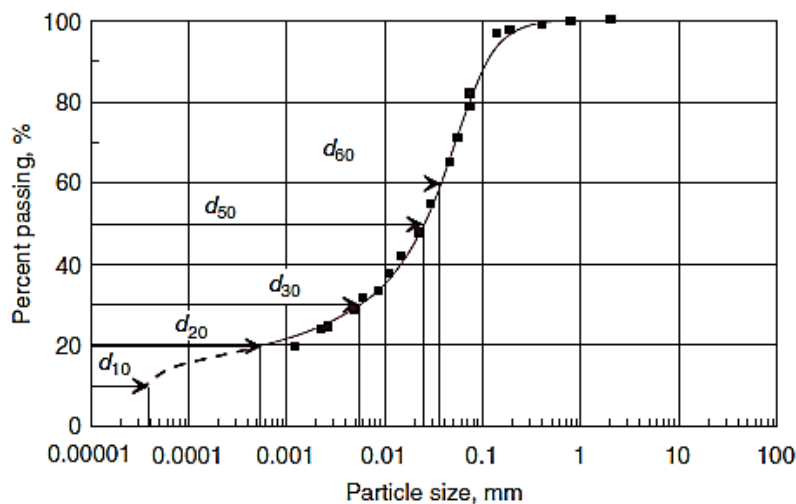


Figure IV.7: Determination of percentage passage for selected particle sizes, d (Fredlund et al., 2000).

- **Estimation of the soil-water characteristic curve from grain size data**

Soil water characteristics (SWCC) have also been estimated using grain size distribution curves (Gupta and Larson, 1979a; Arya and Paris, 1981; Haverkamp and Parlange, 1986; Ranjitkar and Sunder, 1989; M.D. Fredlund et al., 2000a). The SWCC explains the relationship between the mass (and/or volume) of water in a soil and the soil suction (fig. 13). The SWCC has been shown to be an interpretative model that uses the basic capillary concept to explain the distribution of water in the cavities.

In the geotechnical industry, a broad consensus has emerged on the methods of measuring and interpreting SWCC laboratory data. Information from the grain size

distribution curve was used to estimate the SWCC of a soil (Fredlund et al 1997). The grain size distribution curve gives information about the air pore value and the desaturation rate of the soil.

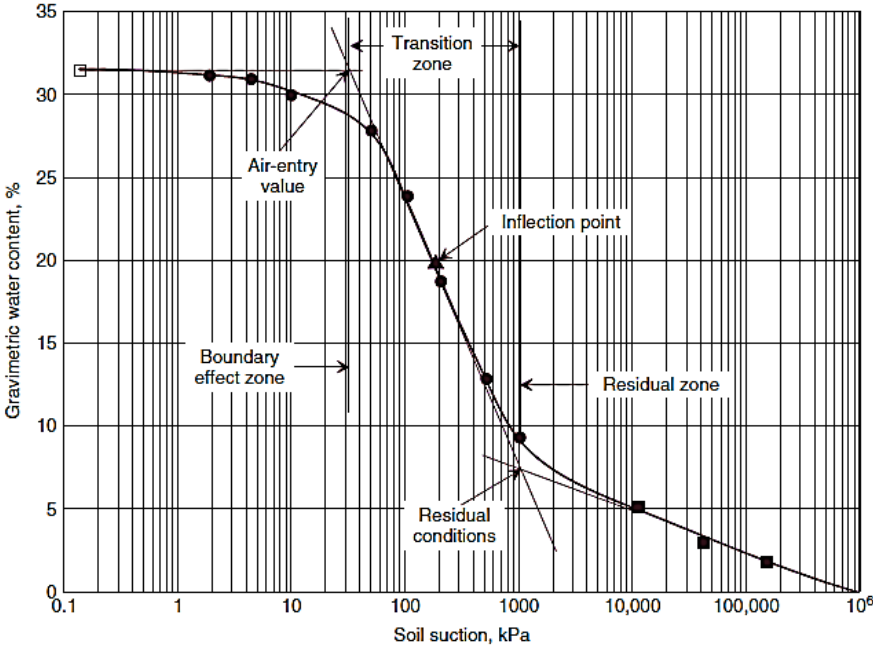


Figure IV.8: Typical desorption SWCC with clear desaturation zones.

8.2- Atterberg Limits

The Atterberg Limits characterize the differentiation of fine-grained soil conditions. Clay constituents can exist in four states depending on their moisture content: liquid, plastic, semi-solid, and solid. These limits are the most commonly used index parameter of all fine soil engineering tests, and are used for a number of technical purposes, including soil classification, earthwork specification, and estimating the geotechnical quality of soils.

More importantly, these tests provide a qualitative picture of how water interacts with solid particles and how the diffuse double layer forms. The plastic limit of a soil is the point at which the transition from a liquid to a semi-solid state occurs. The Shrinkage Curve Measuring an initially muddy soil provides information about the consistency of the soil in terms of gravimetric water content. If the soil is allowed to dry, the shrinkage curve starts in the liquid state and progresses through the plastic state, the semi-solid state and the solid state. In response to an increase in soil suction caused by soil drying, the soil goes through various phases. It is helpful to understand the shrinkage curve in response to changes in stress state (e.g. soil suction or negative pore water pressure).

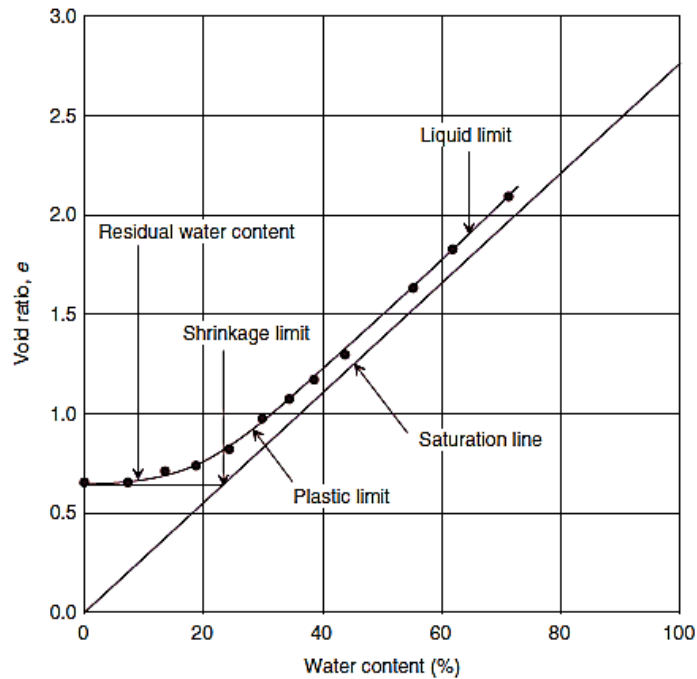


Figure IV.9: Relationship of Atterberg limits to shrinkage curve for initially highly plastic clay (data points generated).

8.3- The shrinkage limit

The Shrinkage Limit is the water content that corresponds to all voids filled with water when the soil has been dried to zero water content (and minimum void ratio) with no external stress. In other words, the shrinkage limit represents the maximum amount of water that can be injected into a completely dried soil without causing a volume change. The Standard Test Method for Wax Shrinkage Factors, ASTM D4943, is an alternative method for determining the shrinkage limit of cohesive material that does not use mercury. The shrinkage curve is part of the constitutive behavior of an unsaturated soil and can be used in conjunction with a SWCC to identify the relationship between volume change, void ratio (or specific volume) and soil suction.

9. Unsaturated soil phase properties

As we mention in the definition, unsaturated soil consists of four phases. Each phase has different properties than the adjacent materials. The amounts of mass and volume associated with each phase of an unsaturated soil are shown in the phase diagram (Fig 10). The contractile skin is very thin and only a few molecular layers thick.

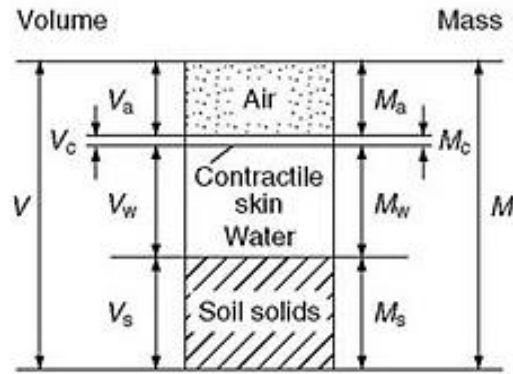


Figure IV.10: Phase diagram for unsaturated soil, it simplifies four phases.

9.1- The contractile skin

From a stress assessment point of view, the contractile skin (air-water interface) plays a crucial role. It also acts as an elastic membrane that influences the mechanical behavior of the soil by pulling the soil particles together through surface tension. The most characteristic property of contractile skin is its ability to exert a tensile force. It behaves like an elastic membrane that is woven under tension throughout the floor structure. Furthermore, when evaluating volume-mass relationships for an unsaturated soil, the water in the contractile skin does not need to be separated from the rest of the water mass (and volume). In other words, an unsaturated soil can be thought of as a three-phase system in terms of volume-mass properties, but as a four-phase system in terms of stress state conditions (Fig11.).

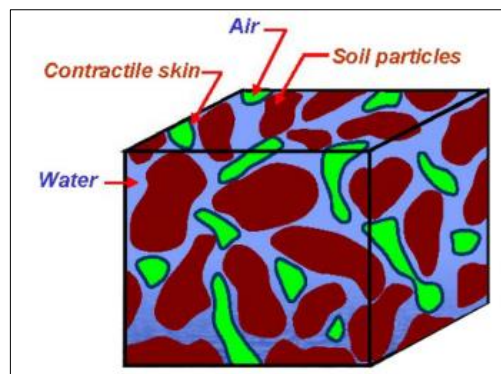


Figure IV.11: Element of unsaturated soil with continuous air phase (modified from Fredlund and Rahardjo).

9.2- Solid phase

This phase plays an important role in soil behavior. When only water is present, saturated soil results, and when water and air are used, unsaturated soil results. It gives the floor its technical properties such as density, specific volume and thermal properties.

- **Density of Solid**

The density of the solid phase, p_s , is defined as a mass to volume ratio as follows:

$$p_s = M_s/V_s$$

M_s = mass of solids and V_s = volume of solids.

Density and specific volume are used to define the volume to mass ratio of each phase. They can also be related to the density of water. Each phase of a soil mixture has a specific density. Soil particle density is commonly expressed as a dimensionless variable called specific gravity G . Soil particle specific gravity is defined as the ratio of the density of soil particles to the density of water at a temperature of 4°C under atmospheric pressure conditions (101.3 kPa). In the SI unit system, this quantity is now referred to as the relative density of the soil particles: $G_s = p_s/p_w$.

The density of water at 4 °C and 101.3 kPa is 1000 kg/m³. Table (02) shows typical specific gravity values for several common minerals.

Table IV.2: Specific Gravity of Several Mineral.

Mineral	Specific Gravity, G_s
Quartz	2.65
K feldspars	2.54–2.57
Na-Ca feldspars	2.62–2.76
Calcite	2.72
Dolomite	2.85
Muscovite	2.7–3.1
Biotite	2.8–3.2
Chlorite	2.6–2.9
Pyrophyllite	2.84
Serpentine	2.2–2.7
Kaolinite	2.61 ^a ; 2.64±0.02
Halloysite (2H ₂ O)	2.55
Illite	2.84 ^a ; 2.60–2.86
Montmorillonite	2.74 ^a ; 2.75–2.78
Attapulgite	2.30

Source: From Lambe and Whitman, 1979.
^aCalculated from crystal structure.

9.3- Water phase

The water phase has a significant impact on soil behavior. There are some physical properties of soils that are particularly interesting. Water exists in three states: liquid, solid, and vapor, and its properties are determined by temperature and pressure.

- **Density of Water**

The density of water, ρ_w , is defined as:

$$\rho_w = M_w/V_w$$

The variation in water density due to temperature differences is more relevant to geotechnical problems than the variation due to applied pressure. McCutcheon et al. (1993) proposed an empirical equation for the density of water with respect to temperature changes. The proposed closed equation for the density of pure water as a function of temperature is as follows:

$$\rho_w = 1000 \left[1 - \frac{(T + 288.9414)(T - 3.9863)^2}{508929.2(T + 68.12963)} \right]$$

where:

ρ_w = density of water, kg/m³, and

T = temperature, °C.

For most geotechnical problems it is generally assumed that the density of water under isothermal conditions is 1000 kg/m³.

Table IV.3 :Shows more accurate water densities over a temperature range.

Temperature (°C)	Density (kg/m ³)
+100	958.4
+80	971.8
+60	983.2
+40	992.2
+30	995.65
+25	997.05
+20	998.21
+15	999.10
+10	999.70
+4	999.97
0	999.84
-10	998.12
-20	993.55
-30	983.85

Source: From Lide, 1990.

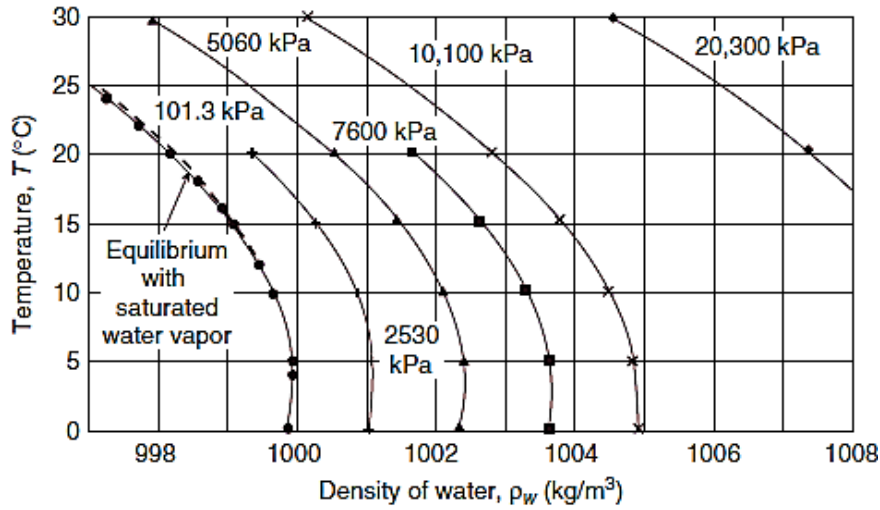


Figure IV.12: Density of pure water for different applied pressures and temperatures (from Dorsey, 1940).

9.4- Air Phase

The physical properties of the air phase change dramatically with temperature and pressure

- **Density of Air**

The density of air, measured in ρ_a , can be written as:

$$\rho_a = \frac{M_a}{V_a}$$

The specific volume of air, v_{a0} is:

$$v_{a0} = \frac{V_a}{M_a}$$

Air behaves like a mixture of several gases table (04) and also different amounts of water vapour.

Table IV.4: Composition of Dry Air

	Percentage by Volume	Density (kg/m ³)	Molecular Mass (Basis of Natural Scale, O = 16) (kg/kmol)
Nitrogen (N ₂)	78.08	1.25055	28.016
Oxygen (O ₂)	20.95	1.42904	32.000
Other gases	0.97		
Air	100.0	1.2929	28.966

^aUnder standard conditions (i.e., 101.3 kPa and 0°C) with no water vapor.

9.5- Interaction of Air and Water

Air and water behave both as an immiscible and miscible mixture. The immiscible mixture is a combination of free air and pure water with no interaction. The immiscible mixture is characterized by liquid-gas separation created by the contractile skin. A miscible air-water mixture can take two forms. First, air dissolves in water and can occupy about 2 percent by volume of the water (Dorsey, 1940). Second, water vapor can be present in the air. Different types of air-water mixtures are discussed in the following sections. The possible water conditions are also taken into account.

9.6- Surface tension

Surface tension is a characteristic of air-water contact (skin contractile). The surface tension phenomenon results from intermolecular forces acting on molecules in the contractile skin. These forces differ from those acting on molecules in water (Fig.13). A molecule in water experiences equal forces in all directions, meaning there is no unbalanced force. A water molecule in the contractile skin experiences an unbalanced force toward the water interior. In order for the contractile skin to be in balance, tension is created along the contractile skin. The ability of contractile skin to exert a tensile force is called surface tension T_s . Surface tension is measured as the tensile force per unit length of contractile skin (units N/m). The surface tension is tangential to the contractile skin surface. Their size decreases with increasing temperature.

Due to the surface tension, the contractile skin behaves like an elastic membrane. The behavior of the contractile skin is similar to that of an inflated balloon, where there is greater pressure inside the balloon than outside. When a flexible two-dimensional membrane is subjected to different pressures on each side, towards the greater pressure the membrane must acquire a concave curvature and exert tension in the membrane in order to be in equilibrium. The pressure difference across the curved surface can be related to the surface tension and the radius of curvature of the membrane (Fig. 13, b). The pressures acting on the membrane are u and $u + \Delta u$. The membrane has a radius of curvature R_s and a surface tension T_s . The horizontal forces along the membrane balance each other. This requires the balance of forces in the vertical direction.

$$2T_s \sin \beta = 2\Delta u R_s \sin \beta \dots\dots\dots 3$$

Where ; $2T_s \sin \beta$ = length of the membrane projected onto the horizontal plane.

Rearranging Eq.3 :

$$\Delta u = \frac{T_s}{R_s} \dots\dots\dots 4$$

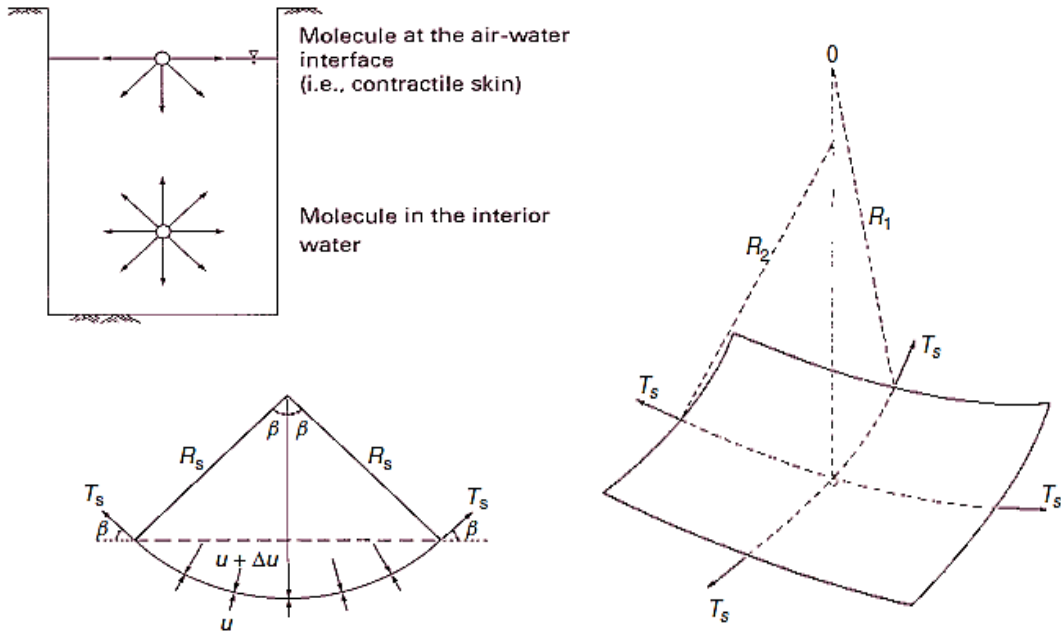


Figure IV.13: Surface tension phenomenon at air-water interface. (a) Intermolecular forces acting on contractile skin. (b) Surface tension forces associated with curved two-dimensional surface. (c) Surface tension on three-dimensional warped membrane.

Figure 13.c gives the pressure difference across a two-dimensional curved surface with a radius R_s and a surface tension T_s . For a warped or saddle-shaped surface (three-dimensional membrane), Eq 4 can be extended using the Laplace equation:

$$\Delta u = T_s \left(\frac{1}{R_1} + \frac{1}{R_2} \right) \dots \dots \dots 5$$

R_1, R_2 : radii of curvature of a warped membrane in two orthogonal principal planes.

if the radius of curvature is the same in all directions (R_1 and R_2 equal R_s), Eq.5 becomes

$$\Delta u = \frac{2T_s}{R_s} \dots \dots \dots 6$$

The contractile skin in an unsaturated soil is exposed to an air pressure u_a , etc., which is greater than the water pressure u_w , etc. The pressure difference $u_a - u_w$, is called matric suction (or capillary pressure) in a soil. The pressure difference causes the contractile skin to bend into a curvature given by Eq.6

$$u_a - u_w = \frac{2T_s}{R_s} \dots \dots \dots 8$$

The radius of curvature of the contractile skin decreases with increasing matrix suction of a soil. The curved contractile skin is often referred to as the meniscus. When the difference between pore air and pore water pressure approaches zero, the radius of curvature R_s approaches infinity. Therefore, a flat air-water interface exists when the matrix suction approaches zero. Interestingly, even under these conditions, the surface tension property of water remains at a constant value.

10. Volume-mass relations

There are a number of volumes, mass, and volume-to-mass relationships that constitute useful properties in geotechnical engineering practice. First the volume relationships are presented, then the mass relationships, and then the volume-to-mass relationships.

10.1- Volume Relationship

- **Porosity**

First, some simple variables for the relative volumes of the phases need to be introduced, as shown in figure 14. The porosity $n\%$ in percent is defined as the ratio of the void volume V_v to the total volume V which is composed of the volume of the voids V_v and the volumes of the solid phase V_s , V_w and V_a for the solid particles, the water and the air, making up the total volume of the soil V , respectively:

$$n = \frac{V_v}{V} (100) \dots 01 \quad , \quad n_s = \frac{V_s}{V} (100) \quad , \quad n_w = \frac{V_w}{V} (100) \quad , \quad n_a = \frac{V_a}{V} (100)$$

Where: n : porosity; n_s : the solid particle porosity; n_w : the water porosity; n_a : porosity of air.

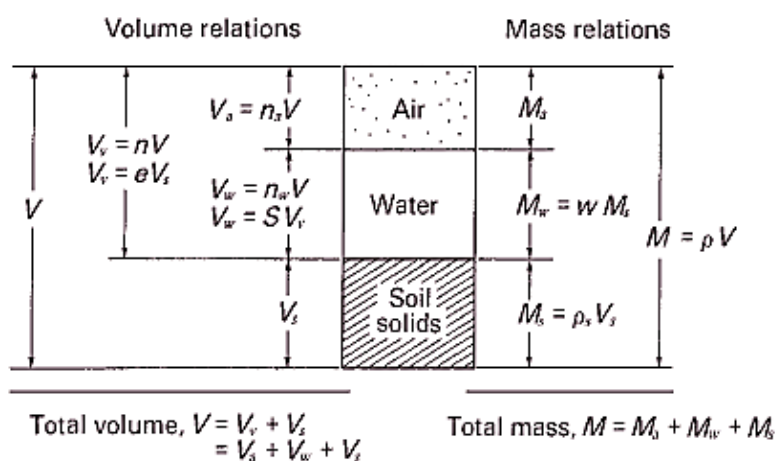


Figure IV.14: Relationship between volume and mass of unsaturated soil.

The porosities of water and air represent their percentage by volume in the soil. The porosity of soil particles can be represented as a percentage of the total volume of soil particles. The sum of the porosities of all phases must be 100%. Therefore, the following soil porosity equation can be written as:

$$n_s + n = n_s + n_a + n_w = 100\%$$

The water porosity n , expressed in decimal form, is generally referred to as the volumetric water content θ_w in the literature on soil science and soil physics.

- **Void Ratio**

The void ratio e is an alternative representation of the volumetric variable and is conveniently used to express volumetric changes in consolidation or compression tests, particularly for saturated soils. The pore ratio expresses the ratio of the volume of the pores to the volume of the solids:

$$e = \frac{V_v}{V_s}$$

The relationship between porosity and pore ratio is obtained by equating the pore volume V_v from the two equations 01 and 02:

$$n = \frac{e}{1 + e}$$

- **The degree of saturation**

The percentage of the void containing water is expressed as degree of saturation S_r (%):

$$S_r = \frac{V_w}{V_v} \times 100$$

With the help of the degree of saturation S_r , soils can be divided into three main groups, which can be described as follows. Dry soils ($S_r = 0\%$) consist of soil particles and air in which water is essentially absent. Saturated soils ($S_r = 100\%$) consist of soils whose cavities are filled with water. Unsaturated soils ($0\% < S_r < 100\%$) consist of a soil in which both air and water occupy the soil void.

An unsaturated soil can be further subdivided according to the continuity of the air phase and the water phase. For example, at high saturation levels ($85\% < S_r < 100\%$) the water phase may contain trapped air bubbles and the air phase is therefore discontinuous. Under these conditions, pore air and pore water combine to form a compressible liquid phase. However, at low saturation levels ($0\% < S_r < 15\%$), it is possible that the water phase becomes discontinuous and liquid flow through the soil practically stops.

Far better variables and ones that emerge naturally from thermodynamic analysis are the specific volume v , the specific water volume v_w and the specific air volume v_a defined as:

$$v = 1 + e = \frac{V}{V_s} \quad v_w = 1 + eS_r = \frac{V_s + V_w}{V_s} \quad v_a = e(1 - S_r) = \frac{V_a}{V_s}$$

- **The specific volume**

The specific volume v is defined as the total volume of soil per unit volume of solid, and the difference ($v - v_w$) is the volume of air voids per unit volume of solid v_a , often defined in the literature as the air void ratio e .

In fine-grained soils in the unsaturated state, the soil particles tend to come together as particle aggregates, typically the size of silt or sand, with relatively large voids between the aggregates. The water phase and the soil particles have a close affinity, and if the aggregates of the soil particles in an unsaturated soil contain all the water, v_w can be defined as the volume of the aggregates per unit volume of solid. Accordingly, the ratio of the specific volume of water to the specific volume expresses the volume of aggregates per unit volume of soil:

$$\frac{v_w}{v} = \frac{V_s + V_w}{V}$$

This equation contains a term for the volume of the solid particles and a term for the volume of the water phase. Since there is a term for the total volume, a term for the air phase is built into the formulation. The equation presents the volumetric terms for all phases in an unsaturated soil in a single formulation.

11. Water content relationships

The amount of water in a soil is generally expressed in two ways. The water content w (often called gravimetric water content) is expressed as:

$$w = \frac{M_w}{M_s} \times 100$$

M_w is the mass of the water and M_s is the mass of the solid particles. Water content w is also known as volumetric water content (gravimetric water content) w which is defined as the ratio of water volume v_w to total volume of soil V :

$$\theta_w = \frac{V_w}{V}$$

Volumetric water content can also be expressed in terms of porosity, degree of saturation and void fraction. This allows the volumetric water content to be written as:

$$\theta_w = \frac{SV_v}{V}$$

The above equation can be rewritten as $\frac{V_v}{V}$ equals the porosity of the soil

$$\theta_w = Sn$$

The volumetric water content equation can also be written as

$$\theta_w = \frac{Se}{1 + e}$$

The relationship between the gravimetric water content w and the volumetric water content can be written using the basic volume-mass relationship ($Se = wG_s$):

$$\theta_w = \frac{wG_s}{1 + e}$$

Given that specific gravity G_s can be written as ρ_s / ρ_w (ρ_s = density of soil solids and ρ_w = density of water) we can write: $G_s = \rho_s / \rho_w$

and using the definition for a soil's dry density, the volumetric water content can be written as dry density and the Density of the water:

$$\theta_w = w \frac{\rho_d}{\rho_w}$$

Gravimetric water content is the most commonly used in geotechnical engineering. It is important to know whether unsaturated soils are referred to as gravimetric water content or volumetric water content. SWCC data is often presented in terms of both volumetric water content and gravimetric water content. However, many geotechnical formulations, particularly those relating to fluid flow, use a volumetric representation of water content when calculating unsaturated soil property functions or performing further process analysis. The term degree of saturation may be the preferred representation of the water in the soil as the volume changes as soil suction is increased.

11.1- Volume-Mass Relations

Density and weight units provide information about the relationship between volume and mass designations of a soil. Saturated and completely dry conditions are special borderline cases of a variety of possible soil conditions.

- **Soil Density**

Two commonly used definitions of soil density are total density and dry density. The total density of a soil is the ratio of the total mass M to the total volume of the soil, V :

$$\rho = \frac{M}{V}$$

The overall density is also called bulk or wet density. The dry density of a soil, ρ_d , is defined as the ratio of the mass of soil solids, M_s , to the total volume of the soil, V :

$$\rho_d = \frac{M_s}{V} \quad \text{or} \quad \rho_d = \frac{G_s}{1+e} \rho_w$$

The total and dry density of the total soil mass can also be expressed in terms of other volume-mass properties of the soil (S_r , e , w and G_s). Assuming that the mass of the air phase, M_a , is negligible, the total mass of the soil is the sum of the mass of the water, M_w and the mass of the soil solids, M_s . The total volume of the soil, V , is divided by the volume of the soil solids, V_s . and the volume of the voids, V_v .

The density of a soil can be rewritten in the following forms:

$$\rho = \frac{M_s + M_w}{V_s + V_v}$$

$$\rho = \frac{G_s \rho_w V_s + w G_s \rho_w V_s}{V_s + V_v}$$

$$\rho = \frac{G_s (1+w)}{1+e} \rho_w$$

Substituting the basic volume-mass relationship ($S_r e = w G_s$) into $\rho = \frac{G_s (1+w)}{1+e} \rho_w$ results in the following equation for the total density:

$$\rho = \frac{G_s S_r e}{1+e} \rho_w$$

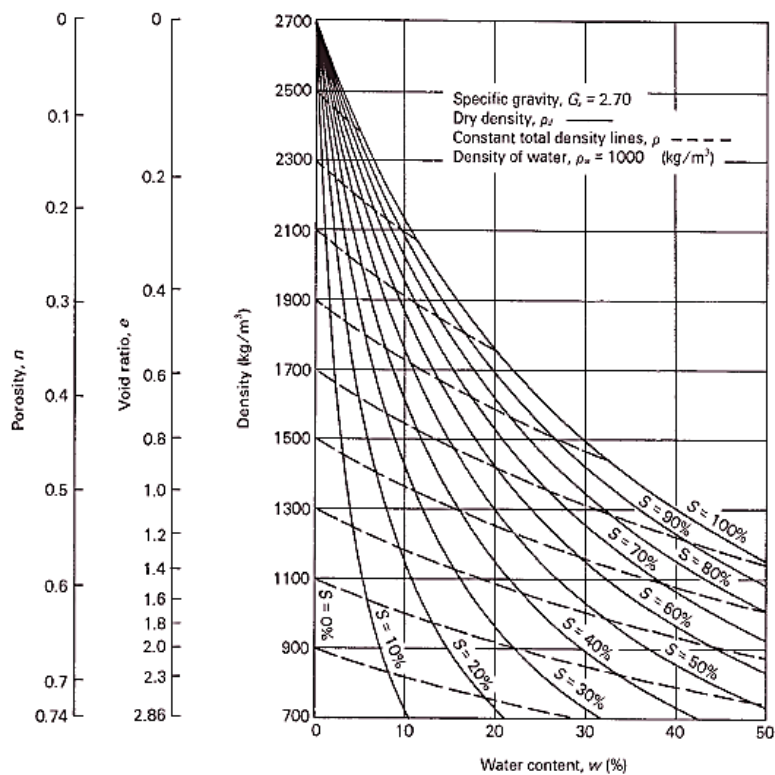


Figure IV.15: Relationship between volume-mass properties of unsaturated soil.

- **Unit Weight**

The unit weight of a mass of soil can be calculated by multiplying the total density of a soil by the acceleration of gravity \mathbf{g} (ρg). The unit weight of a floor is often referred to as the body force involved when gravity acts on the floor. The above equations for density can be written in the following unit weight forms:

$$\gamma = \frac{G_s (1+w)}{1+e} \gamma_w$$

$$\gamma = \frac{G_s S_r e}{1 + e} \gamma_w$$

12. Basic Volume-Mass Relationship

The basic volume-mass relationship is an equation commonly used to calculate phase relationship properties in unsaturated soil.

Volume and mass for each phase can be related to each other using basic relationships from the phase diagram fig 16. The mass of water in a soil, M_w , is the product of the volume and density of the water:

$$M_w = \rho_w V_w$$

Where $V_w = S_r e V_s$ so, we can write: $M_w = \rho_w S_r e V_s$

we can also write The mass of the water, $M_w = w M_s \dots \dots \dots 9$

from the diagram fig 15 The mass of the soil solids $M_s = G_s \rho_w V_s \dots \dots \dots 10$

Equating Eq. 9 and 10 gives a basic volume-to-mass relationship for soil:

$$S_r e = w G_s$$

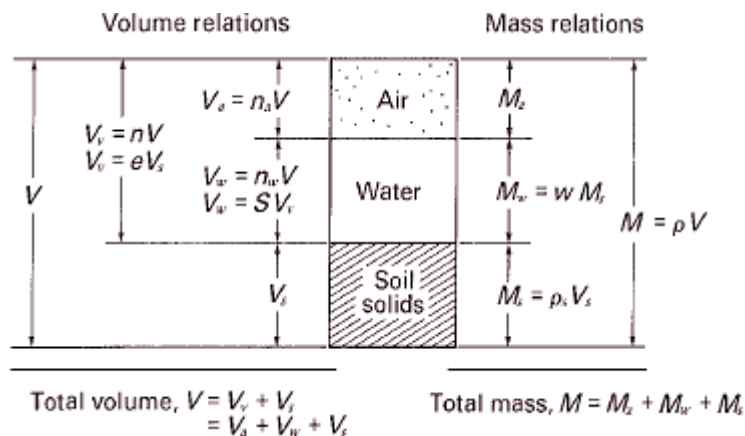


Figure IV.16: Relationship between volume and mass of unsaturated soil.

13. Shear strength of unsaturated soils

The shear strength of soils is a constitutive relationship. It is a one-valued equation that expresses the relationship between state variables. In more complex models such as the Barcelona base model (Alonso et al. 1990), the model formulation maintains the separation of load state variables and constitutive behavior. The most likely reason for the separation of stress state variables and constitutive behavior in these models is that there is more than one constitutive relationship and the use of two stress state variables allows more flexibility in formulating the constitutive relationships. The problem with effective stress for unsaturated soils is that they require a different form of effective stress for the constitutive relationships

of shear strength and volume change and therefore the stress state variables can be more easily separated (Fredlund 2015, Leong 2008).

The main controversy regarding the effective stress for unsaturated soils arises especially when only a constitutive relationship is examined. Sometimes this is due to a misunderstanding of the definition of the stress state variable combined with the form of the constitutive relationship. This is illustrated by a review of the shear strength equations proposed for unsaturated soils, as summarized in Table 05

The shear strength equation should apply to the full range of saturation . from dry to fully saturated. All of the shear strength equations in Table 2 satisfy this condition and revert to the shear strength equation for saturated soils.

$$\tau = c' + (\sigma + u_w) \tan \phi' = c' + \sigma' \tan \phi'$$

All of the shear strength equations in Fig. 16 can also be easily rewritten into the form of the Bishop and Blight (1961) shear strength equation:

$$\tau = c' + [(\sigma - u_a) + X(u_a - u_w)] \tan \phi'$$

Where X is Bishop's effective stress parameter. The equivalent forms of X for the shear strength equations are shown in Table 06. From Table 06 it can be seen that X can be expressed in terms of volumetric water content, degree of saturation, due suction and shear strength parameters. The different shapes suggest that X is not unique for different soil types. A fact well supported by experimental evidence is shown in Fig. 16

Table IV.5: Shear strength equations for unsaturated soils.

References	Shear strength equation	Notations
Fredlund et al. (1978)	$\tau = c' + (\sigma - u_a) \tan \phi' + (u_a - u_w) \tan \phi^b$	τ = shear strength c^0 = effective cohesion ϕ' = effective friction angle ϕ^b = angle indicating a change in shear strength related to matric suction
Lambom (1986)	$\tau = c' + (\sigma - u_a) \tan \phi' + \theta(u_a - u_w) \tan \phi'$	θ = volumetric water content
Vanapalli et al. (1996)	$\tau = c' + (\sigma - u_a) \tan \phi' + \frac{\theta - \theta_r}{\theta_s - \theta_r} (u_a - u_w) \tan \phi'$	θ_r = residual volumetric water content θ_s = saturated volumetric water content
Oberg and Salfors (1997)	$\tau = c' + (\sigma - u_a) \tan \phi' + S(u_a - u_w) \tan \phi'$	S = degree of saturation
Bao et al. (1998)	$\tau = c' + (\sigma - u_a) \tan \phi' + \left\{ \frac{\log \left[\frac{(u_a - u_w)_r}{(u_a - u_w)_b} \right]}{\log \left[\frac{(u_a - u_w)_r}{(u_a - u_w)_b} \right]} \right\} \times (u_a - u_w) \tan \phi'$	$(u_a - u_w)_r$ = residual matric suction $(u_a - u_w)_b$ = air - entry value
Khalili and khabbaz (1998)	$\tau = c' + (\sigma - u_a) \tan \phi' + \left[\frac{(u_a - u_w)}{(u_a - u_w)_b} \right]^{-0.55} \times (u_a - u_w) \tan \phi'$	
Aubeny and Lytton (2003)	$\tau = c' + (\sigma - u_a) \tan \phi' + f_1(\theta)(u_a - u_w) \tan \phi'$	8 $f_1(\theta)$ $= \begin{cases} \frac{1}{\theta} & \text{for } S = 100\% \\ 1 + \frac{S-85}{15} \left(\frac{1}{\theta} - 1 \right) & \text{for } 85\% \leq S \leq 100 \\ 1 & \text{for } S \leq 85\% \end{cases}$
Tekinsoy et al. (2004)	$\tau = c' + (\sigma - u_a) \tan \phi' + [(u_a - u_w) + P_a] \times \ln \left[\frac{(u_a - u_w) + P_a}{P_a} \right] \tan \phi'$	P_a = atmospheric pressure
Garven and Vanapalli (2006)	$\tau = c' + (\sigma - u_a) \tan \phi' + \left(\frac{\theta - \theta_r}{\theta_s - \theta_r} \right)^k (u_a - u_w) \tan \phi'$	$k = -0.00161I_p^2 + 0.0975I_p$
Vilar (2006)	$\tau = c' + (\sigma - u_a) \tan \phi' + \left[\frac{(C_{ult} - c')}{(C_{ult} - c') + (u_a - u_w) \tan \phi'} \right] \times (u_a - u_w) \tan \phi'$	C_{ult} = ultimate shear strength

Table IV.6: Equivalent X for shear strength equations listed in Table 5.

References	$\chi =$
Fredlund et al. (1978)	$\frac{\tan \phi^b}{\tan \phi^c}$
Lamborn (1986)	θ
Vanapalli et al. (1996)	$\left(\frac{\theta - \theta_r}{\theta_s - \theta_r} \right)$
Oberg and Salfors (1997)	S
Bao et al. (1998)	$\left\{ \frac{\log \left[\frac{(u_a - u_w)_r}{(u_a - u_w)} \right]}{\log \left[\frac{(u_a - u_w)_s}{(u_a - u_w)_b} \right]} \right\}$
Khalili and Khabbaz (1998)	$\left[\frac{(u_a - u_w)_r}{(u_a - u_w)_b} \right]^{-0.55}$
Aubeny and Lytton (2003)	$f_1(\theta)$
Tekinsoy et al. (2004)	$\frac{[(u_a - u_w) + P_a]}{(u_a - u_w)} \ln \left[\frac{(u_a - u_w) + P_a}{P_a} \right]$
Garven and Vanapalli (2006)	$\left(\frac{\theta - \theta_r}{\theta_s - \theta_r} \right)^k$
Vilar (2006)	$\left[\frac{(c_{uh} - c^c)}{(c_{uh} - c^c) + (u_a - u_w) \tan \phi^c} \right]$

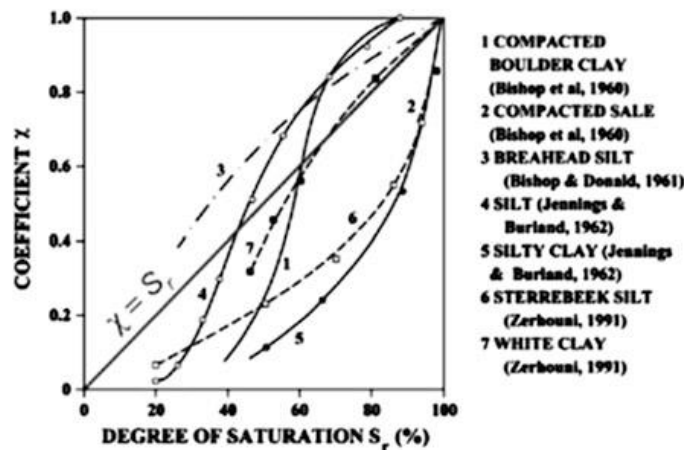


Figure IV.17: Effective stress parameter χ versus degree of saturation (from Zerhouni 1991).

14. Effective stress equations

Numerous equations have been proposed that relate one or more of the stress variables affecting a soil property to other stress variables. It is important to distinguish between the role of these equations and the description of the state of stress at a point on a continuum. There are theoretical and formulation limitations associated with the use of effective stress equations. The oldest and most frequently cited univalent effective stress relationship is that proposed by Bishop (1959).

The equation is commonly referred to as Bishop's effective stress equation for unsaturated soils and has the form:

$$\sigma' = (\sigma - u_a) + X(u_a - u_w)$$

σ' : effective stress X : a soil parameter related to degree of saturation and ranging from 0 to 1.

14.1- Stress State Variables for Unsaturated Soils

The technical performance of soil materials is governed by the same stress variables that control the balance of soil structure. For unsaturated soils these are the total stress s , the pore water pressure u_a and the pore air pressure u_w . These are the quantities required to describe the equilibrium of the soil structure and can be used as stress state quantities for the same soil.

14.2- Stress state variables

The independent sets of normal stresses from the equilibrium equation for soils in Fig 18 are:

$(\sigma_y - u_a)$, $(u_a - u_w)$ and u_a , which control the equilibrium stress state quantities for unsaturated soils. Therefore, contractile skin and soil structure independent tensors $(\sigma_y - u_a)$ and $(u_a - u_w)$ are considered stresses that can be used to represent the full form of the stress condition. Figure 18 shows two independent tensors acting on a component in unsaturated soils.(Augustin & Takoukam, 2018) .

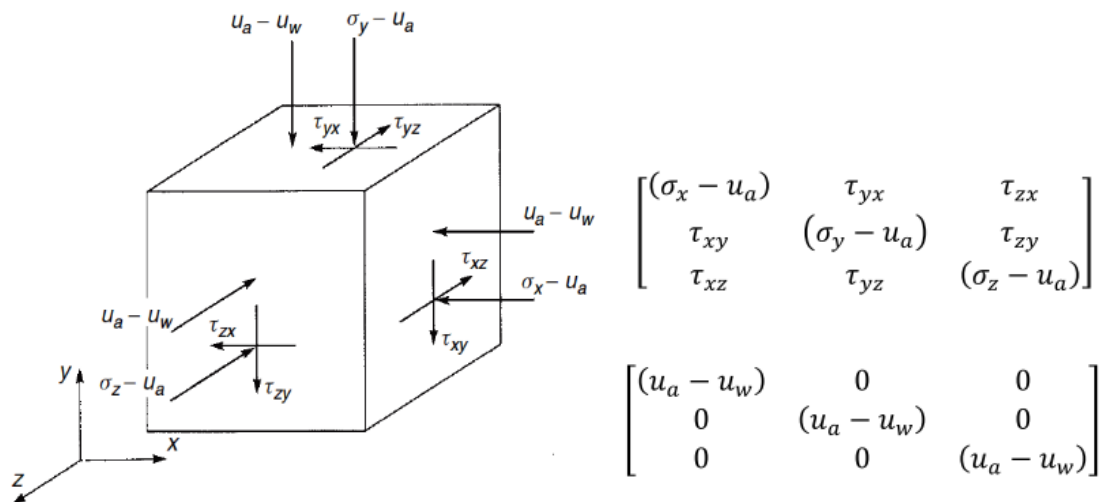


Figure IV.18: Stress state variables for unsaturated soil.

15. Equations for Mohr circle

The state of stress at a point in the ground is three-dimensional, but often practical engineering problems can be represented in two-dimensional form. In two dimensions, there is always a set of two mutually orthogonal principal planes with real-valued principal stresses. The principal planes are the planes where no shear stresses occur. The direction of

the principal planes depends on the general state of stress at a point. The largest principal stress is called the major principal stress and is given the symbol σ_1 . The smallest principal stress is called the minor principal stress and is given the symbol σ_3 . The horizontal and vertical planes form the principal plane for a horizontal ground surface. The vertical net normal stress is often close to the net major principal stress ($\sigma_1 - u_a$) and the horizontal net normal stress is close to the net secondary principal stress ($\sigma_3 - u_a$).

If the magnitude and direction of the stresses acting on two mutually orthogonal planes (the principal planes) are known, the stress state on each inclined plane can be determined. In other words, the net normal stress and the shear stress on each inclined plane can be calculated from the known net principal stresses. The matric suction ($u_a - u_w$) on any inclined plane through a point is constant since it is an isotropic tensor. Therefore, only the net normal stress and the shear stress on an inclined plane need to be considered.

Let's consider an unsaturated soil under quiescent conditions under a horizontal soil surface. The net normal stress and the shear stress on a plane with an angle of inclination α to the horizontal plane are shown in Fig 18. The inclined plane has an infinitesimal length d_s and results in a triangular free-body element with horizontal and vertical planes. The horizontal plane has an infinitesimal length of d_x . Its length can be written by the slope length d_s and the angle.

$$d_x = d_s \cos a \dots\dots\dots 11$$

The vertical plane has an infinitesimal length of d_y :

$$d_y = d_s \sin a \dots\dots\dots 12$$

All planes have unit thickness in the perpendicular direction. The balance of the triangular element requires that the sum of the forces in the horizontal and vertical directions is zero.

The horizontal summation of the forces gives:

$$-(\sigma_a - u_a)d_s \sin a + \tau_a d_s \cos a + (\sigma_3 - u_a)d_y = 0 \dots\dots\dots 13$$

The vertical summation of the forces gives:

$$-(\sigma_a - u_a)d_s \cos a - \tau_a d_s \sin a + (\sigma_1 + u_a)d_x = 0 \dots\dots\dots 14$$

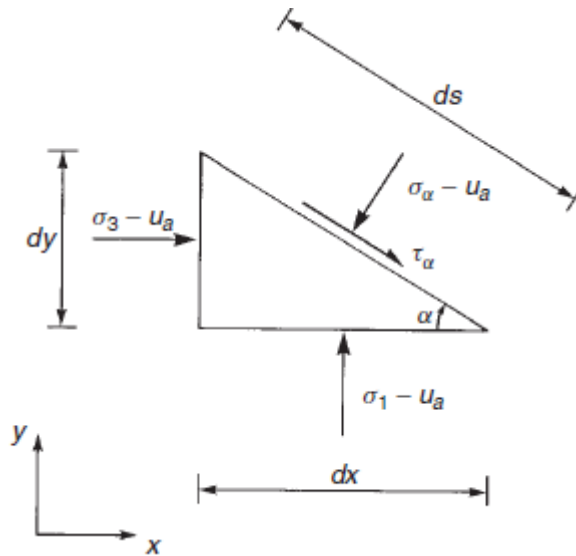


Figure IV.19: Net normal and shear stresses on inclined plane at point in soil mass below horizontal ground surface.

Substituting d_x and d_y (Eqs. 11 and 12 into Eq. 13 or 14 and multiplying Eq. 13 by $\sin a$ and 14 from $\cos a$ there:

$$-(\sigma_a - u_a)d_s \sin^2 a + \tau_a d_s \sin a \cos a + (\sigma_3 - u_a)d_s \sin^2 a = 0 \dots\dots\dots 15$$

$$(\sigma_a - u_a)d_s \sin^2 a + \tau_a d_s \sin a \cos a + (\sigma_1 - u_a)d_s \cos^2 a = 0 \dots\dots\dots 16$$

When Eqs. 15 and 16 are added together, we get:

$$-(\sigma_a - u_a)d_s(\sin^2 a + \cos^2 a) + (\sigma_3 - u_a)d_s \sin^2 a + (\sigma_1 - u_a)d_s \cos^2 a = 0$$

Using trigonometric relationships to solve for $\sigma_a - u_a$ gives:

$$\sigma_a - u_a = (\sigma_1 - u_a) \left(\frac{1 + \cos^2 a}{2} \right) + (\sigma_3 - u_a) \left(\frac{1 - \cos 2a}{2} \right) \dots\dots\dots 17$$

Eq. 17 is rewritten to give: $\sigma_a - u_a = \left(\frac{\sigma_1 + \sigma_3}{2} - u_a \right) + \left(\frac{\sigma_1 - \sigma_3}{2} \right) \cos^2 a \dots\dots\dots 18$

The shear stress is obtained by inserting d_x and d_y (Eq 11 and 12) into Eq.13 or 14 and multiplying Eq. 13 by $\cos a$ and Eq. 14 of $\sin a$:

$$-(\sigma_a - u_a)d_s \sin a \cos a + \tau_a d_s \cos^2 a + (\sigma_3 - u_a)d_s \sin a \cos a = 0 \dots\dots\dots 19$$

$$-(\sigma_a - u_a)d_s \sin a \cos a + \tau_a d_s \sin^2 a + (\sigma_3 - u_a)d_s \sin a \cos a = 0 \dots\dots\dots 20$$

Subtracting Eq. 19 from Eq.20 results:

$$\tau_a d_s (\sin^2 a + \cos^2 a) + (\sigma_3 - u_a)d_s \sin a \cos a + (\sigma_1 - u_a)d_s \sin a \cos a = 0$$

Using trigonometric relationships it is possible to solve for:

$$\tau_a = \left(\frac{\sigma_1 + \sigma_3}{2}\right) \sin 2a \dots \dots \dots 21$$

Equations 18 and 21 give the net normal stress and the shear stress on an inclined plane through a point. The term $\sigma_1 - \sigma_3$ is called the deviatoric stress and is a measure of the shear stress in the soil. The maximum shear stress for a given stress state $\frac{\sigma_1 - \sigma_3}{2}$ occurs on a plane with such an inclination a angle that $\sin 2a$ equals one.

$$\left[(\sigma_a - u_a) - \left(\frac{\sigma_1 + \sigma_3}{2} - u_a\right) \right]^2 + \tau_a^2 = \left(\frac{\sigma_1 - \sigma_3}{2}\right)^2 \dots \dots \dots 22$$

The circle is known as a Mohr diagram and represents the state of stress at a point. In saturated soils, the Mohr diagram is often plotted with the effective principal normal stress on the abscissa and the shear stress on the ordinate. For unsaturated soils, an extended form of the Mohr diagram can be used, as shown in Fig.20.

The extended Mohr chart uses a third orthogonal axis to represent matric suction . The one in Eq (22) is drawn in a plane with the net normal stress as $\sigma - u_a$ the abscissa and the shear stress τ as the ordinate. The center of the circle has an abscissa defined by $\left(\frac{\sigma_1 + \sigma_3}{2} - u_a\right)$. and a radius defined by $\frac{\sigma_1 - \sigma_3}{2}$. The matric suction must also be included in the description of the state of stress. The matrix pull determines the position of the Mohr diagram along the third axis. The matrix suction goes to zero when the soil is saturated and the Mohr diagram reverts to a single $(\sigma - u_w)$ versus plane τ .

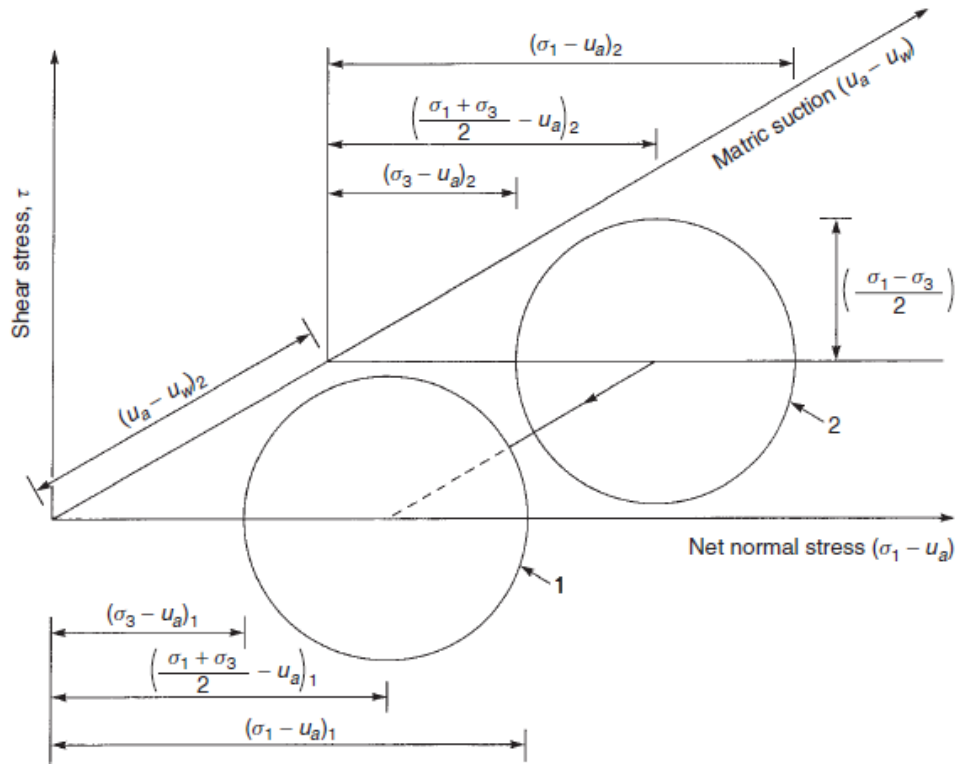


Figure IV.20: Using the Extended Mohr Diagram to represent stress states in unsaturated soils.

15.1- Construction of Mohr circles for unsaturated soils

The structure of the Mohr diagram on the $(\sigma - u_a)$ against $-\tau$ plane is shown in Fig 20. A compressive net normal stress is plotted as a positive net normal stress according to the sign convention for the Mohr diagram. A shear stress that creates a counterclockwise moment about a point within the element is represented as a positive shear stress. This sign convention for shear stresses differs from the convention normally used in continuum mechanics (Desai and Christian, 1977). This convention should only be used for drawing the Mohr diagram. The major and minor net principal stresses, $\sigma_1 - u_a$ and $\sigma_3 - u_a$ are plotted on the abscissa while the center of the Mohr circle is at $\frac{\sigma_1 + \sigma_3}{2} - u_a$. The radius of the circle is $\frac{\sigma_1 - \sigma_3}{2}$.

The Mohr circle represents the net normal stress and shear stress at each plane through a point in unsaturated soil. The net normal stress and shear stress at each plane can be determined if the pole point or origin of the planes is known. Each plane drawn through the pole point intersects the Mohr diagram and gives the net normal stress and shear stress acting on that plane. On the other hand, if the net normal stress and the shear stress on a plane are known and plotted as a stress point on the Mohr circle, the direction of the plane considered is given by the orientation of a line connecting the stress point and the pole point.

The pole point for the condition shown in fig 21 is determined from the known net normal stress and shear stress in a given plane. For example, consider the case where the greatest principal stress acts on a horizontal plane. The state of stress in the horizontal plane is represented by stress point $\sigma_1 - u_a$ and others on the Mohr circle.

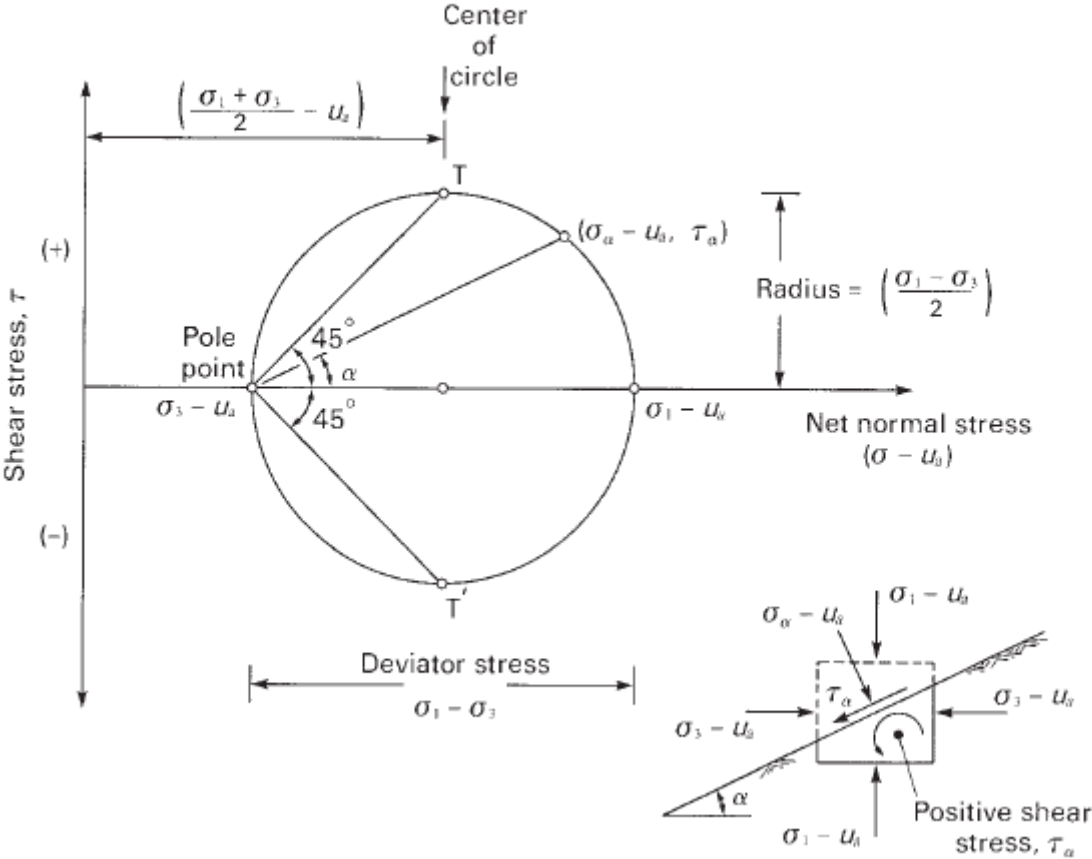


Figure IV. 21: Construction of Mohr circle using net normal stresses

16. Hydraulic properties

The soil property required for the analysis of the steady and transient (or unsteady) flow of an incompressible fluid through a porous medium is the permeability coefficient. When analyzing flow through saturated soil, it is generally assumed that the permeability coefficient is constant. However, the permeability coefficient for an unsaturated soil can vary greatly depending on the state of stress (or degree of saturation) of the soil. The permeability coefficient of an unsaturated soil takes the form of a mathematical function. In fact, any change in floor suction power beyond the air intake value will have a large impact on the permeability coefficient.

17. Flow of water in unsaturated soils

Similar to saturated soils, the flow of water is in the direction of the lower mechanical energy. In unsaturated soils however, the flow is in the direction of the more negative total potential. This total potential is the sum of the gravimetric potential (elevation and pressure heads) and the matric potential ψ . The permeability coefficient for unsaturated soils is dependent on the water content of the soils. The higher the moisture content the higher the permeability. The permeability of the soil is at its maximum when the soil reaches saturation. The hydraulic conductivity for unsaturated soils is however a function of matric potential ($k(\psi)$) or volumetric water content ($k(\theta)$).

Buckingham has extended Darcy law to the unsaturated soils to become the extended Darcy-Buckingham law. It is given by

$$q_z = -k(\psi) \frac{dh}{dz} = -k(\psi) \frac{d(z + \psi)}{dz}$$

From the continuity equation which is:

$$\frac{dq_z}{dz} = \frac{d\theta}{dt}$$

When replacing dz by its expression we get:

$$\frac{d}{dz} \left(k(\psi) \frac{dh}{dz} \right) = \frac{d\theta}{dt} \implies k(\psi) \left(\frac{dz}{dz} + \frac{d\psi}{dz} \right) = \frac{d\theta}{dt} \implies k(\psi) \left(\frac{d\psi}{dz} + 1 \right) = \frac{d\theta}{dt}$$

This equation is known by Richard equation.

To solve this equation commercial software such as HYDRUS 1D is well suited for it. For more rigorous work, HYDRUS 2D and 3D are commonly used.

18. Factors affecting unsaturated hydraulic conductivity

As we know, in unsaturated soil there is a fourth phase in which the pores are filled with an air-water mixture flowing under the influence of negative suction and gravimetric potential. It has been observed that during the water flow path in unsaturated soils, the total matrix suction and water volume vary as the wetting front progresses, and the grade and consequently the hydraulic conductivity vary accordingly. Figure 22 shows how hydraulic conductivity changes when both matric potential and volumetric water content are varied.

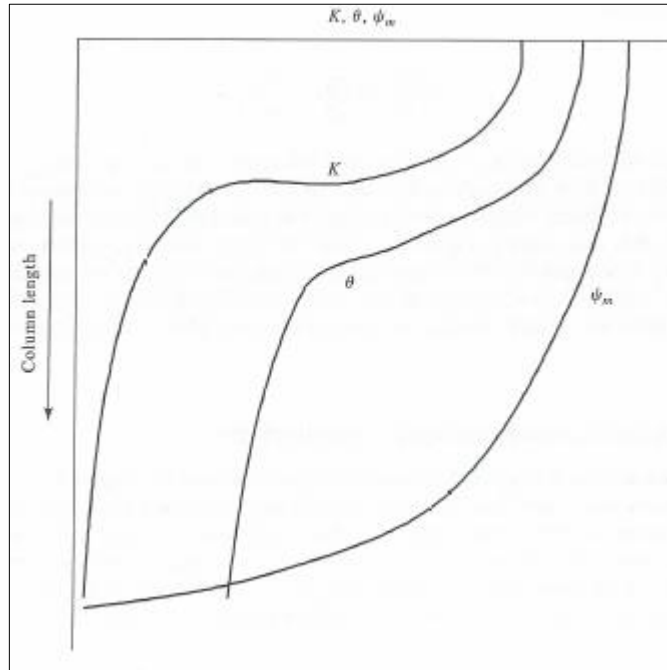


Figure IV.22: Illustration demonstration non-uniform wetness and thus, variation in unsaturated hydraulic conductivity k , volumetric water content θ and matric potential ψ_m (after Hillel 1971).

19. Conclusion

Here are some reasons why unsaturated soil mechanics are important:

- 1- Soil-water curve: Unsaturated soils exhibit unique water retention properties. The relationship between soil suction (negative pore water pressure) and water content is described by the Soil-Water Characteristic Curve (SWCC). The SWCC is critical for understanding soil moisture movement, predicting volume changes, and assessing soil strength.
- 2- Suction and Shear Strength: In unsaturated soils, suction power plays a crucial role in determining shear strength. The suction is created by capillary forces between soil particles and water. The magnitude of suction affects the soil's ability to withstand shear stresses and influences slope stability, bearing capacity and foundation design.
- 3- Soil Volume Change: Unsaturated soils undergo significant volume changes with changes in moisture content. As the water content increases or decreases, the soil swells or shrinks. These volume changes can have a significant impact on engineering projects, affecting settlement, soil compaction, and the behavior of support structures.
- 4- Soil-water interaction: The mechanics of unsaturated soils take into account the interaction between air, water and soil particles. The movement of air and water in soil cavities affects pore pressure distribution, soil strength, and transport of contaminants. Understanding these interactions is critical to assessing fluid flux, permeability, and the behavior of unsaturated soils in response to loading.
- 5- Climatic and environmental aspects: The mechanics of unsaturated soils becomes particularly important in regions with seasonal variations in moisture content or in arid and semi-arid soils. dry climate. It is also relevant in environmental studies, for example when assessing the transport of pollutants through unsaturated soils or when designing landfills and waste container systems. The mechanics of unsaturated soils has its own theories, experimental techniques and modeling approaches to understand and predict the behavior of unsaturated soils. It complements the knowledge of the mechanics of saturated soils and promotes the understanding of soil behavior in different technical and ecological contexts.

**Chapter V: Inventory of
Shallow Landslides and
Soil Characterization of
The area Study**

1. Introduction

In order to study the shallow landslide activity in the Souk Ahras region, we can monitor this external geodynamic activity under the influence of the hydrological events during a specific time period. According to (Wu & Sidle, 1995) there are two main groups of factors affecting landslide activity: the quasi-static variables and the dynamic variables. Quasi-static variables are those that show very little or no observable variation over the short-term scale. In this group we can include all the soil properties (mechanical properties, depth, permeability, etc.) and the topographical features (elevation, slope, curvature, etc.). The static variables are of great importance to determine the probability of landslides occurring in the individual areas and to determine the susceptibility of the slopes to failure. Instead, the dynamic variables are those that can change very rapidly over time and control the generation of disturbances along the slopes, such as the amount of storm water infiltration and the degree of saturation. In this work, we use ground-based weather data as input for the dynamic variables and data collected during fieldwork for the near-static variables. The precipitation maps obtained from ground-based weather radar devices are used to assess the degree of saturation and, in conjunction with the mechanical properties of the soil, to assess the distributed slope stability (Lorenzo Leoni 2008).

2. Methodology

The methodology used in this study is summarized in Figure (01). The study begins by examining the geology of the area, which is believed to be a significant contributor to landslide susceptibility. In addition, the precipitation properties and the geomorphology of the study area are determined. This is followed by the investigation of the hydraulic and mechanical properties of the soil. The collected data was then entered into the numerical simulation software Seep/w and Slope/w Geoslope International Ltd., 2004a and b) for coupled stability analysis. Analysis of transient seepage through the slope is performed using Seep/w and the results are used in Slope/w to calculate the stability of the slope at a given time and rainfall intensity. The flowchart below schematically illustrates the methodology used in this study.

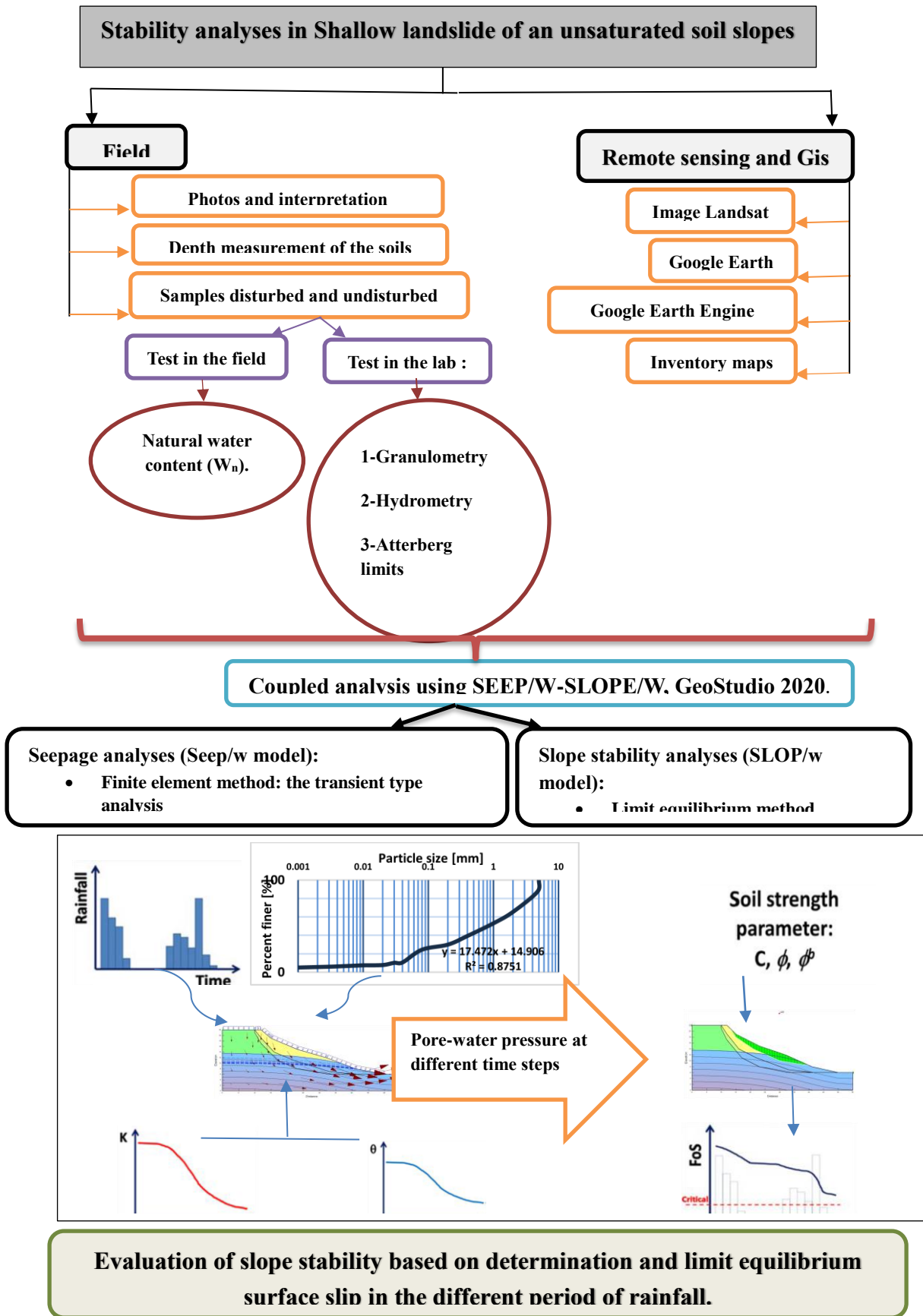


Figure V.1: Generalized flowchart adopted in the current study.

3. Landslide inventory

Landslide processes in Souk Ahras and the surrounding areas have caused unrest among the population and those passing through. They mainly affect road infrastructure, water supply, electricity lines and buildings. The problem is that despite the corrective measures taken by the authorities, landslides continue to occur every rainy season. They become a burden and eat up the resources that should be devoted to the development and well-being of the population.

After the heavy rains of 2004 (150 mm per month), a large landslide severely damaged the RN 81 at PK114 and PK116 in Hammam Tassa, photo. (01). The road surface was damaged and the traffic jam was terrible for days. At the same time, the road slopes at Mechrouha, Zaarouria and Hammam Tassa were affected by other landslides of lesser magnitude and impact. There are numerous instabilities affecting agricultural land, but they have not attracted the attention of the authorities as they have less impact on the daily activities of the population. In order to act efficiently and reduce the damage caused by this natural phenomenon, it is mandatory to report a maximum number of landslides with their geometric, geological, geomorphological and all the conditions of their occurrence throughout the study area. This can actually be summed up by conducting a landslide inventory.

The term landslide inventory refers to the reporting in a defined format (map) of the spatial distribution of the destabilized masses, as well as their size, volume, extent, typology, topography, geology and activity status (Hansen, 1984a, Hansen, 1984b).), McCalpin, 1984, Wiczorek, 1984, Brabb, 1991 (Guzzetti et al., 2000).



a- Hammam Tassa PK 114



b- Hammam Tassa PK116

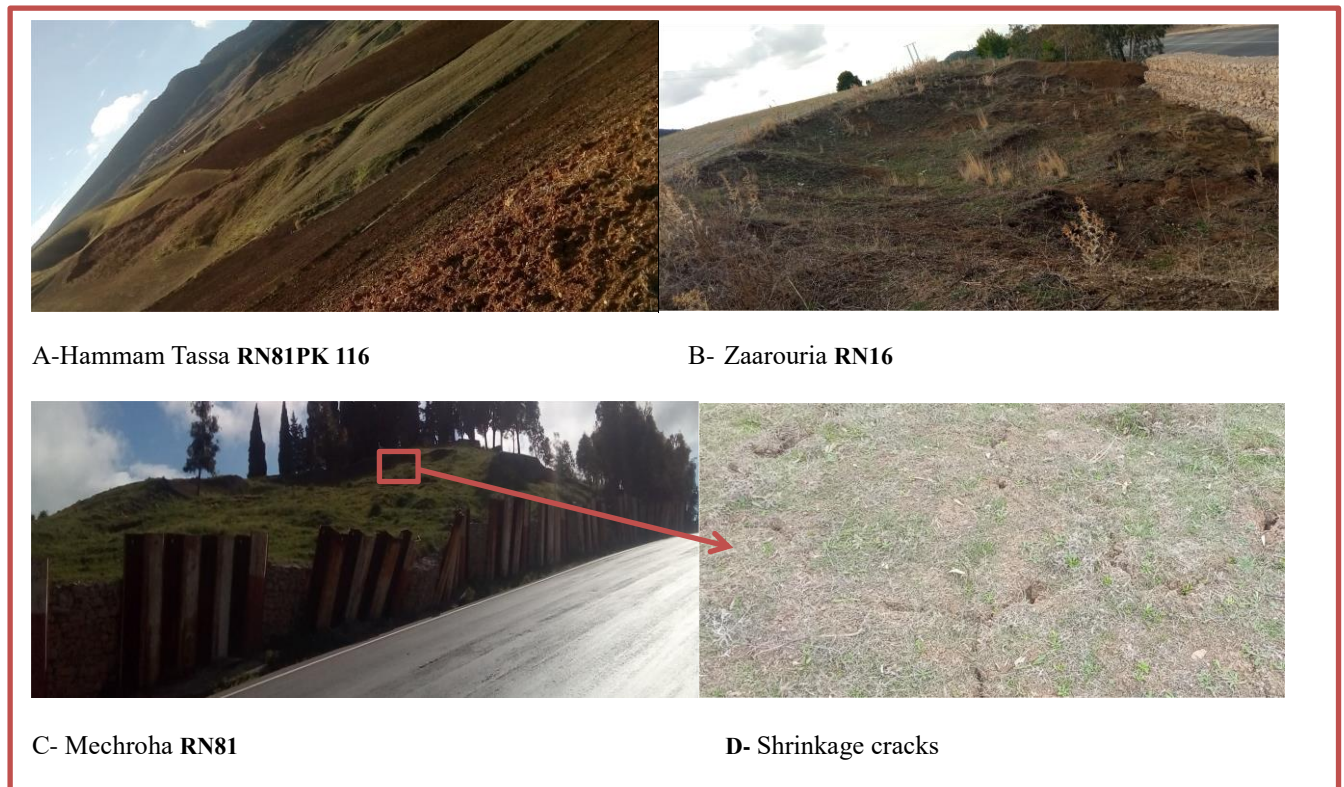


c- Zaarouria

Photo V.1: Shallow landslide in the study area (Hammam Tassa and Zaarouria).

4. Landslide material characterization

Field observations and previous studies conducted in the area since 2004 indicate that landslides have occurred throughout the Souk Ahras area, up to a level where the RN81 national road meets the PK 114, due to excessive deformation was interrupted several times by the slide. This dangerous event happened in 2004, when more than 150 mm of precipitation fell in January. Landslides have also affected other roads and agricultural land, particularly in the towns of Mechroha, Zaarouria and Hammam Tassa. The common character of the slide mass at these sites is that they are all flat and between (1 and 2.5 m) thick. They are all triggered after prolonged periods of precipitation, usually in late winter and early spring (Atiali, 1998; Bozhinova-Haapanen, 2016; Bozo & Cela, 2016). To better understand this behavior, landslide material is characterized using a methodology essentially based on laboratory testing, field observations and numerical analysis.



Photos V.2: Photos of shallow landslides from the three studied areas.

5. Laboratory and field tests

In order to perform stability calculations for some landslides in the study area, it is necessary to determine the physical and mechanical properties of the soil. These engineering properties directly control the hydraulic, strength, and deformability properties of the sample-scale soil, and hence the entire slope. Representative samples were collected from unstable masses throughout the area. Standard sampling procedures (ASTM 6519) were followed. Sampling focused on the most affected sites such as Zaarouria RN16, Mechroha RN81 and Hammam Tassa RN81 PK116 (photo. 02). On average, two undisturbed samples were collected from each landslide of major importance at the above locations. During sampling, a bulk sample was taken from the cliffs of each landslide at a depth of 0.5 m, using a plastic-coated hammer to drive the sampler down (McKenna et al., 2012; Pramusandi et al., 2015).

The first sampling campaign was conducted in the winter season to determine the maximum natural water content (W_n). It was determined on site by weighing the sample after pressing it out of the sample tube with a balance with an accuracy of + 0.1 g. It was then packed in a waterproof bag and transported to the laboratory oven, where it was oven dried for 24 hours. The natural water content was between 30 and 35%. During the dry season, on

the other hand, the suction pressure is measured. Shrinkage cracks were also observed, which are open to a width of 3 cm and more photo 02 (D).

5.1- Atterberg Limits

In the area of landslides, the plasticity of the soil, related to its water content, plays an important role for its geotechnical properties and behavior. Soil Liquid Limit (LL), Plastic Limit (PL), and Plastic Index (PI) were determined using the methods described in ASTM Standard D4318. The determined mean values of the Atterberg limit values are summarized in Table (01). The soils of Mechrouha are plastic to highly plastic, while the soils of Hammam Tassa and Zaarouria are of low plasticity due to their predominantly muddy character. In addition, empirical formulas were derived from these limit values, which made it possible to determine the undrained shear strength of fine-grained soils (Ylmaz & Ylmaz, 2000).

5.2- Grain size distribution

To characterize soil particle sizes, we used two different experimental tests. Sieve analysis is used to characterize soil particles larger than $75 \mu m$ and classifies different soil particle fractions using a stack of standard sieve meshes. With the hydrometer, on the other hand, soil particles smaller than $75 \mu m$ are measured. It is used to assess the grain size distribution curve of soils that, due to their small size, cannot be distinguished by mechanical shaking (Dante Fratta, Jennifer Aguetant, 2007). Both tests are defined in ASTM Standard Method D421 D422 for Particle Size Analysis of Soils. The Unified Soil Classification System (USCS) (Dante Fratta, Jennifer Aguetant, 2007; Dirx et al., 2020; Ephrem, 2019; Pramusandi et al., 2015) is used in this study. The granulometric properties of soils are often used to estimate their porosity (Carman, 1939), permeability Hazen (Dolzyk & Chmielewska, 2014), Terzaghi (Carman, 1939) and suction (D.G. Fredlund & Zhang, 2013; MacRobert & Blight, 2013; LL Zhang et al., 2013).

5.3- Soil water characteristic curve

The soil water property is the most important property function for the investigation of unsaturated soils. It represents the relationship between matrix wicking and water content and either gravimetric water content (ω), volumetric water content θ_s or degree of saturation (S) (Azmi et al., 2019; M.D. Fredlund & Wilson, 2020; Freund & Ph, n.d.; Ng et al., 2003). It is considered the most important function for implementing the mechanics of unsaturated soils in geotechnical practice.

The shape of this curve is significantly influenced by the properties of the soil texture. The curve is determined either directly from the field with a tensiometer or indirectly via the grain size distribution of the soil.

Van Genuchten (1980) proposed a SWCC equation using three parameters which are θ, n, m and a as follow:

$$\theta(\psi) = \frac{\theta_s}{[1+(a\psi)^n]^m} \dots\dots\dots 01$$

The parameter a is the soil suction value greater than the actual air-entry value.

The parameter n and m are fitting parameters.

The above Van Genutchen (1980) equation can be written for soil suction in the following manner:

$$\psi = \frac{1}{a} \left[\left(\frac{\theta_s}{\theta} \right)^{\frac{1}{m}} - 1 \right]^{1/n} \dots\dots\dots 02$$

$$m = (n - 1)/n.$$

The estimation of soil suction has been dealt with by many researcher among whom are (Ku et al., 2017) and (Pham & Fredlund, 2008)...etc.

6. Landslide analysis

Before performing a landslide analysis, it is important to create a geological model that is a good match for field conditions. These include the thickness of the soil layer, the water table, the geotechnical properties of the soil, and the opening (width) and depth of shrinkage cracks. In this model, the precipitation amounts determined from the ANRH data (Souk Ahras station) and the Google Earth Engine platform are superimposed (Table 02).

The stability analysis is performed with the software package GeoStudio (2020) (Download GeoStudio 2020 from GEOSLOPE). International Ltd., undated). In this package a coupled analysis with SEEP/W-SLOPE/W is used (Dahal et al., 2009; Hasegawa et al., 2009; L.M. Lee et al., 2009; H. Rahardjo et al., 2007).

Seep/w simulates water infiltration and determines the SWCC, while Slope/w performs the stability analysis and presents it in the form of a safety factor.

SEEP/W

Seep/w is a finite element program for simulating water infiltration and pore water pressure in porous materials such as soils. In general, it is an analytical model for infiltration analysis in both saturated and unsaturated flow. Two main types of analysis can be implemented with the software: steady-state and transient analysis. In this study, a transient type analysis is used; It consists in solving the following Richards flow equation in 1D for unsaturated soil. It can be described by (Ali et al., 2014; Richards, 1931; Zhan et al., 2013).

$$\frac{d\theta}{dt} = \frac{d}{dz} \left(K_{\psi} \left[\frac{d\psi}{dz} + 1 \right] \right) \dots\dots\dots 03$$

Where, θ is the volumetric water content, t is the time, ψ is the soil matric suction, K_{ψ} is the hydraulic conductivity at a given soil suction.

To solve the above equation numerically, one must define the SWCC and the hydraulic conductivity functions.

We assume θ the moisture content to vary with ψ , S_e is the effective degree of saturation given by Van Genuchten (1980) model (Ali et al., 2014; Azmi et al., 2019; Van Genuchten, n.d.).

$$S_e = \frac{\theta_w - \theta_r}{\theta_s - \theta_r} = \left(\frac{1}{1 + (\xi u)^n} \right)^m \dots\dots\dots 04$$

θ_s represents the moisture content at the saturated state of the soil; θ_r represents the residual moisture content of the soil; and ξ is the suction scaling parameter, n , and m are fitting parameters of the Genuchten & Wierenga, 1976 water retention function.

The hydraulic conductivity function as related to a function of degree of saturation is given by Van Genuchten and Moualem (Van Genuchten, n.d.).

$$K_{\psi} = K_{sat} S_e^{1/2} \left[\left(1 - \left(1 - S_e^{1/m} \right) \right)^m \right]^2 \dots\dots\dots 05$$

Given appropriate initial conditions, boundary conditions, soil hydraulic properties, and precipitation, the three equations can be solved to obtain soil water content and soil suction at any considered slope and under various saturation conditions (Baum & Godt, 2010; Lu et al., 2010).

SLOPE/W

Slope/w is a slope stability program that uses limit equilibrium analysis and determines the safety factor. It can efficiently analyze both simple and complex instabilities for a variety of slip surface shapes, pore water pressures, climatic conditions, soil properties

and loading conditions Fig. (03) (Chinkulkijniwat et al., 2016). The stability calculations are usually given in the form of a single value called the safety factor. It is defined by the ratio of the available shear force to the mobilized shear force (shear force). It is given by :

$$FOS = \frac{\tau_f}{\tau} = \frac{\text{shear strength}}{\text{shear stress}} \dots\dots\dots 06$$

Shear strength parameters of unsaturated soils are needed to estimate the safety factor using the extended Mohr-Coulomb criterion (Delwyn G. Fredlund et al., 2012).

$$\tau_f = c' + (\sigma_n - u_a) \tan \varphi' + X(u_a - u_w) \tan \varphi^b \dots\dots\dots 07$$

Where τ_f : effective stress, u_a : the pore air is pressure, u_w : is the pore water pressure, φ' : is effective internal friction angle of soil, c' : effective cohesion, σ_n : total normal stress and φ^b : is an angle defining the increase in shear strength for an increase in soil suction. $(\sigma_n - u_a)$ is the net normal stress on failure plane and $(u_a - u_w)$ is soil suction.

The factor of safety for unsaturated soils is given by:

$$FS = \frac{c' - S_e \cdot \gamma_w \cdot u \cdot \tan \varphi'}{\gamma \cdot z_w \cdot \cos \theta \cdot \sin \theta} + \frac{\tan \varphi'}{\tan \theta} \dots\dots\dots 08$$

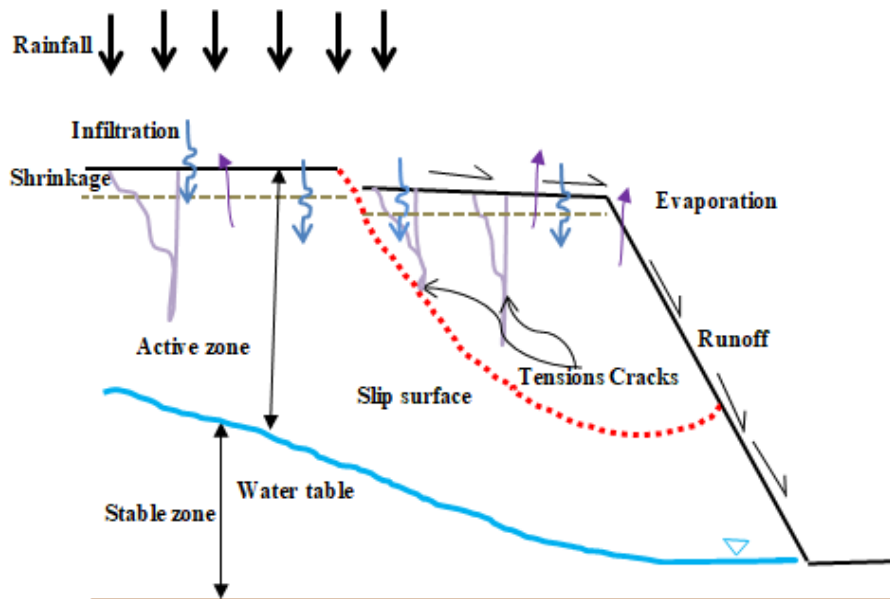


Figure V.2: Deformation and infiltration phenomena in a near-surface deposit of unsaturated expansive soil.

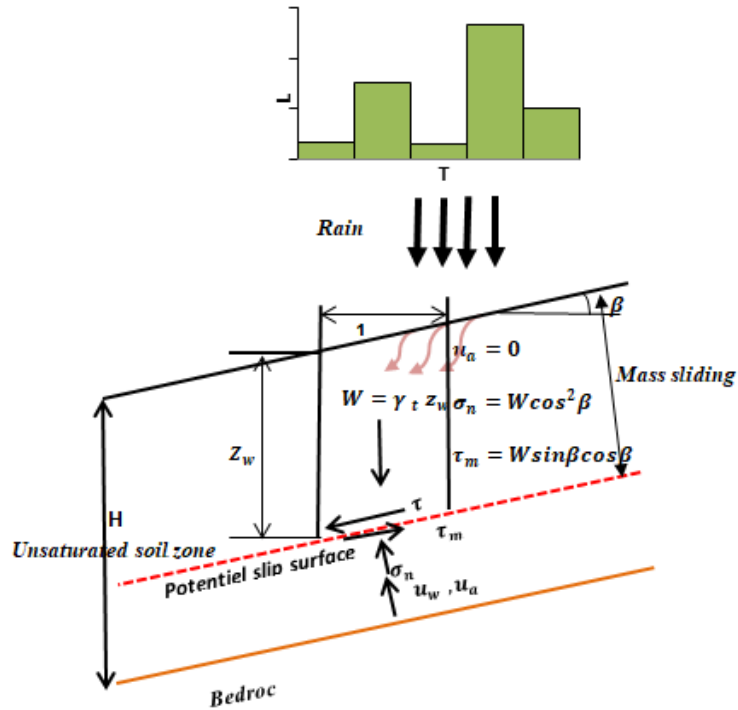


Figure V.3: Forces on an element of infinite slope.

Cohesion friction angle and unit weight are the main data in this model.

The stability analysis using the safety calculation factor is performed using a coupled Seep/w Slope/w stability analysis. The matric suction at each soil saturation condition is determined in seep/w and then used in slope/w for the safety factor calculation.

Chapter VI: Numerical Simulation, Results and Discussion

1. Introduction

This chapter presents the results of the as-built map, laboratory and field test data, and numerical simulations that evaluate the predictive capabilities of the two developed shallow landslide occurrence models. Since there were no significant landslides in the three sectors (Hammam Tassa, Zaarouria and Mechrouha).

2. Interpretation of map's inventory

In this study, as a first step in locating landslides, the landslide inventory is generated using Google Earth Pro imagery. Several field trips were then undertaken to complete the mapping process. In fact, field trips have made it possible to verify the actual existence of the landslides and to identify their nature, extent, volume and size, the slope on which they are evolved and the material involved. Using this technique, 60 landslide masses were identified and mapped, fig.1

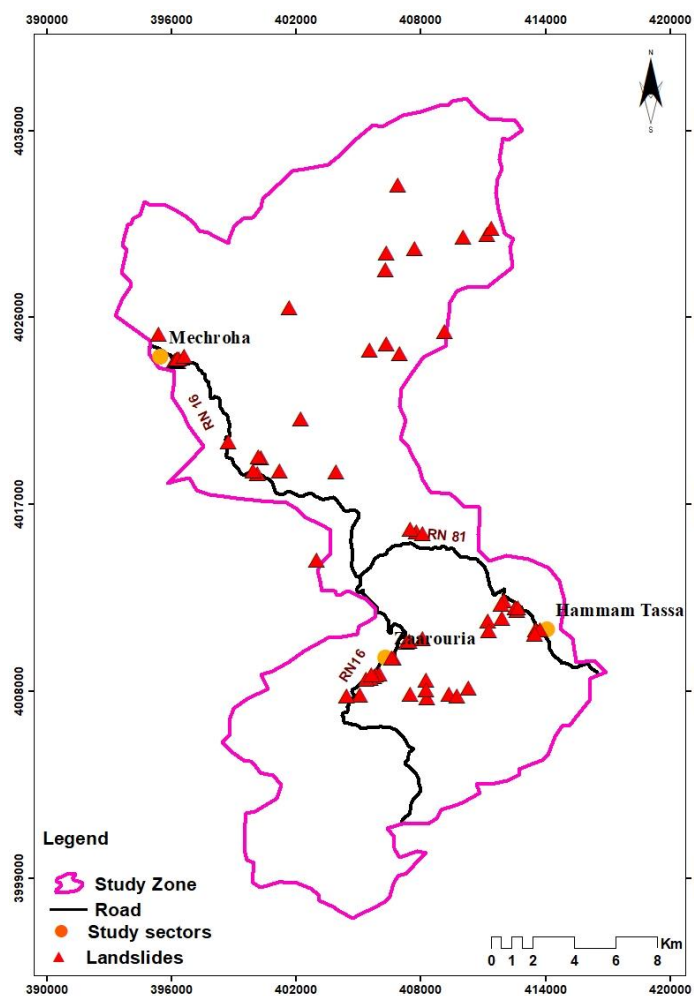


Figure VI.1: The landslide inventory map.

In order to understand the susceptibility to landslide occurrence, factor maps such as land cover, slope inclination etc. were made.

2.1- Land use and cover

Land use/cover is also an important factor in landslide occurrence, as barren slopes are more prone to landslides. Planted areas, on the other hand, tend to minimize the effects of climatic influences such as rain and snow and prevent erosion by being naturally anchored by root trees, thereby reducing susceptibility to landslides. In our case, the land use/coverage map was created using a Landsat 8 image and field visits. Five land use/cover groups that could affect landslide activity in the area were considered. Forest, bare fields, agricultural land, water and urban areas are the different land types fig. 2. Using the raster operation in ArcGIS, they were converted into a raster land cover map. In this regard, it has been observed that the most active flat landslide areas are those bordering road networks, undeveloped land and some agricultural land. Insufficient city expansions have also produced some dramatic events (Arabameri et al., 2019; Bousta & Ait Brahim, 2018; Intarawichian & Dasananda, 2010; L et al., 2018).

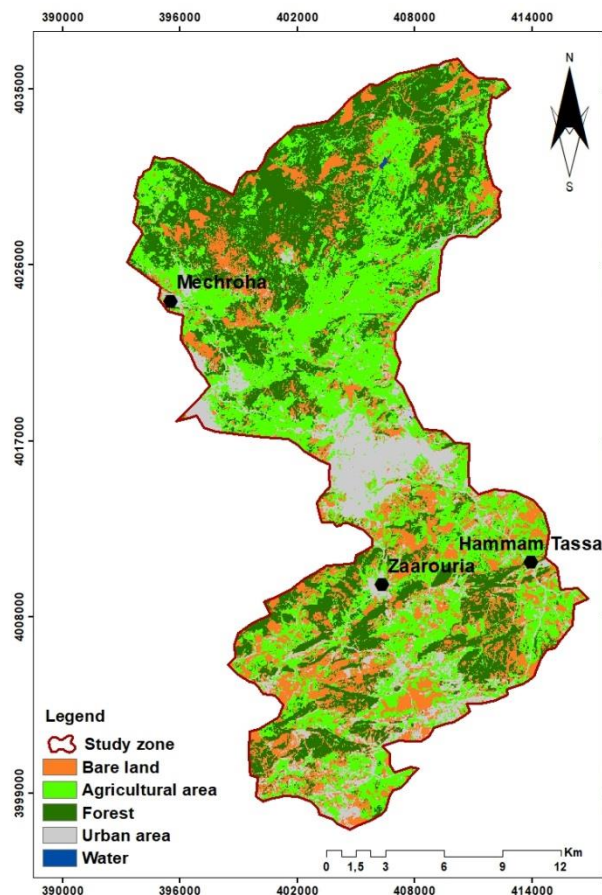


Figure VI.2: Land use / cover map

2.2- Slope inclination map

Slope inclination or gradient is the factor with the greatest influence on ground slip, as it enters the equations used to calculate the safety factor. Many authors such as Da (2007); Hasekioullar (2011); ellek (2013); ellek (2020); Szen & Doyuran, 2004; Budimir et al. (2015) stated that more than 90% of the studies considered slope gradient as the most influential parameter in assessing landslide susceptibility. In addition, Guzzetti et al. is considered an important factor for GIS-based mapping of landslide susceptibility. (1999), Lee and Min (2001), Dai and Lee (2002), and Ohlmacher and Davis (2003). In general, the inclination angle receives the highest rating in landslide susceptibility analyzes (Dlek and Avc 2016, Mehrotra et al.). 1992).

The slope inclination map is created in Arg Gis. The method used a detailed spatial database of the area. In our study area, the slope gradient is divided into five degrees, with the steepest value being 56.5. However, it must be borne in mind that large slope gradients are not always associated with the greatest occurrence of landslides. Our field observations revealed that grade 17-24 is the more active. Erosion channels are also less pronounced in this class, since they are constantly covered and filled with sliding material (fig.3).

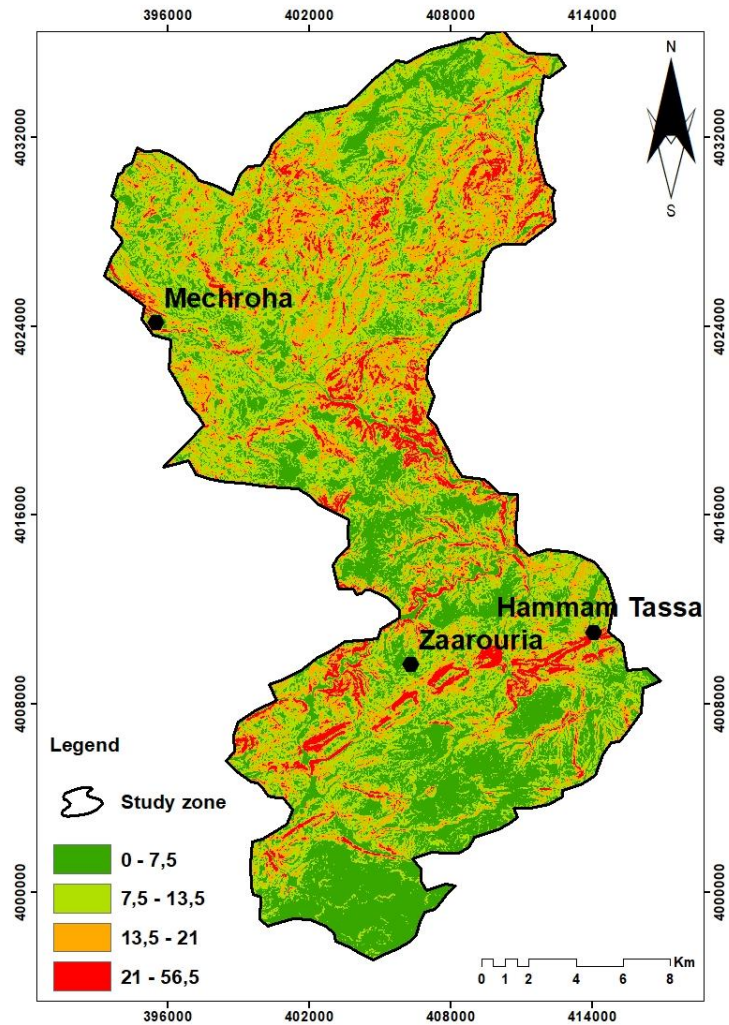


Figure VI.3: Slope inclination map

2.3- Slope aspect ratio map

The slope aspect ratio refers to the north orientation of the terrain slopes. In the study area, the orientation of the slope normal was divided into five classes: flat, north, northeast-east, southeast-east, southwest-west, and northwest-N. The slope aspect is important because rain exposure can vary from windward to leeward in many places around the world. Consequently, further land instabilities can be expected on the west side of the relief Fig. 04.

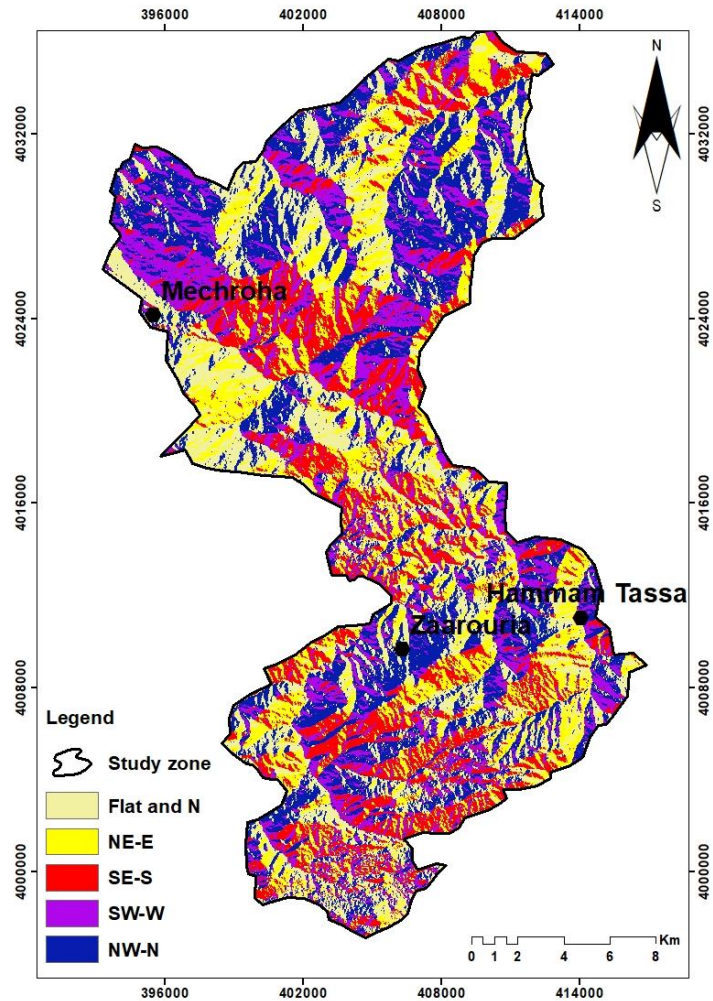


Figure VI.4: Slope aspect ratio map

2.4- Elevation map

The elevation map shows the slope elevation from the reference point at sea level. We have identified different geomorphological zones: low-altitude zones between 277 and 400 m near Oued Cheham, medium-altitude zones between 600 and 800 m corresponding to Souk Ahras, Zaarouria and Mechroha. Altitude zones are between 1000 m and 1359 m in the mountains of Mechrouha and Zaarouria. It can be seen that most of the landslides developed in intermediate and high altitude areas Fig. 05.

All slope gradient maps, slope aspect ratio maps, elevation maps, and land cover maps were created in ArcGIS from DEM at 12.5 m resolution. The characteristics of the landslide prone areas were identified and verified by overlaying all slope aspect maps, geological maps, elevation maps, slope gradient maps, etc. over the landslide inventory map.

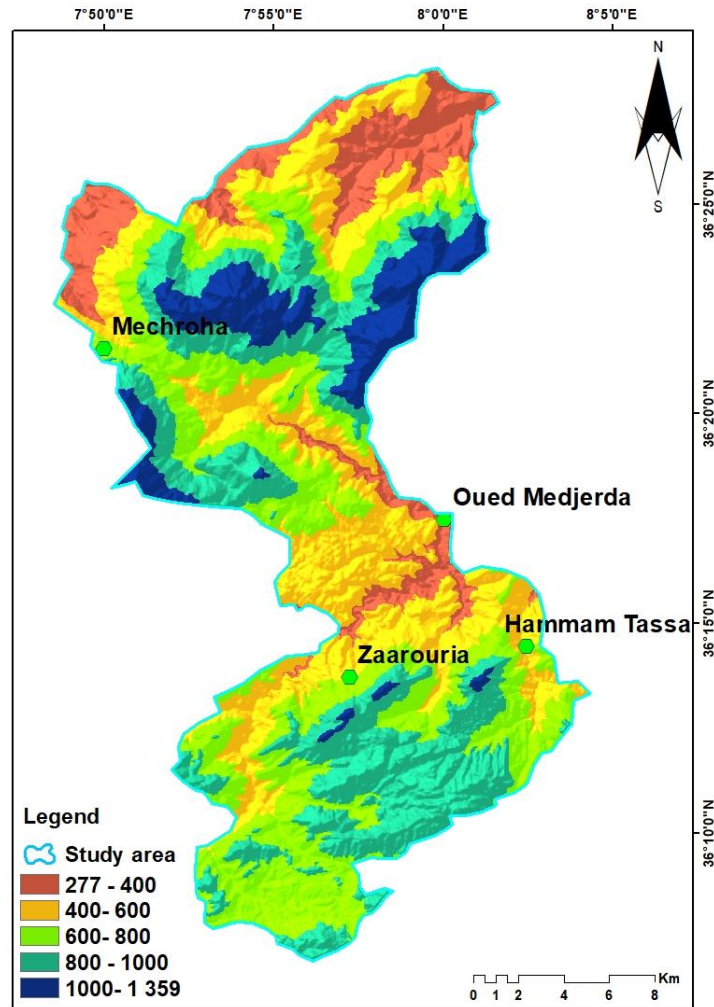


Figure VI 05: Elevation map

3. Laboratory and field data analysis

To determine the physical and mechanical properties of the soils, laboratory tests were carried out on undisturbed soil samples from a depth of 0.3 to 0.5 m. As already mentioned, the soil samples were taken from unstable soil masses. The natural water content achieved is between 30 and 35%. The plasticity limits vary between 58 and 61 for the liquidity limit and between 28 and 48 for the plasticity limit. The plasticity index varies between 15 and 30, indicating medium to high plasticity soils.

The particle size distribution was determined in the laboratory using sieve and hydrometer analyses. It is conducted according to USCS. The soils in the Hammam Tassa area have been found to be silty sand (SM). For Zaarouria, on the other hand, it is well sorted sand with silt

and gravel (SW-SM). In Mechrouha soils it is mainly clayey sand with gravel (CS-SM) (SC). These are the main soil types encountered.

Table VI.1: Summary of the laboratory test results

		Hammam Tassa	Zaarouria	Mechrouha
No	Description	Silty Sand	Well Graded Sand With Silt and Gravel	Clayey Sand with Gravel
1	Unified Soil Classification System (USCS)	SM	SW- SM	SC
	Depth (m)	0.5	0.5	0.5
	Specific Gravity , Gs	2.7	2.7	2.7
	Grain size and Hydrometer analysis			
	- Gravel content (%)	12.6	29.8	34.1
	- Sand content (%)	63	64.9	53.1
	- Silt content (%)	19.1	4	12.1
	- Clay content (%)	5.3	1.4	0.7
	- D ₁₀ (mm)	0.0211	0.3327	0.0635
	- D ₃₀ (mm)	0.2137	1.524	0.9209
	- D ₆₀ (mm)	1.5614	3.8906	4.0146
	- C _u	74.08	11.7	63.2
	- C _c	1.39	1.79	3.33
	Atterberg limit			
	- Liquid limit ,LL(%)	61	63	58
	- Plastic limit, PL(%)	46	48	28
	- Plasticity index, PI (%)	15	15	30
	Saturated coefficient of permeability, K _s (m/s)	0.00045	0.11	0.004

In addition to (SW-SM) and (CS-SM), the silt sand (SM) occurs in practically all areas. The particle size distribution curves obtained are more or less identical for all locations (Fig. 7.3). For soils south of Souk Ahras, the topsoil consists of 19.1% silt and 5.3% clay, while the soils of Zaarouria contain about 4% silt and 1.4% clay (Table 01). For soils in the northwest of the city (Mechrouha), it is 12.1% silt and 0.7% clay (Jeong et al., 2017).

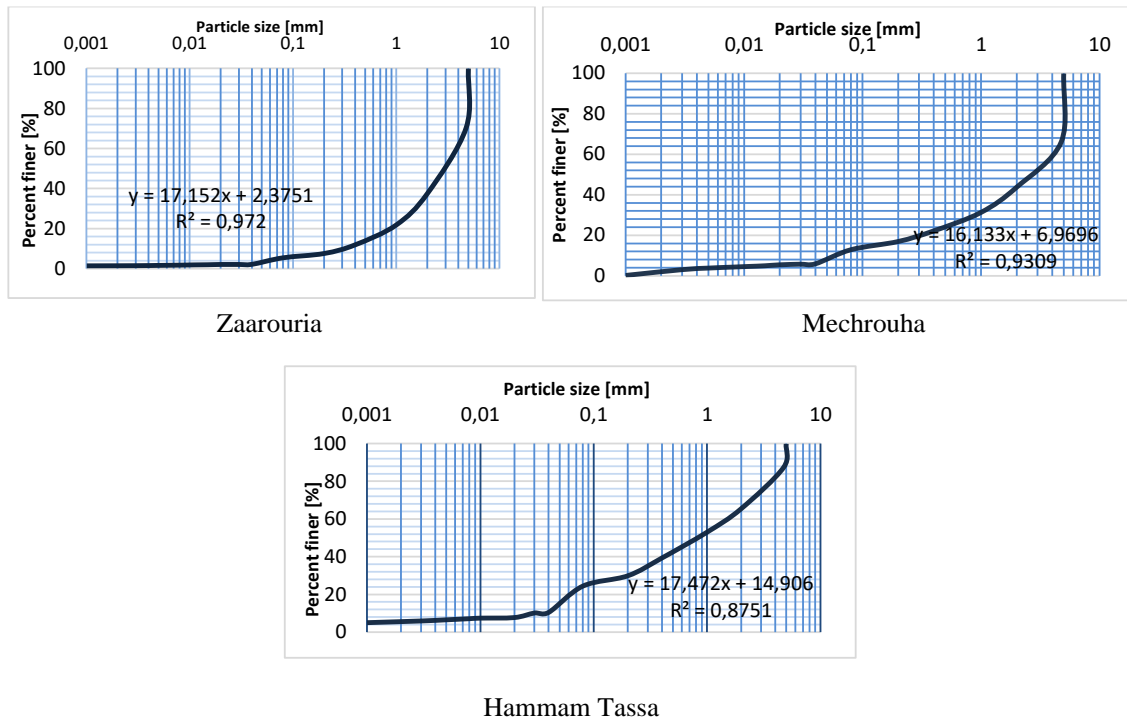


Figure VI.6: Grain size distribution curves of representative samples from the three studied areas.

The calculated permeability varies between $4.5 \cdot 10^{-6}$ to $4 \cdot 10^{-5}$ and 10^{-3} m/s. As described in Sections 4.2 and 4.3, both parameters were used in modeling infiltration and slope stability. The direct shear tests carried out in the civil engineering laboratory with the shear box apparatus resulted in values of $C = 3.6, 3.44$ and 0.8 kg/m² and an internal friction angle of $= 19.20, 14.62$ to 6.43 . These values partially agree with those of the LTPE laboratory (Table 01).

4. Rainfall and landslide

According to Google Earth Engine Platform (GEE), the average annual precipitation in 2019 is about 718.11 mm. The amount of precipitation reached 128 mm in January, 60 mm in February and 111 mm in March 2019. Diagram Fig. 07 shows the monthly rainfall variation for 2019, while Table (3) shows the rainfall variation for 2019 for three rainiest months of the year. The water budget 2019 shows a surplus table (02).

From December to June 2019, the agricultural deficit is zero. This means that the soil has reached the saturated state, where the built up pore pressure will continue to increase as long as it keeps raining.

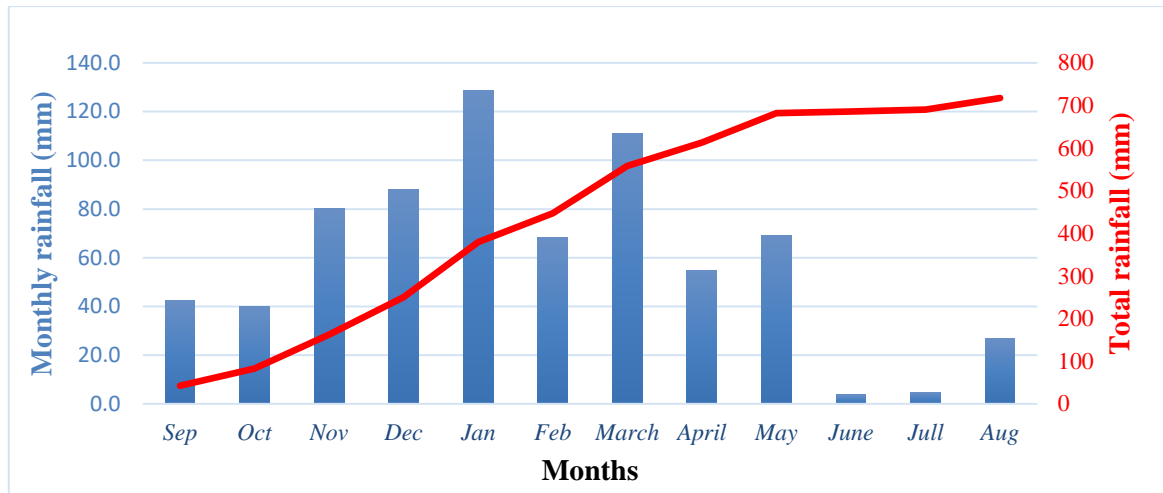


Figure VI.7: Rainfall intensity and cumulative rainfall from GEE for 2019.

Table VI.2: Table showing the rainfall data from GEE for 2019.

2019	Sep	Oct	Nov	Dec	Jan	Feb	March	April	May	June	Jul	Aug
Precipitation	42.5	40	80.2	87.9	128.7	68.1	110.9	54.6	69	3.9	4.8	27
Deficit	64	26	0	0	0	0	0	0	0	23	162	142
Deficit (GEE)	90,5	53,3	0	0	0	0	0	26,7	50,7	162,5	222,6	171,4

In fact, the landslide activity observed in 2019 began manifesting itself in January and widened in March. In reality, this observation has been reported by many researchers elsewhere (Klime & Escobar, 2010; Richards, 1931). (Echeverri and Valencia 2004) found a correlation between a precipitation threshold and the triggering of landslide areas with high precipitation levels. The relationship is given by the following empirical equation:

$$A = R_3 - 0.55 R_{15} \dots \dots \dots 01$$

Where A is the hazard of landslide triggered by rainfall, R_3 is the 3-days antecedent rainfall, and R_{15} is the accumulated rainfall of 15 days preceding the R_3 .

While in areas where rainfall is reduced, the threshold for the amount of water at which failure occurs is rain accumulation over a 15 to 90 day period (Brunetti et al., 2010; H. Chen & Lee, 2004; Ko, n.d.) .

The failure threshold for the saturation state coincides at least with the complete saturation of the soil. Some researchers such as (Alves et al., 2016; CA Hidalgo et al., 2018) have found

that most landslides occur when the ground is saturated to a critical depth due to the effects of accumulated precipitation.

For Souk Ahras Although no studies have been conducted linking landslides to triggering precipitation, it can be observed that all major landslide events occurred after the rainy periods from late winter to early spring. 2019 saw significant rainfall: 128.7 mm in January, 68.1 mm in February and 110.9 mm in March. The shallow landslide activity was intense and we recorded several dozen instabilities in the three locations Hammam Tassa, Zaarouria and Mechrouha (Fig. 7.03).

5. Numerical analyses

As recommended by Freedland (M.D. Fredlund et al., n.d.), soil particle size distribution, soil dry density, voids ratio and specific gravity can be used to determine SWCC in SoilVision software and then validated by field measurements. In this study, the SWCC is established directly in the Seep/W software, similar to ground sighting. The hydraulic conductivity function is calculated from the SWCC and the saturated permeability (K_{sat}) (Fig. 08).

In this study, the Van Genuchten model was used (Eq. 05) as shown in Fig. (09). Based on the field and laboratory test results, the slope for the transient infiltration analysis is modeled with SEEP/W (GeoSlope International Ltd., 2004a), while the pore water pressure profile calculated from the infiltration analysis is integrated into the stability calculations with Slope/W. W (GeoSlope International Ltd., 2004b) (Nishimura and Fredlund 2000, Suryo et al. 2015)

For this analysis, the precipitation amounts for 2019 are taken into account (Table 02). The analysis resulted in a safety factor between 0.6 to 1.05 and 1.1 for the slopes in the three sectors. The decreasing pattern shown in the safety factor versus time graph (Fig. 10) varies by soil type.

For instance, the safety factor for Mechrouha slopes steadily decreases during prolonged rain events fig. (09 C), while a sudden decrease was observed for Hammam-Tassa soils after 15 days of rain (Fig. 09A). For Zaarouria slopes, the relationship between the safety factor and precipitation time is a negative power-law relationship (Fig. 10 B).

The field observations have shown that when it rains in Mechrouha, the first landslides to appear are relatively reduced in size and extent. However, in Hammam Tassa, they sometimes

appear after those of Mechrouha. The last and more frequent instabilities occur in the locality of Zaarouria. The results of the coupled analysis Seep/w Slope/w in the form of optimized critical slip surfaces and the respective safety factors at the time of failure are shown in fig. (11) (Acharya et al., 2016)

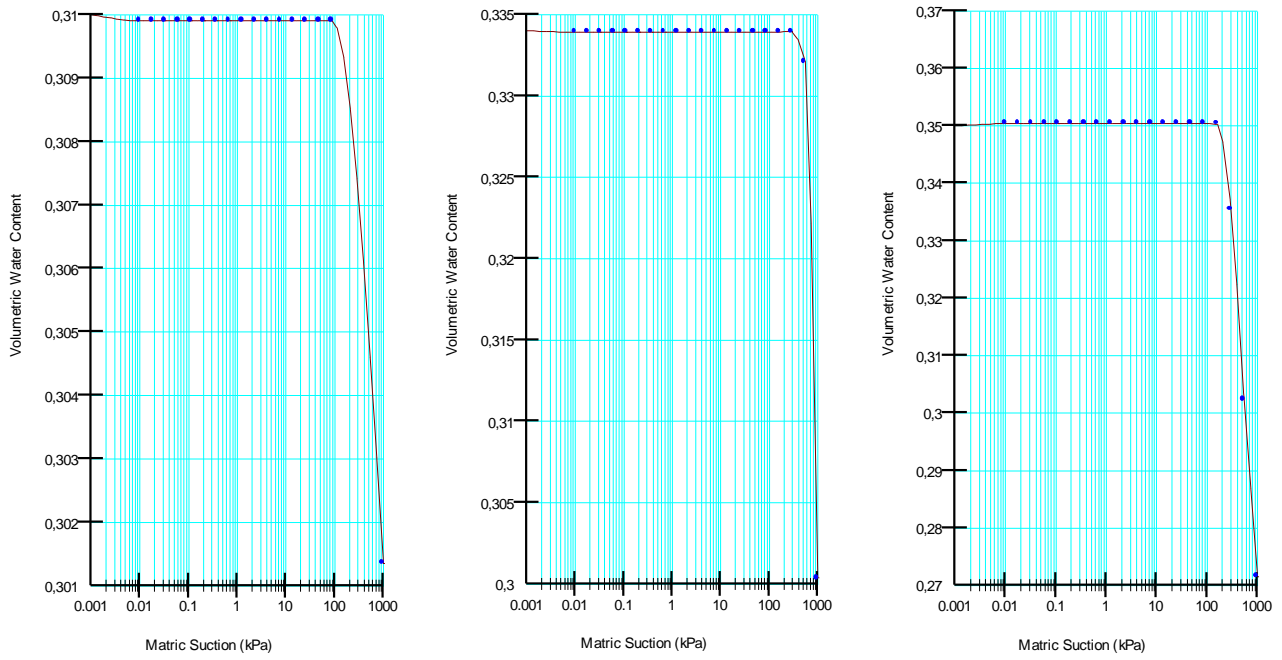


Figure VI.8: The SWCC for soils from the three sectors studies

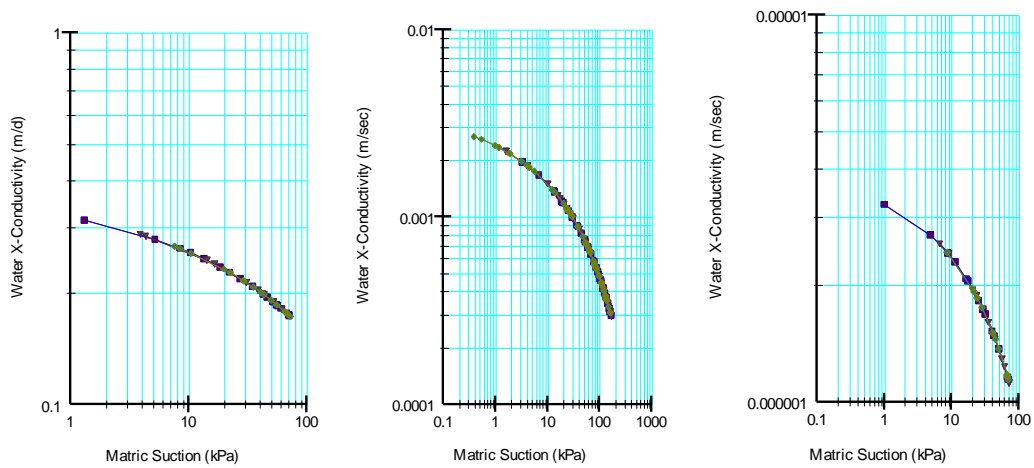


Figure VI.9: Soil conductivity and matric suction

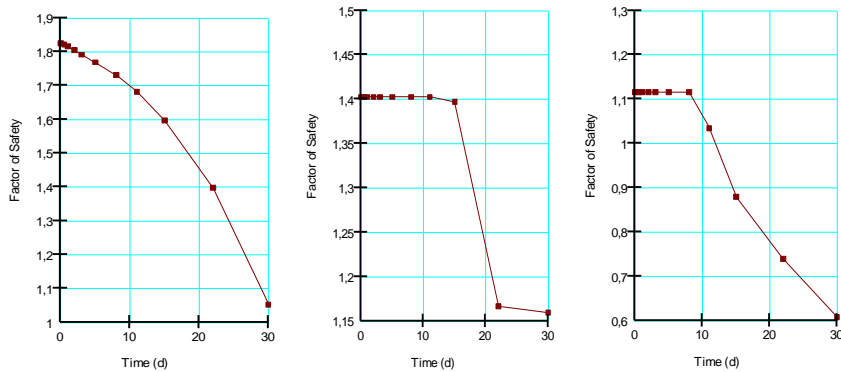
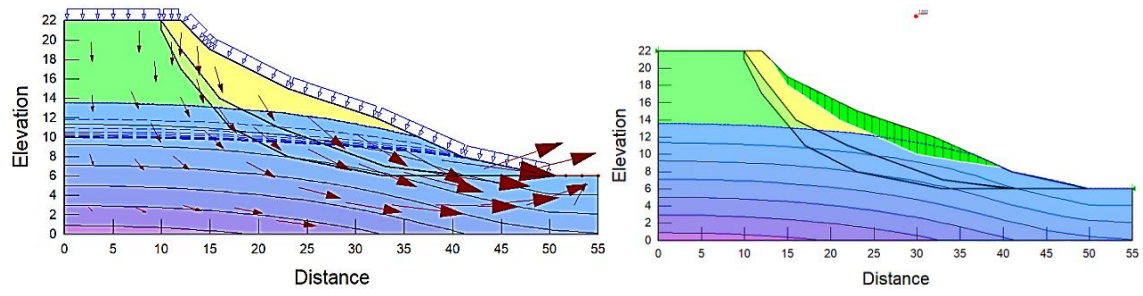
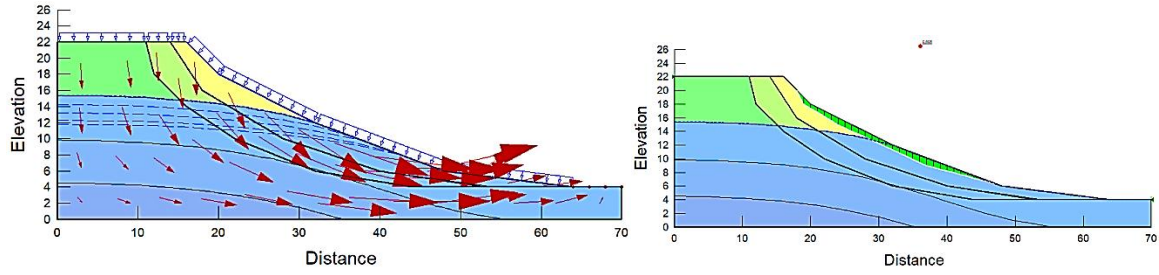


Figure VI.10: The results of safety factor (FOS)

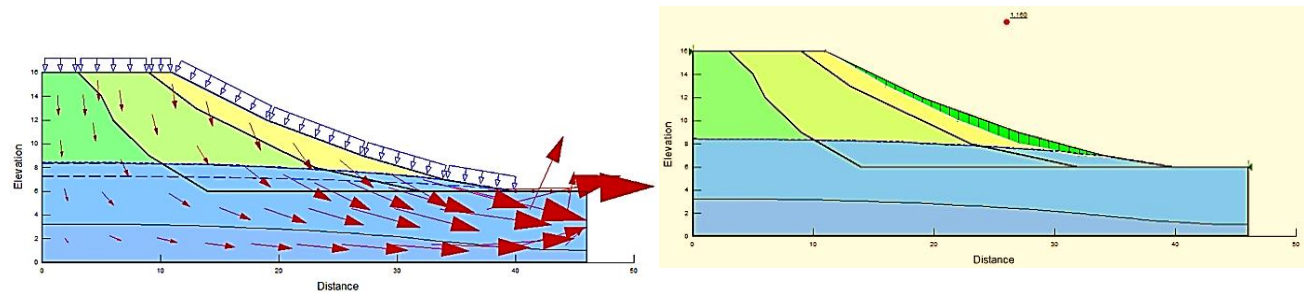
A-Hammam Tassa B-Zaarouria C- Mechrouha



A-Hammam Tassa



B-Mechrouha



C-Zaarouria

Figure VI.11: Numerical slope model in coupled of seep/w –slop/w of the Geoslope Software (2020).

6. Conclusion

The aim of this work is to investigate the mass wasting process in the Souk Ahras area and the interaction of geology, topography, soil type and precipitation in the formation of shallow landslides as the dominant process. For this purpose we have selected three sectors (Hammam Tassa, Zaarouria and Mechrouha) in the Souk Ahras region. This study has shown that, in addition to the predisposing factors, precipitation is the main trigger, since landslides usually occur after the rainy seasons in winter and early spring. According to conservative estimates, soil unsaturation leads to instability after heavy rainfall, which typically accumulates 100 mm per month. A coupled stability analysis using Seep/w-Slop/w software on established geological models and considering different precipitation scenarios has shown flat failure planes with safety factors between (0.6 and 1.8). The stability analysis was performed on completely dry soil, where matric suction is highest, and on completely saturated soil, where matric suction is lowest. For almost dry soils, the safety factor reaches values of 1.4 and 1.8, respectively, while in the same soil in a fully saturated state, a safety factor of only 1.1 was determined. From this it can be deduced that the suction part of the shear strength can significantly improve the safety factor.

The relationship between the safety factor and the amount of precipitation shows different patterns depending on the soil permeability. In soils with high permeability, such as those of Mechrouha and Zaarouria, there is a sudden drop in the safety factor when the accumulated precipitation reaches a value of around 100 mm. For Hammam Tassa, however, the decrease in the safety factor shows an inversely linear relationship. However, in all analyzes performed, the sliding process began when the accumulated amount of precipitation for a continuous event reached about 100 mm in all areas studied.

**GENERAL
CONCLUSION AND
RECOMMENDATION
S**

Conclusion and recommendation

Conclusion and recommendation

In this research work we studied shallow landslides in the region of Souk Ahras. The study area is almost exclusively covered by Triassic formations except the southern part where the Miocene covers the slopes. These materials are generally clays and silts for the Miocene and varicolor clays for the Trias.

Three sites (Hammam Tassa, Zaarouria and Mechrouha) were chosen for the study of this shallow landslide phenomenon as they are prone to the occurrence of shallow landslides, though characterized by different lithology. The research elaborated in the land instability archive shows that the majority of landslides are superficial and recurrent. They occur after heavy rainfall at the end of winter.

Anthropotization, slope conditions, drainage networks, clay formations, tectonic accidents and heavy rainfall, etc. are the main factors affecting the spatial distribution of these shallow landslides. The inventory allowed us to map **60** landslides. The thickness of moving masses does not exceed three meters and is often located near roads and drainage networks. On the Triassic materials, landslides develop on embankments with a slope of around 10° . On clayey silts, landslides develop on slopes of around **18 to 20°**.

During fieldwork in these sectors, numerous data on soil properties were collected through in situ tests (natural water content) and laboratory analyzes (Atterberg limits, hydrometer and grain size distribution, cohesion, friction angle) on the collected samples.

Since it was not possible to reach all points in the sectors during field work, a new resolution satellite image was taken by Google Earth Pro as well as Landsat 8 and DEM (12.m). The image was orthorectified and then performed using photo interpretation. A new landslide database was created in a GIS environment.

The generated inventory map and its factors (slope, slope, aspect, land use/cover, elevation, etc.) using Arc Gis software helped to identify the newly occurring shallow landslides.

The susceptibility to landslides of the different cartographic units through the study terrain is then evaluated and mapped using ArcGIS 10.2 software.

Under ArcGis several layers of information (rasters and shapefiles) have been developed. These are the Slopes, Aspect, Elevation, Distance to Roads, and Distance to Drainage Layer.

Conclusion and recommendation

The susceptibility interval is then reclassified into five classes. These are high, medium high, medium, medium low and low susceptibility.

The stability computation of the slopes with respect to landslides, were established using a two-dimensional geological model for slopes of the selected areas. For the calculation of the stability, the soil is considered unsaturated with the suction characteristics, taken from the SWCC established with the Soil Vision software from the granulometric data. The safety factor is then calculated by the Slope/w software using the model previously presented. The stability computation was undertaken using, GeoStudio software 2020, a coupled analysis where the Seep/W simulates the seepage and the Slope/W for the safety factor. The safety factor varies between 0.8 , 1.16 and 0.8.

Shallow landslides caused by precipitation often occur with transient infiltration into initially unsaturated soils. Heavy rains, especially when preceded by prolonged periods of rain, can lead to an increase in pore water pressure coupled with a loss of apparent cohesion leading to failure of the top soil layers.

Moreover, study has shown that, in addition to the predisposing factors, precipitation is the main triggering factor, since landslides usually occur after the rainy seasons in winter and early spring. According to conservative estimates, soil saturation leads to instability after heavy rainfall, which typically accumulates 100 mm per month.

As future research work, we aim to develop a model for predicting precipitation-related landslides on the basis of statistical analysis of past slope failure records and actual precipitation data. However, such studies are limited by the availability, completeness, precision, and bias of these records. Therefore, in order to develop a useful early warning system, the physical mechanisms of landslides should be considered. A prototype for early warning system should integrate three main components:

- (1) A vulnerability mapping and hotspot identification component based on a land surface geospatial database (topographic information, soil property maps and local landslide inventory, etc.);
- (2) A satellite-based precipitation monitoring system and precipitation forecast model (i.e., Weather Research Forecast) and;
- (3) A physically based prediction model for precipitation-related landslides SLIDE.

Conclusion and recommendation

The system uses the modified physical model to calculate a safety factor that accounts for the contribution of precipitation infiltration and partial saturation to soil shear strength in topographically complex terrains. In use, the land surface information is integrated with the precipitation triggered by the landslide prediction model to predict potential slope failures as a function of time and location.

In such a system, one should use precise geomorphological data, a high resolution digital elevation model (DEM) and a soil maps and an accurate rainfall record. The system's predictive performance should then be evaluated using a local landslide inventory.

Reference

Reference

Reference

- Acharya KP, Bhandary NP, Dahal RK, Yatabe R (2016) Seepage and slope stability modelling of rainfall-induced slope failures in topographic hollows. *Geomat Nat Haz Risk* 7(2):721–746. <https://doi.org/10.1080/19475705.2014.954150>
- Ahmadi-adli, M., Huvaj, N., & Toker, N. K. (2017). Rainfall-triggered landslides in an unsaturated soil: a laboratory flume study. *Environmental Earth Sciences*, 76(21). <https://doi.org/10.1007/s12665-017-7049-z>
- Ahmadi-adli, Mohammad, Nejan Huvaj, and Nabi Kartal Toker. 2017. “Rainfall-Triggered Landslides in an Unsaturated Soil: A Laboratory Flume Study.” *Environmental Earth Sciences* 76(21). doi: 10.1007/s12665-017-7049-z.
- Aleotti P, Chowdhury R (1999) Landslide hazard assessment: summary review and new perspectives. *Bull Eng Geol Env* 58:21–44. <https://doi.org/10.1007/s100640050066>
- Ali A, Huang J, Lyamin AV, Sloan SW, Cassidy MJ (2014) Boundary effects of rainfall-induced landslides. *Comput Geotech* 61:341–354. <https://doi.org/10.1016/j.compgeo.2014.05.019>
- Ali, A., Huang, J., Lyamin, A. V., Sloan, S. W., & Cassidy, M. J. (2014). Boundary effects of rainfall-induced landslides. *Computers and Geotechnics*, 61, 341–354. <https://doi.org/10.1016/j.compgeo.2014.05.019>
- Alves ME, Omotoso O, Anderson MA, Antoni M, Rossen J, Martirena F, Scrivener KL, Avet F, Snellings R, Alujas Diaz A, Ben Haha M, Scrivener KL, Barrer RMM, Jones DL, Mainwaring DE, Bediako M, Gawu SK, Adjaottor AA, Solomon Ankrah J, ... Karstunen M (2016) Correlation of the undrained shear strength and plasticity index of tropical clays. *Cement Concrete Res*, 6(1), 1–11
- Anbalagan R (1992) Landslide hazard evaluation and zonation mapping in mountainous terrain. *Eng Geol* 32:269–277
- Arabameri A, Pradhan B, Rezaei K, Lee CW (2019) Assessment of landslide susceptibility using statistical- and artificial intelligence-based FR-RF integrated model and multiresolution DEMs. *Remote Sensing*, 11(9). <https://doi.org/10.3390/rs11090999>
- Atiali JR (1998) *Avant propos*. *Diabetes Metab* 24(SUPPL. 3):5–6 Augusto Filho O, Fernandes MA (2019) Landslide analysis of unsaturated soil slopes based on rainfall and matric suction data. *Bull Eng Geol Env* 78(6):4167–4185. <https://doi.org/10.1007/s10064-018-1392-5>
- Augustin, A., & Takoukam, F. (2018). CHARACTERIZATION OF SWELLING STRESS AND SOIL MOISTURE DEFICIENCY RELATIONSHIP FOR. June.
- Azmi M, Ramli MH, Hezmi MA, Mohd Yusoff SAN, Arel MNA (2019) Estimation of soil water characteristic curves (SWCC) of mining sand using soil suction modelling. *IOP Conference Series: Materials Science and Engineering*, 527(1). <https://doi.org/10.1088/1757-899X/527/1/012016>

Reference

- Azmi, M., Ramli, M. H., Hezmi, M. A., Mohd Yusoff, S. A. N., & Alel, M. N. A. (2019). Estimation of Soil Water Characteristic Curves (SWCC) of mining sand using soil suction modelling. *IOP Conference Series: Materials Science and Engineering*, 527(1). <https://doi.org/10.1088/1757-899X/527/1/012016>
- Baeza C, Corominas J (2001) Assessment of shallow landslide susceptibility by means of multivariate statistical techniques. *Earth Surf Proc Land* 26:1251–1263. <https://doi.org/10.1002/esp.263>
- Baum RL, Godt JW (2010) Early warning of rainfall-induced shallow landslides and debris flows in the USA. *Landslides* 7(3):259–272. <https://doi.org/10.1007/s10346-009-0177-0>
- Begueria S (2006) Changes in land cover and shallow landslide activity: a case study in the Spanish Pyrenees. *Geomorphology* 74:196–206. <https://doi.org/10.1016/j.geomorph.2005.07.018>
- Blight, Geoffrey E. n.d. *Unsaturated Soil Mechanics in Geotechnical Practice*.
- Bousta M, Ait Brahim L (2018) Weights of evidence method for landslide susceptibility mapping in Tangier. *Morocco MATEC Web of Conferences* 149:02042. <https://doi.org/10.1051/mateconf/201814902042>
- Bozhinova-Haapanen A (2016) Stabilizing the Landslide on Road E87 Burgas - Malko Tarnovo, Bulgaria. *Procedia Engineering*, 143(Ictg), 650–657. <https://doi.org/10.1016/j.proeng.2016.06.092>
- Bozo L, Cela K (2016) Problems with landslide stabilization of Dukat in the Road Vlora – Saranda. *Procedia Engineering*, 143(Ictg), 1435–1442. <https://doi.org/10.1016/j.proeng.2016.06.169>
- Brabb EE (1991) The world landslide problem. *Episodes* 14(1):52–61 Brunetti MT, Peruccacci S, Rossi M, Luciani S, Valigi D, Guzzetti F (2010) Natural Hazards and Earth System Sciences Rainfall thresholds for the possible occurrence of landslides in Italy. In *Hazards Earth Syst. Sci* (Vol. 10). www.nat-hazards-earth-syst-sci.net/10/447/2010/
- Budimir MEA, Atkinson PM, Lewis HG (2015) A systematic review of landslide probability mapping using logistic regression. *Landslides* 12:419–436. <https://doi.org/10.1007/s10346-014-0550-5>, 2 Campbell RH (1975) Soil slips, debris flows, and rainstorms in the Santa Monica mountains and vicinity, Southern California. U.S. Geological Survey Professional Paper 851, 51 pages. <http://pubs.usgs.gov/pp/0851/report.pdf>
- Carman PC (1939) Permeability of saturated sands, soils and clays. *J Agric Sci* 29(2):262–273. <https://doi.org/10.1017/S0021859600051789>
- Castro CD, Lombardo L, Martin MP, Dou J, Huser R (2017) Handling high predictor dimensionality in slope unit based landslide susceptibility models through LASSO-penalized Generalized Linear Model. *Environ Model Soft* 97:145–156. <https://doi.org/10.1016/j.envsoft.2017.08.003>
- Çellek S (2013) Landslide susceptibility analysis of Sinop-Gerze region, Doctora Thesis (in Turkish), KTU, Turkey.

Reference

- Çellek S (2020) Effect of the slope angle and its classification on landslide, Nat Hazards Earth Syst Sci. 10.5194/nhess-2020-87, 2020
- Cevasco A, Pepe G, Brandolini P (2014) (2013): The influences of geological and land use settings on shallow landslides triggered by an intense rainfall event in a coastal terraced environment. Bull Eng Geol Environ 73:859–875. <https://doi.org/10.1007/s10064-013-0544-x>
- Cevasco A, Robbiano A, Sacchini A, Vincenzi E (2008) Hydro-logical thresholds for triggering shallow landslides in the area of the Municipality of Genoa: the case study of the Bisagno Valley. Rendiconti Online Societa` Geologica Italiana 3(1):212–213
- CHABBI Abdallah. (2017). Les nappes telliennes de la région Nord de Souk Ahras (NE algérien) : Etude géologique et structurale.
- CHABBI Abdallah. 2017. “Les Nappes Telliennes de La Région Nord de Souk Ahras (NE Algérien) : Etude Géologique et Structurale.”
- Chen CW, Chen H, Wei LW, Lin GW, Iida T, Yamada R (2017) Evaluating the susceptibility of landslide landforms in Japan using slope stability analysis: a case study of the 2016 Kumamoto earthquake. Landslides 14(5):1793–1801. <https://doi.org/10.1007/s10346-017-0872-1>
- Chen H, Lee CF (2004) Geohazards of slope mass movement and its prevention in Hong Kong. Eng Geol 76(1–2):3–25. <https://doi.org/10.1016/j.enggeo.2004.06.003>
- Chinkulkijniwat A, Yubonchit S, Horpibulsuk S, Jothityangkoon C, Jeeptaku C, Arulrajah A (2016) Hydrological responses and stability analysis of shallow slopes with cohesionless soil subjected to continuous rainfall. Can Geotech J 53(12):2001–2013. <https://doi.org/10.1139/cgj-2016-0143>
- Cohen AS, Coe AL, Harding SM, Schwark L (2004) Osmium isotope evidence for the regulation of atmospheric CO₂ by continental weathering. Geology 32(2):157–160. <https://doi.org/10.1130/G20158.1>
- Crosta GB, Dal Negro P, Frattini P (2003) Soil slips and debris flows on terraced slopes. Nat Hazards Earth Syst Sci 3(1/2):31–42. <https://doi.org/10.5194/nhess-3-31-2003>
- Dağ S (2007) Landslide susceptibility analysis of Çayeli (Rize) and its surrounding by statistical methods, Doctora Thesis (in Turkish), KTU, Turkey
- Dahal RK, Hasegawa S, Nonomura A, Yamanaka M, Masuda T, Nishino K (2009) Failure characteristics of rainfall-induced shallow landslides in granitic terrains of Shikoku Island of Japan. Environ Geol 56(7):1295–1310. <https://doi.org/10.1007/s00254-008-1228-x>
- Dai FC, Lee CF (2002) Landslide characteristics and slope instability modeling using GIS Lantau Island, Hong Kong. Geomorphology 42:213–238
- Dai FC, Lee CF, Ngai YY (2002) Landslide risk assessment and management: an overview. Eng Geol 64(1):65–87. [https://doi.org/10.1016/S0013-7952\(01\)00093-X](https://doi.org/10.1016/S0013-7952(01)00093-X)

Reference

- Dante Fratta, Jennifer Aguettant LR-S (2007) Introduction to soil mechanics laboratory testing by Dante Fratta, Jennifer Aguet- tant, Lynne Roussel-Smith (z-lib.org).pdf (p. 246 pages). <http://www.taylorandfrancis.com>
- David L (1956) Etude géologique des Monts de la Haute Medjerda. Thesis sc. Paris, PSCGANS, bull. N° 11, 289 pp
- De Vita P, Allocca V, Manna F, Fabbrocino S (2012) Coupled dec- adal variability of the North Atlantic Oscillation, regional rain- fall and karst spring discharges in the Campania region (south- ern Italy). *Hydrol Earth Syst Sci* 16(5):1389–1399. <https://doi.org/10.5194/hess-16-1389-2012>
- Di Crescenzo G, Santo A (2005) Debris slides–rapid earth flows in the carbonate massifs of the Campania region (Southern Italy): morphological and morphometric data for evaluating trigger- ing susceptibility. *Geomorphology* 66(1–4):255–276. <https://doi.org/10.1016/J.GEOMORPH.2004.09.015>
- Dias, A. S., Pirone, M., & Urciuoli, G. (2017). Review on the Methods for Evaluation of Root Reinforcement in Shallow Landslides. In *Advancing Culture of Living with Landslides* (pp. 641–648). Springer International Publishing. https://doi.org/10.1007/978-3-319-53498-5_74
- Dias, Ana Sofia, Marianna Pirone, and Gianfranco Urciuoli. 2017. “Review on the Methods for Evaluation of Root Reinforcement in Shallow Landslides.” Pp. 641–48 in *Advancing Culture of Living with Landslides*. Springer International Publishing.
- Dirx WJ, van Beek R, Bierkens M (2020) The influence of grain size distribution on the hydraulic gradient for initiating backward erosion. *Water (Switzerland)*, 12(9). <https://doi.org/10.3390/w12092644>
- Djazair : Réaménagement des forêts de chêne-liège à Souk Ahras. (n.d.). Retrieved March 15, 2023, from <https://www.djazair.com/fr/liberte/463694>
- Dölek İ, Avcı V (2016) Determination of areas with landslide sus- ceptibility in Arguvan district (Malatya province) and its sur- rounding by multi-criteria decision analysis method (MDAM). *J Acad Soc Sci* 4(33):106–129
- Dolzyk K, Chmielewska I (2014) Predicting the coefficient of perme- ability of non-plastic soils. *Soil Mech Found Eng* 51(5):213– 218. <https://doi.org/10.1007/s11204-014-9279-3>
- Drewa PB, Platt WJ, Moser EB (2002) Community structure along elevation gradients in headwater regions of longleaf pine savannas. *Plant Ecol* 160(1):61–78. <https://doi.org/10.1023/A:1015875828742>
- Echeverri O, Valencia Y (2004) Analysis of landslides in the basin of the Iguana river from Medellín city based on rainfall-slope- geological formation interaction. *Dyna* 71(142):33–45
- Ephrem G (2019) Characteristics of grain size distribution and the shear strength analysis of Chenjiaba long runout. *Coseismic Landslide* 16:2110–2125

Reference

- Ermini L, Catani F, Casagli N (2005) Artificial neural networks applied to landslide susceptibility assessment. *Geomorphology* 66:327–343. <https://doi.org/10.1016/j.geomorph.2004.09.025>
- Fredlund DG, Rahardjo H, Fredlund MD (2012) *Unsaturated soil mechanics in engineering practice*. John Wiley & Sons, Inc
- Fredlund DG, Zhang F (2013) Combination of shrinkage curve and soil-water characteristic curves for soils that undergo volume change as soil suction is increased. In: 18th International Conference on Soil Mechanics and Geotechnical Engineering: Challenges and Innovations in Geotechnics, ICSMGE 2013, 2, pp 1109–1112
- Fredlund MD, Fredlund DG, Wilson GW (n.d.) Prediction of the soil-water characteristic curve from grain-size distribution and volume-mass properties
- Fredlund MD, Wilson GW (2020) Indirect procedures to determine unsaturated soil property functions, *Proceedings of the 50 Canadian Geotechnical Conference*. April
- Galve JP, Cevasco A, Brandolini P, Soldati M (2015) Assessment of shallow landslide risk mitigation measures based on land use planning through probabilistic modelling. *Landslides* 12:101–114. <https://doi.org/10.1007/s10346-014-0478-9>
- Genuchten, M. T. van, & Wierenga, P. J. (1976). Mass Transfer Studies in Sorbing Porous Media I. Analytical Solutions. *Soil Science Society of America Journal*, 40(4), 473–480. <https://doi.org/10.2136/SSSAJ1976.03615995004000040011X>
- GeoSlope International Ltd. (2004a) *Seep/W user's guide for finite element Seepage Analysis*. GEO-SLOPE International Ltd, Calgary, Alta
- GeoSlope International Ltd. (2004b) *Seep/W User's guide for slope stability analysis*. GEO-SLOPE International Ltd, Calgary, Alta
- GeoStudio 2020 by GEOSLOPE International Ltd (2020) Retrieved February 19, 2023, from <https://geostudio2020.software.informer.com/download/>
- Goetz JN, Brenning A, Petschko H, Leopold P (2015) Evaluating machine learning and statistical prediction techniques for landslide susceptibility modelling. *Comput Geosci* 81:1–11. <https://doi.org/10.1016/j.cageo.2015.04.007>
- Goetz JN, Guthrie RH, Brenning A (2011) Integrating physical and empirical landslide susceptibility models using generalized additive models. *Geomorphology* 129(3–4):376–386. <https://doi.org/10.1016/j.geomorph.2011.03.001>
- Greco R, Guida A, Damiano E, Olivares L (2010) Soil water content and suction monitoring in model slopes for shallow flowslides early warning applications. *Phys Chem Earth* 35:127–136. <https://doi.org/10.1016/j.pce.2009.12.003>
- Grelle G, Revellino P, Donnarumma A, Guadagno FM (2011) Bedding control on landslides: a methodological approach for
- Guzzetti F, Cardinali M, Reichenbach P, Carrara A (2000) (2000): Comparing landslide maps: a case study in the upper Tiber River Basin Central Italy. *Environ Manag* 25(3):247–363

Reference

- Hadji R, Achour Y, Hamed Y (2018) Using GIS and RS for slope movement susceptibility mapping: Comparing AHP, LI and LR methods for the Oued Mellah Basin, NE Algeria. In: *Advances in Science, Technology and Innovation*. Springer Nature, pp 1853–1856.
https://doi.org/10.1007/978-3-319-70548-4_536
- Hadji R, Boumazbeur A, Limani A, Beghem Y, Chouabi M, demdoum A, (2013) Geologic, topographic and climatic controls on land- slide hazard assessment using GIS modeling: a case study of Souk Ahras region, NE Algeria. *Quat Int* 302:224–237.
- Hansen A (1984a) Strategies for classification of landslides. In: Prior DB (ed) Brunsden D. *Slope Instability*. Wiley, New York, pp 523–602
- Hansen A (1984b) Engineering geomorphology: the application of an evolutionary model of Hong Kong. *Z Geomorphol* 51(1984):39–50
- Harmoko U, Yuliyanto G, Yulianto T (2020) Vulnerability assessment in landslide risk analysis. *Int J Recent Trends Eng Res* 6(5):7–13. <https://doi.org/10.23883/ijrter.2020.6026.hl2zm>
- Hasegawa S, Dahal RK, Nishimura T, Nonomura A, Yamanaka M (2009) DEM-Based analysis of earthquake-induced shallow land-slide susceptibility. *Geotech Geol Eng* 27(3):419–430. <https://doi.org/10.1007/s10706-008-9242-z>
- Hasekiogulları GD (2011) Assessment of parameter effects in producing landslide susceptibility maps, Master Thesis (in Turkish), Hacettepe University, Turkey
- Hidalgo CA, Vega JA, Obando MP (2018) Effect of the rainfall infiltration processes on the landslide hazard assessment of unsaturated soils in tropical mountainous regions. In *Engineering and Mathematical Topics in Rainfall*. InTech. <https://doi.org/10.5772/intechopen.70821>
- Hidalgo CH, de Assis AP (2013) A rainfall threshold for the occurrence of landslides in manmade slopes in residual soils in the northwest of Colombia. *Advances in Unsaturated Soils* 579–584.
<https://doi.org/10.1201/B14393-86/RAINFALL-THRESHOLD-OCCURRENCE-LANDSLIDES-MANMADE-SLOPES-RESIDUAL-SOILS-NORTHWEST-COLOMBIA-HIDALGO-DE-ASSIS>
- Intarawichian N, Dasananda S (2010) Analytical hierarchy process for landslide susceptibility mapping in lower Mae Chaem watershed, northern Thailand. In *Suranaree J Sci Technol* 17(3):277–292
- Iverson RM (2000) Landslide triggering by rain infiltration. *Water Resour Res* 36:1897–1910.
<https://doi.org/10.1029/2000WR900090>
- Iverson RM, Major JJ (1986) Groundwater seepage vectors and the potential for hillslope failure and debris flow mobilization. *Water Resources Research* 22(11):1543–1548. <https://doi.org/10.1029/WR022I011P01543>

Reference

- Jeong S, Lee K, Kim J, Kim Y (2017) Analysis of rainfall-induced landslide on unsaturated soil slopes. *Sustainability (Switzerland)* 9(7):1280. <https://doi.org/10.3390/su9071280>
- Klimeš J, Escobar VR (2010) A landslide susceptibility assessment in urban areas based on existing data: an example from the Iguaná Valley, Medellín City, Colombia. *Natural Hazards Earth Syst Sci* 10(10):2067–2079. <https://doi.org/10.5194/nhess-10-2067-2010>
- Ko FW (2005) Correlation between rainfall and natural terrain landslide occurrence in Hong Kong. *Geotech Eng* 168:77
- Ku CY, Liu CY, Xiao JE, Yeh W (2017) Transient modeling of flow in unsaturated soils using a novel collocation meshless method. *Water (Switzerland)*, 8(12). <https://doi.org/10.3390/w9120954>
- Ku, C. Y., Liu, C. Y., Xiao, J. E., & Yeh, W. (2017). Transient modeling of flow in unsaturated soils using a novel collocation meshless method. *Water (Switzerland)*, 8(12). <https://doi.org/10.3390/w9120954>
- L AB, Bousta M, Jemmah IA, I EH, Elmahsani A, Abdelouafi A, Sos-sey F, Lallout I (2018) Landslide susceptibility mapping using AHP method and GIS in the peninsula of Tangier (Rif-northern morocco) Landslide susceptibility mapping using AHP method and GIS in the peninsula of Tangier (Rif-northern morocco). *MATEC Web of Conferences* 149:02084. <https://doi.org/10.1051/mateconf/201814902084>
- Lee ML, Gofar N, Rahardjo H (2009) A simple model for preliminary evaluation of rainfall-induced slope instability. *Eng Geol* 108(2009):272–285
- Lee S (2005) Application of logistic regression model and its validation for landslide susceptibility mapping using GIS and remote sensing data. *Int J Remote Sens* 26:1477–1491. <https://doi.org/10.1080/01431160412331331012>
- Lee S, Min K (2001) Statistical analysis of landslide susceptibility at Yongin, Korea. *Environ Geol* 40:1095–1113
- Lee S, Ryu JH, Won JS, Park HJ (2004) Determination and application of the weights for landslide susceptibility mapping using an artificial neural network. *Eng Geol* 71:289–302. [https://doi.org/10.1016/S0013-7952\(03\)00142-X](https://doi.org/10.1016/S0013-7952(03)00142-X)
- Leoni, L. (2008). Shallow landslides triggered by rainfall: integration between ground-based weather radar and slope stability models in near-real time. <https://core.ac.uk/download/pdf/301562848.pdf>
- Leoni, Lorenzo. 2008. “Shallow Landslides Triggered by Rainfall: Integration between Ground-Based Weather Radar and Slope Stability Models in near-Real Time.”
- Lin WT, Lin CY, Chou WC (2006) Assessment of vegetation recovery and soil erosion at landslides caused by a catastrophic earthquake: a case study in Central Taiwan. *Ecol Eng* 28(1):79–89. <https://doi.org/10.1016/j.ecoleng.2006.04.005>

Reference

- Lu N, Godt JW, Wu DT (2010) A closed-form equation for effective stress in unsaturated soil. *Water Resour Res* 46(5):1–14. <https://doi.org/10.1029/2009wr008646>
- MacRobert CJ, Blight GE (2013) A field study of the in situ moisture regime during active hydraulic tailings deposition. *J South Afric Instit Civil Eng* 55(3):57–68. http://www.scielo.org.za/scielo.php?script=sci_arttext&pid=S1021-20192013000300007&lng=en&nrm=iso&tlng=en.
- Mahdadi F., (2018): Approche par les méthodes statistiques à l'étude de l'influence de la géologie et de la minéralogie sur la distribution spatiale de la susceptibilité aux glissements de terrain dans la région de Souk Ahras, NE de l'Algérie. PhD Thesis, University Constantine
- Marjanovic M, Kovačević M, Bajat B, Vozenilek V (2011) Landslide susceptibility assessment using SVM machine learning algorithm. *Eng Geol.* 123:225–234 <https://doi.org/10.1016/j.enggeo.2011.09.006>
- McCalpin J (1984) Preliminary age classification of landslides for inventory mapping, Proceedings 21st annual Engineering Geology and Soils Engineering Symposium. University Press, Moscow, Idaho, pp 99–111
- McKenna JP, Santi PM, Amblard X, Negri J (2012) Effects of soil engineering properties on the failure mode of shallow landslides. *Landslides* 9(2):215–228. <https://doi.org/10.1007/s10346-011-0295-3>
- Mehrotra R, Namuduri K, Ranganathan N (1992) Gabor filter-based edge detection. *Pattern Recogn* 25(12):1479–1494. [https://doi.org/10.1016/0031-3203\(92\)90121-X](https://doi.org/10.1016/0031-3203(92)90121-X)
- Montgomery DR, Dietrich WE (1994) A physically based model for the topographic control on shallow landsliding. *Water Resour Res* 30:1153–1171. <https://doi.org/10.1029/93WR02979>
- Montrasio L, Schilirò IL, Terrone IA, (2016) Physical and numerical modelling of shallow landslides, 13, pages 873–883, <https://doi.org/10.1007/s10346-015-0642-x>
- Montrasio L, Valentino R (2008) A model for triggering mechanisms of shallow landslides. *System Sciences*, 1149–1159
- Moser M, Hohensinn F (1983) Geotechnical aspects of soil slips in alpine regions. *Eng Geol* 19:185–211. [https://doi.org/10.1016/0013-7952\(83\)90003-0](https://doi.org/10.1016/0013-7952(83)90003-0)
- Nations U (2003) Human Development Report 2003. *Hum Dev Rep* Ng CWW, Zhan LT, Bao CG, Fredlund DG, Gong BW (2003) Performance of an unsaturated expansive soil slope subjected to artificial rainfall infiltration. *Géotechnique* 53(2):143–157. <https://doi.org/10.1680/geot.53.2.143.37272>
- Nishimura T, Fredlund DG, (2000) Relationship between shear strength and matric suction in an unsaturated silty soil. Proceedings of the Asian Conference on Unsaturated Soils, UNSAT ASIA 2000 Singapore, May 18 – 19, 2000 Ohlmacher CG, Davis CJ (2003) Using multiple regression and GIS technology to predict landslide hazard in northeast Kansas, USA. *Eng Geol* 69:331–343

Reference

- Persichillo MG, Bordoni M, Meisina C, Bartelletti C, Barsanti M, Giannecchini R, D'Amato AG, Galanti Y, Cevasco A, Brandolini P (2016) Shallow landslides susceptibility assessment in different environments. *Geomat Nat Hazards Risk* 8:748–771. <https://doi.org/10.1080/19475705.2016.1265011>
- Pham BT, Bui DT, Prakash I, Dholakia MB (2017) Hybrid integration of multilayer perceptron neural networks and machine learning ensembles for landslide susceptibility assessment at Himalayan area (India) using GIS. *CATENA* 149:52–63. <https://doi.org/10.1016/j.catena.2016.09.007>
- Pham HQ, Fredlund DG (2008) Equations for the entire soil-water characteristic curve of a volume change soil. *Can Geotech J* 45(4):443–453. <https://doi.org/10.1139/T07-117>
- Pham, H. Q., & Fredlund, D. G. (2008). Equations for the entire soil-water characteristic curve of a volume change soil. *Canadian Geotechnical Journal*, 45(4), 443–453. <https://doi.org/10.1139/T07-117>
- Piacentini D, Troiani F, Soldati M, Notarnicola C, Savelli D, Schneiderbauer S, Strada C (2012) Statistical analysis for assessing shallow-landslide susceptibility in South Tyrol (south-eastern Alps, Italy). *Geomorphology* 151–152:196–206. <https://doi.org/10.1016/j.geomorph.2012.02.003>
- Pramusandi S, Rifa'i A, Suryolelono KB, (2015) Determination of unsaturated soil properties and slope deformation analysis due to the effect of varies rainfall. *Procedia Eng* 125:376–382. <https://doi.org/10.1016/j.proeng.2015.11.090>
- Rahardjo H, Kim Y, Satyanaga A (2019) Role of unsaturated soil mechanics in geotechnical engineering. *Intl J Geo-Eng*, 1–23. <https://doi.org/10.1186/s40703-019-0104-8>
- Rahardjo H, Li XW, Toll DG, Leong EC (2001) The effect of antecedent rainfall on slope stability. *Geotech Geol Eng* 19(3–4):371–399. <https://doi.org/10.1023/A:1013129725263>
- Rahardjo H, Ong TH, Rezaur RB, Leong EC (2007) Factors controlling instability of homogeneous soil slopes under rainfall. *J Geotech Geoenviron Eng* 133(12):1532–1543. [https://doi.org/10.1061/\(asce\)1090-0241\(2007\)133:12\(1532\)](https://doi.org/10.1061/(asce)1090-0241(2007)133:12(1532))
- Rahardjo, H., Kim, Y., & Satyanaga, A. (2019). Role of unsaturated soil mechanics in geotechnical engineering. *International Journal of Geo-Engineering*, 10(1), 1–23. <https://doi.org/10.1186/s40703-019-0104-8>
- Ran Q, Hong Y, Li W, Gao J (2018) A modelling study of rainfall-induced shallow landslide mechanisms under different rainfall characteristics. *J Hydrol* 563:790–801. <https://doi.org/10.1016/j.jhydrol.2018.06.040>
- Rengers N (1973) Landslides and their control. In *Engineering Geology* (Vol. 7, Issue 3). [https://doi.org/10.1016/0013-7952\(73\)](https://doi.org/10.1016/0013-7952(73))

Reference

- Revellino P, Grelle G, Donnarumma A, Guadagno FM (2010) Structurally controlled earth flows of the Benevento province (Southern Italy). *Bull Eng Geol Environ* 69(3):487–500.
<https://doi.org/10.1007/s10064-010-0288-9>
- Richards LA (1931) Capillary conduction of liquids through porous mediums. *J Appl Phys* 1(5):318–333. <https://doi.org/10.1063/1.1745010>
- Rihab, H. 2013. (2013). Avant propos. In thesis phd (Vol. 24, Issue SUPPL. 3).
- Rihab, Hadji 2013. 2013. Avant Propos. Vol. 24.
- Rouaibia, F. 2018. (2018). Ministère de l'Enseignement Supérieur et de la Recherche Scientifique و. البحث العلمي وزارة التعليم العالي
- Rouaibia, Farid 2018. 2018. Ministère de l'Enseignement Supérieur et de La Recherche Scientifique و. البحث العلمي وزارة التعليم العالي
- Sassa K, Canuti P, Yin Y (2014) Landslide science for a safer geoenvironment. *Lands Sci Safer Geoenviron* 1:1–486. <https://doi.org/10.1007/978-3-319-04999-1>
- Schilirò L, Cevasco A, Esposito CS, Mugnoz G (2018) Shallow landslide initiation on terraced slopes: inferences from a physically-based approach. *Geomat Nat Haz Risk* 9(1):295–324.
<https://doi.org/10.1080/19475705.2018.1430066>
- Suryo, Eko Andi, Gallage, Chaminda, & Trigunaryah, Bambang (2015) A method for predicting rain-induced instability of an individual slope. In Barnes, Paul H. & Goonetilleke, Ashantha (Eds.) *The 9th Annual International Conference of the International Institute for Infrastructure Renewal and reconstruction*. (8–10 July 2013), Queensland University of Technology, Brisbane, Australia, pp. 118–127
- Süzen ML, Doyuran V (2004) (2014): A comparison of the GIS based landslide susceptibility assessment methods: multivariate versus bivariate. *Environ Geol* 45:665–679.
<https://doi.org/10.1007/s00254-003-0917-8>
- Trigila A, Iadanza C, Esposito C, Scarascia MG (2015) 2015): Comparison of Logistic Regression and Random Forests techniques for shallow landslide susceptibility assessment in Giampileri (NE Sicily, Italy). *Geomorphology* 249:119–136. <https://doi.org/10.1016/j.geomorph.2015.06.001>
- Van Genuchten MT (1980) A Closed-form equation for predicting the hydraulic conductivity of unsaturated soils 1
- van Genuchten MT, Wierenga PJ (1976) Mass transfer studies in sorbing porous media I. Analytical solutions. *Soil Sci Soc Am J* 40(4):473–480. <https://doi.org/10.2136/SSSAJ1976.0361599500>
- Van Genuchten, M. T. (n.d.). A Closed-form Equation for Predicting the Hydraulic Conductivity of Unsaturated Soils 1.
- Vila JM (1980) la chaîne Alpine de l'Algérie Nord Orientale et des confins Algéro-Tunisien. These Doc. Univ. P. et M. Curie Paris VI, 665p

Reference

- WHO (2022): https://www.who.int/health-topics/landslides#tab=tab_3 Wiczorek GF (1984) (1984):
Preparing a detailed landslide-inventory map for hazard evaluation and reduction. Bull Assoc
Eng Geol
- Yılmaz I, Yılmaz II (2000) Evaluation of shear strength of clayey soils by using their liquidity index.
In Bull Eng Geol Env (Vol. 59). Springer-Verlag 227
- Youssef AM, Pourghasemi HR, Pourtaghi ZS, Al-Katheeri MM (2016) Landslide susceptibility
mapping using random forest, boosted regression tree, classification and regression tree, and
general linear models and comparison of their performance at Wadi Tayyah Basin, Asir Region,
Saudi Arabia. Landslides 13:839–856. <https://doi.org/10.1007/s10346-015-0614-1>
- Zhan TLT, Jia GW, Chen YM, Fredlund DG, Li H (2013) An analytical solution for rainfall
infiltration into an unsaturated infinite slope and its application to slope stability analysis. Int J
Numer Anal Meth Geomech 37(12):1737–1760. <https://doi.org/10.1002/nag.2106>
- Zhang H, Chen G, Zheng L, Zhang Y (2013) Mechanism of shallow rainfall-induced landslide and
simulation of initiation with DDA. Proceedings of the 11th Int. Conf. on Analysis of Discontinu-
ous Deformation, ICADD, pp 289–293. <https://doi.org/10.1201/b15791-38>
- Ziemer, R. R. (1981). The role of vegetation in the stability of forested slopes. Proc. Int. XVII IUFRO
World Congress, 297–308. <https://www.fs.fed.us/psw/publications/ziemer/ZiemerIUFRO1981.PDF>

Annexes

Annex I

Annexe II

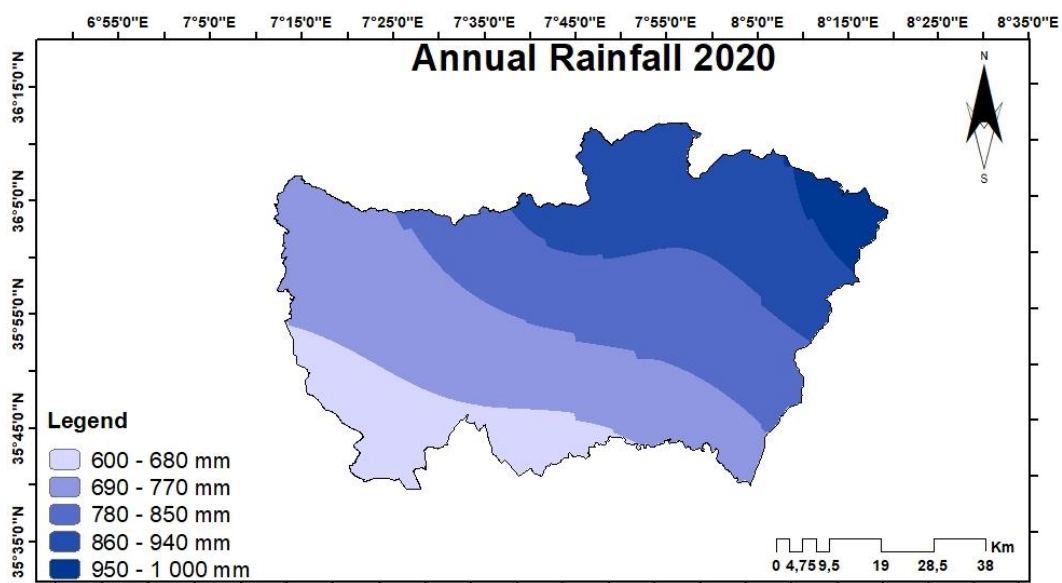


Figure 2: Rainfall map of Souk Ahras area (2020).

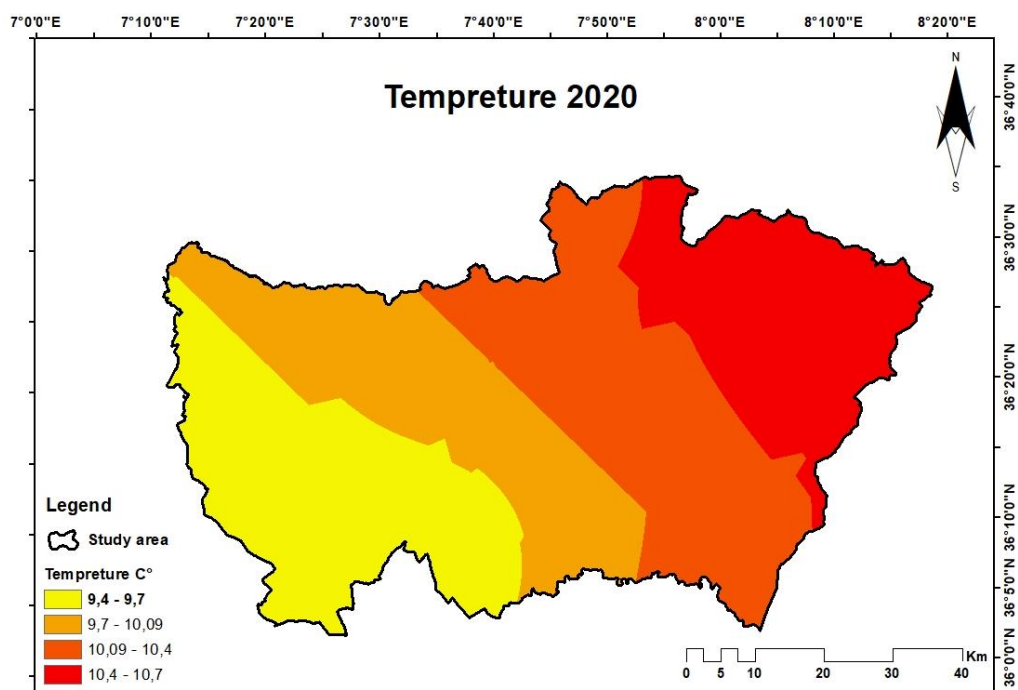
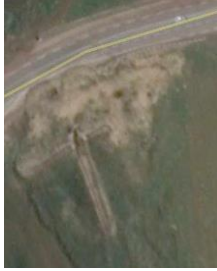







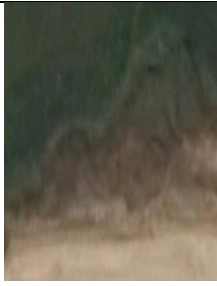



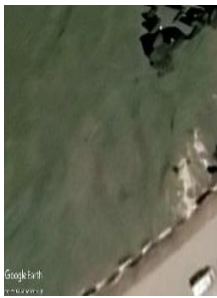





Figure 3: Temperature map of Souk Ahras area (2020).

Annex III

	2014	2015	2016	Real photos
Shallow landslide of Hammam Tassa PK114				 
Shallow landslide Hammam Tassa pk116				
Shallow landslide Zaarouria				
Shallow landslide Mechroha				

Some images satellite and real photos in three sectors in the table:

Annex IV

Some pictures of the sample collection procedure are:



Mechrouha



Zaarouria



Hammam Tassa

Annex V

Calculations and results with Soil Office software

SO-Sieve [Sample project]

- File
- Main
- USCS
- Atterberg limits
- Export
- Settings
- Scientific manual
- Index
- License
- About

Sieve Analysis

Visual examination Generation

BH/TP: TP-01 Depth [m]: 1 USCS: SC

PEAT Organic Cobble Boulder

Dry mass: 2000 [g] Load sieve set Used sieves

Dispersant: NaPO3 Separation sieve: No. 200

Temp.: Constant 20 [°C] Passing: 12.84 [%]

Hydrometer details

Type: 152H Dispersant: NaPO3 Hydrometer: ASTM D422

GC: 2.7 Temp.: Constant 20 [°C]

Md: 80 [g]

Normal Composite

Miscous - Cn: 1 [g/L]

Load correction

No.	T [°C]	Tr [°C]	Cc-1 [g/L]
1	16.4	16	-1.19
2	16.4	16	-1.19
3	16.4	16	-1.19
4	16.3	16.3	-1.19
5	16.2	16.2	-1.19
6	16.1	16.1	-1.19
7	16.1	16.1	-1.19
8	16.2	16.2	-1.19
9	17.3	17.3	-1.19

Note: Report Cc

Results Summary

Organic	Cobble	Boulder	Plus 3-in. [%]	Gravel [%]	Sand [%]	Silt [%]	Clay [%]	D30 [mm]	D60 [mm]
			0	34.1	22.2	21.5	9.3	0.3	0.0634
			0	0	22.2	21.5	9.3	0.3	0.0634
			0	0	22.2	21.5	9.3	0.3	0.0634
			0	0	22.2	21.5	9.3	0.3	0.0634
			0	0	22.2	21.5	9.3	0.3	0.0634
			0	0	22.2	21.5	9.3	0.3	0.0634
			0	0	22.2	21.5	9.3	0.3	0.0634
			0	0	22.2	21.5	9.3	0.3	0.0634
			0	0	22.2	21.5	9.3	0.3	0.0634
			0	0	22.2	21.5	9.3	0.3	0.0634

Atterberg Limits

Pin [g]: 256.7

Result: LL 57.8 PI 27.8

Result: Fines as "Cl" PI 30

Percent finer [%]

No.	Elapsed time [min]	Temp. T [°C]	Reading R [g/L]	Corrected readings [g/L]	Fall distance H [cm]	Diameter D [mm]	Percent finer [%]
1	1	16.4	37	38.12	11.19	0.04715	47.12
2	2	16.4	35	36.12	11.59	0.03993	44.05
3	5	16.4	32	33.12	12.59	0.02201	40.94
4	10	16.3	30	31.14	13.59	0.01584	38.49
5	20	16.2	28	29.16	14.59	0.01139	36.04
6	40	16.1	25	26.17	15.59	0.00825	32.35
7	80	16.1	20	21.17	16.59	0.00604	26.17
8	240	16.2	2	3.16	18.19	0.00389	3.9
9	1440	17.3	1	1.97	18.39	0.00157	2.43

USCS Classification

USCS: SC

Depth [m]: 1

Mechrouha

SO-Sieve [Sample project]

File Main UCSX Antberg limits Edit Export Blank Settings Scientific manual Help License About

Sieve Analysis

Visual examination Generation

PEAT Organic Cobble Boulder

Dry mass: 2000 [g] Used sieves

No.	Sieve	Opening [mm]	Mass retained [g]	Mass retained [%]	Cumulative percent [%]	Coarser	Finer
1	No. 4	4.75	595	29.75	70.25	62.55	37.45
2	No. 10	2	656	32.8	78.2	88.125	11.875
3	No. 18	1	313	15.65	92.45	94.6	5.4
4	No. 40	0.425	198.5	9.925	94.6		
5	No. 70	0.212	86.5	4.325			
6	No. 200	0.075	43	2.15			

Load sieve set Used sieves

Part [g]: 108 **Delete test**

Atterberg limits tests are not performed.

NP Visual examination Free input

Results: LL [63.1] PL [47.7] PI [15.4]

Result: Finest as "MH" **Delete test**

Organic: Cobble Boulder Plus 3-in. [%] 0 Gravel [%] 29.8

BH/TP: TP-Q1 Depth [m] 1 Cu 11.7 Cc 1.79 Ll 63 Pl 15 USCS SW-SM

Hydrometer

Hydrometer test Test Generation

Type: 152H ASTM D7928 ASTM D422

Dispersant: NaPO3 Normal Composite

Meniscus - Cm: 1 [g/l]

Gas: 2.7 Constant Variable

Temp: 20 [°C]

Load Hydrometer: Load correction

No.	H [cm]	W [g]	W ₁ [g]	W ₂ [g]
1	15	15	17.1	
2	12.5	12.5	0.89	

Separation sieve: No. 200 Peening: 5.4 [%]

Correction

No.	Elapsed time t [min]	Temp. T [°C]	Reading R [g/l]	Corrected readings [g/l]	Rect.	Sill distance H [cm]	Diameter D [mm]	Percent finer [%]
1	1	15.8	32	30.89	33	12.19	0.0496	38.18
2	2	15.8	32	30.89	33	12.19	0.03907	38.18
3	5	15.8	30	27.89	31	12.59	0.02154	35.71
4	10	15.8	29	27.89	30	12.79	0.01607	34.47
5	20	15.8	27	25.89	28	13.19	0.01154	32
6	40	15.8	25	23.89	26	13.59	0.00828	29.53
7	80	15.8	23	21.89	24	13.99	0.00594	27.06
8	240	15.8	22	20.89	23	14.19	0.00345	25.82
9	1440	17.1	17	16.11	18	15.19	0.00143	15.91

Results Summary

Sand [%]	Silt [%]	Clay [%]	Silt [%]	Clay [%]
N/A	78.43	21.57		

Delete test

Percent Finer [%]

Properties

Organic: PEAT Organic Cobble Boulder

Load sieve set Used sieves

SO-Sieve [Sample project]

File Main USCIS Atherberg Imms Edit Export Blank Settings Scientific manual Index License About

File menu Main USCIS Atherberg Imms Edit Export Blank Settings Scientific manual Index License About

Test Visual examination Generation

Sieve Analysis

PEAT Organic Cobble Boulder

Dry mass: 2000 [kg]

Load sieve set Used sieves

No.	Sieve	Opening [mm]	Mass retained [kg]	Mass retained [%]	Cumulative percent [%]	Coarser	Finer
1	No.4	4.75	251.5	12.575	12.575	87.425	
2	No.10	2	439.5	21.975	34.55	65.45	
3	No.18	1	248.5	12.425	46.975	53.025	
4	No.40	0.425	273.5	13.675	60.65	39.35	
5	No.70	0.212	188.5	9.425	70.075	29.925	
6	No.200	0.075	110	5.5	75.575	24.425	

More ... Pan [kg]: 488.5 Delete test

Atherberg Limits

Atherberg limits tests are not performed.

NR

Visual examination:

Free input: LL [] PI []

Result: LL [60.5] PI [46.3]

Test data: LL [60.5] PI [46.3] Delete test

Result: Fines as "NM"

Depth [m] 1

Cu 74.1 Cc 1.39

LL 61 PI 15 USCS SM

Organic Cobble Boulder Plus 3 in. [%] 0

Gravel [%] 12.6 Sand [%] 22 Medium Fine

Coarse 0

LL 61 PI 15 USCS SM

TP-01

Percent Finer [%]

0.001 0.01 0.1 1 10 100

Diameter [mm]

4200 44

Depth [m] 1

USCS SM

Hydrometer test Test Generation

ASTM D7928 ASTM D422

Hydrometer

Type: 125H

Dispersant: NaPO3

Temp: 20 [°C]

Separation sieve: No.200

Passing: 24.42 [%]

Properties

Gr: 2.7

Md: 80.1 [g]

Temp: Variable

Correction

Normal Composite

Mendocino - Cnt: 1 [g/l]

No.	Temp. T [°C]	Reading R [g/l]	Corrected readings [g/l]	Recp	Recl	Fall distance H [cm]	Diameter D [mm]	Percent finer [%]
1	17.6	34	34.8	35	34	11.79	0.04766	42.96
2	17.6	34	34.8	35	34	11.79	0.0317	10.49
3	17.6	33	33.8	34	34	11.99	0.0215	41.73
4	17.6	25	25.8	26	25	13.59	0.01618	31.85
5	17.4	24	24.78	25	24	13.79	0.01155	30.59
6	17.4	23	23.78	24	23	13.99	0.00823	29.36
7	17.4	21	21.78	22	21	14.39	0.0059	26.89
8	17.7	19	19.81	20	19	14.79	0.00344	24.46
9	17.8	16	16.82	17	16	15.39	0.00143	20.77

Load correction

No.	T [°C]	Cc1 [g/l]	Cc2 [g/l]
1	17	-0.74	-0.75
2	17.1		

Note: no-p-c

Results Summary

Sand [%]	Silt [%]	Clay [%]	D10 [mm]	D30 [mm]	D60 [mm]
78.19	19.1	5.3	0.0211	0.2137	1.6514

Site [%] 19.1 Clay [%] 5.3 D10 [mm] 0.0211 D30 [mm] 0.2137 D60 [mm] 1.6514

Description: [SM] Silt SAND with Organic Fines, Cobbles and Boulders

© 2017 2019 Soil Office Software Group Version 11.7151.1 [Time Spent: 9 days remaining]

Hammam Tassa

